Electronic Supplementary Information for

Solvatochrony: Solvatochronic Photocatalysts and Their Applications in Intermolecular [2+2] Cycloaddition Reaction of Unactivated Styrenes

Sohee Lee,[a] Seoyeon Kim,[b] Byung Hak Jhun,[a] Hyokyung Kim,[c] Jaeheung Cho,[c,] Eun Jin Cho,[b,]* and Youngmin You[a,]**

[a] Department of Chemical and Biomolecular Engineering, Yonsei University, Seoul 03722, Republic of Korea.
[b] Department of Chemistry, Chung-Ang University, 84 Heukseok-ro, Dongjak-gu, Seoul 06974, Republic of Korea.
[c] Department of Chemistry, Ulsan National Institute of Science and Technology (UNIST), Ulsan 44919, Republic of Korea.

e-mail: jaeheung@unist.ac.kr (J.C.); ejcho@cau.ac.kr (E.J.C); odds2@yonsei.ac.kr (Y.Y.)

CONTENTS

Fig. S21 | a, Photoluminescence spectra of 10 μM Au(^{Dipp}Im)(Cz) dissolved in Ar-saturated 1-propanol and DMSO. **b**, Photoluminescence decay traces of of 10 μM Au(^{Dipp}Im)(Cz) dissolved in Ar-saturated 1-propanol and DMSO. **c**, Photoluminescence of 10 μM Au(^{Dipp}Im)(Cz) dissolved in Ar-saturated THF and diethyl ether. **d**, Photoluminescence decay traces of of 10 μM Au(^{Dipp}Im)(Cz) dissolved in Ar-saturated THF and diethyl ether.

Fig. S22 | UV–Vis absorption spectra of 10 μM Au(^{Dipp}Im)(Cz) and 10 μM **1a** in DMSO.

Fig. S23 | a, Determination of the turn-over numbers and the quantum yields for the photocatalytic [2+2] cycloaddition reaction ($\Phi_{[2+2]s}$) with increased amounts of **1a**. **b**, UV–Vis absorption spectra of 6.0 mM $K_3[Fe(C_2O_4)_3]\cdot 3H_2O$ photoirradiated using 365 nm LEDs for a period of 5 min. **c**, A plot of $\Phi_{[2+2]}$ as a function of the added amount of **1a**.

Fig. S24 | UV–Vis absorption spectra of 100 μM Au(^{Dipp}Im)(Cz) recorded during continuous photoirradiation at 365 nm (10 mW) in deaerated DMSO.

Fig. S25 | Nonlinear least-squares fit analyses for photoluminescence decay traces of 100 μM Au(^{Dipp}Im)(Cz) recorded at a wavelength of 432 nm after nanosecond pulsed laser photoexcitation at 377 nm with increasing the concentration of **1a** (0–1.5 mM).

Fig. S26 | a, Heat map of transient absorption spectra of an Ar-saturated DMSO containing 100 μM Au(^{Dipp}Im)(Cz) and 1.5 mM **1a** recorded after nanosecond pulsed laser excitation at 355 nm. **b**, Time traces of the photoinduced absorption of 100 μM Au(^{Dipp}Im)(Cz) in the presence of 1.5 mM **1a**, monitored at wavelengths of 400, 430, and 595 nm. **c,d**, Time traces of the photoinduced absorption of 100 μM Au(DippIm)(Cz) with the increased concentration of **1a** (0–1.5 mM; Ar-saturated DMSO), monitored at wavelengths of 400 (**c**) and 430 nm (**d**). **e,f**, Corresponding pseudo-first-order kinetics analyses of the quenching rate recorded at wavelengths of 400 (**e**) and 430 nm (**f)** as a function of added **1a**.

Fig. S27 | UV–Vis absorption spectra of 100 μM Au(^{Dipp}Im)(Cz) (DMSO) recorded with increased concentration of styrene (1a) (0–3.0 mM).

Fig. S28 | a, Cyclic and differential pulse voltammograms of 2.0 mM Au(^{Dipp}Im)(Cz) dissolved in Ar-saturated CH_3CN containing 0.10 M $TBAPF_6$. **b**, Comparisons of the electrochemical potentials of the ground and excited states of Au(^{Dipp}Im)(Cz) with the oxidation potential of styrene (**1a**).

Fig. S29 | ^{1}H NMR (300 MHz, CD_2Cl_2) spectrum of Au(^{Dipp}Im)(Cz).

Fig. S30 | $^{13}C\{^1H\}$ NMR (126 MHz, CD_2Cl_2) spectrum of Au(^{Dipp}Im)(Cz).

Fig. S31 | High-resolution mass spectrum of Au(^{Dipp}Im)(Cz).

Fig. S32 | ^{1}H NMR (300 MHz, CD_2Cl_2) spectrum of Au(^{Dipp}Im)(CNCz).

Methods

General procedures. Commercially available chemicals were used as received unless otherwise stated. Dichloromethane (CH_2Cl_2, ≥ 99.8%), sodium *tert*-butoxide (2.0 M in THF), and styrene (≥ 99%) were purchased from Sigma-Aldrich. Carbazole (> 99.0%) and gold chloro[1,3-bis(2,6-diisopropylphenyl)imidazol-2-ylidene] (Au(^{Dipp}Im)Cl, > 98.0%) were purchased from Tokyo Chemical Industry. Gold chloro[1,3-bis(2,6-diisopropylphenyl)benzoimidazol-2-ylidene] (Au(^{Dipp}BZI)Cl), Au(^{Dipp}BZI)(Cz), and Au(^{Dipp}BZI)(TMCz) were prepared, following the previous procedure.[1] Dimethyl sulfoxide (DMSO, > 99.0%) was purchased from Kanto Chemical. Tetrahydrofuran (THF, > 99.5%), toluene (PhMe, ≥ 99.9%) and pentane (98%) were purchased from Daejung Chemicals. *N,N*-Dimethylformaide (DMF, ≥ 99.7%) and ethyl acetate (EtOAc, ≥ 99.8%) were purchased from Wako Pure Chemical Corporation. Acetonitrile (CH_3CN, ≥ 99.8%) was purchased from Junsei. ^{1}H, ^{13}C{^{1}H} and ^{19}F{^{1}H} NMR spectra were collected using Bruker, Avance III-300, 400, and 500 NMR spectrometers. Chemical shifts were referenced to tetramethylsilane. Copies of ^{1}H, ^{13}C{^{1}H}, and ^{19}F{^{1}H} NMR spectra can be found in the supplementary information. High-resolution mass spectra were acquired using JEOL, JMS-700GC or Agilent, 6890 series instruments. Elemental analyses were performed using a Thermo Fisher Scientific, Flash 2000 instrument. FT–IR spectra were recorded on a Nicolet 6700 Thermo Scientific FT-IR spectrometer. Reactions were monitored by thin layer chromatography and GC–MS using the Agilent GC 7890B/5977A inert MSD with Tripel-Axis Detector.

Synthesis of Au(^{Dipp}Im)(Cz). The synthesis of Au(^{Dipp}Im)(Cz) was performed following previous procedures.[2-3] Carbazole (0.296 g, 1.771 mmol) and Au(^{Dipp}Im)Cl (1.00 g, 1.61 mmol), were suspended in freshly distilled THF (120 mL) in a 250 mL two-necked round-bottom flask equipped with a magnetic stir bar. Sodium *tert*-butoxide (2.0 M in THF) (1.61 mL, 3.22 mmol) was added dropwise to the stirred solution at room temperature. The reaction mixture was stirred overnight at room temperature under dark and an Ar atmosphere. The reaction solution was allowed to pass a Celite pad to remove insoluble particulates. The filtrate was concentrated using a rotavap under a reduced pressure. The concentrated solution was then added dropwise to pentane (300 mL) to form precipitates which were subsequently triturated, filtered and washed with pentane (100 mL × three times). The reprecipitation was repeated to afforded white powder in a 91% yield. ^{1}H NMR (300 MHz, CD_2Cl_2) δ (ppm): 7.88 (dd, J = 7.7, 1.3 Hz, 2H), 7.65 (dd, J = 8.2, 7.4 Hz, 2H), 7.43 (d, J = 7.8 Hz, 4H), 7.35 (s, 2H), 7.02 (ddd, J = 8.3, 7.0, 1.3 Hz, 2H), 6.85 (dd, J = 7.9, 7.0 Hz, 2H), 6.72 (d, J = 8.1 Hz, 2H), 2.72 (hept, J = 6.9 Hz, 4H), 1.38 (d, J = 6.9 Hz, 12H), 1.28 (d, J = 6.9 Hz, 12H). ^{13}C{^{1}H} NMR (126 MHz, CD_2Cl_2) δ (ppm): 179.18, 149.91, 146.72, 134.90, 131.18, 124.79, 124.01, 123.92, 123.87, 119.63, 116.14, 113.99, 29.53, 24.73, 24.45. HR MS (FAB$^+$): Calcd for

$C_{39}H_{44}AuN_3$, 751.32; Found: 751.3201.

Synthesis of Au(^{Dipp}Im)(CNCz). Au(^{Dipp}Im)(CNCz) was synthesized following the protocols identical to the synthesis of Au(^{Dipp}Im)(Cz), except using 3,6-dicyanocarbazole in place of carbazole. A white powder was obtained in a 92% yield. ^{1}H NMR (300 MHz, CD_2Cl_2) δ (ppm): 8.23 (d, *J* = 1.7 Hz, 2H), 7.73–7.62 (m, 2H), 7.44 (d, *J* = 7.8 Hz, 4H), 7.42 – 7.30 (m, 4H), 6.69 (d, *J* = 8.5 Hz, 2H), 2.67 (hept, *J* = 6.8 Hz, 4H), 1.31 (d, *J* = 6.9 Hz, 24H). ^{13}C{^{1}H} NMR (126 MHz, CD_2Cl_2) δ (ppm): 177.01, 152.58, 146.74, 134.61, 131.39, 128.37, 125.47, 124.90, 124.24, 123.62, 121.63, 115.17, 99.96, 29.52, 24.76, 24.42. HR MS (FAB$^+$): Calcd for $C_{41}H_{42}AuN_5$, 801.31; Found: 802.3183.

Synthesis of Au(^{Dipp}Im)(Cz_3). Au(^{Dipp}Im)(Cz_3) was synthesized following the protocols identical to the synthesis of Au(^{Dipp}Im)(Cz), except using 9,3':6',9''-tercarbazole in place of carbazole. A white powder was obtained in a 99% yield. ^{1}H NMR (300 MHz, CD_2Cl_2) δ (ppm): 8.12 (dd, *J* = 0.8 Hz, 4H), 8.01 (d, *J* = 1.7 Hz, 2H), 7.63 (t, *J* = 8.3, 7.4 Hz, 2H), 7.46 (d, *J* = 7.8, 4H), 7.41 (s, 2H), 7.37–7.32 (m, 4H), 7.29–7.26 (m, 4H), 7.24–7.20 (m, 4H), 7.19–7.18 (m, 2H), 6.96 (d, *J* = 8.2 Hz, 2H), 2.77 (hept, *J* = 6.8, 4H), 1.46 (d, *J* = 6.9, 12H), 1.31 (d, *J* = 6.9, 12H). ^{13}C{^{1}H} NMR (126 MHz, CD_2Cl_2) δ (ppm): 178.40, 149.98, 146.78, 142.78, 134.84, 131.31, 126.67, 126.14, 124.89, 124.64, 124.18, 124.10, 123.27, 120.71, 120.48, 119.65, 119.27, 115.19, 110.54, 110.28, 29.59, 24.87, 24.47. HR MS (FAB$^+$): Calcd for $C_{63}H_{58}AuN_5$, 1081.44; Found: 1081.4366.

Synthesis of Au(^{Dipp}Im)(αCb). Au(^{Dipp}Im)(αCb) was synthesized following the protocols identical to the synthesis of Au(^{Dipp}Im)(Cz), except using 9*H*-pyrido[2,3-*b*]indole in place of carbazole. A white powder was obtained in a 91% yield. ^{1}H NMR (300 MHz, CD_2Cl_2) δ (ppm): 8.21–8.08 (m, 2H), 7.87 (dd, *J* = 7.7, 1.3 Hz, 1H), 7.59 (dd, *J* = 8.2, 7.4 Hz, 2H), 7.39 (d, *J* = 7.8 Hz, 4H), 7.32 (s, 2H), 7.08 (ddd, J = 8.3, 7.1, 1.4 Hz, 1H), 6.97–6.86 (m, 1H), 6.85–6.71 (m, 2H), 2.74 (hept, *J* = 6.9 Hz, 4H), 1.42 (s, 12H), 1.27 (d, *J* = 6.9 Hz, 12H). ^{13}C{^{1}H} NMR (126 MHz, CD_2Cl_2) δ (ppm): 178.47, 160.71, 149.42, 146.63, 145.49, 134.98, 131.11, 126.94, 126.92, 124.80, 124.76, 124.04, 122.31, 120.25, 116.97, 116.56, 114.37, 112.40, 29.54, 29.36, 24.68, 24.41. HR MS (FAB$^+$): Calcd for $C_{38}H_{43}AuN_4$, 752.32; Found: 753.3281 $[M+H]^+$.

Synthesis of Au(^{Dipp}Im)(βCb). Au(^{Dipp}Im)(βCb) was synthesized following the protocols identical to the synthesis of Au(^{Dipp}Im)(Cz), except using 9*H*-pyrido[3,4-*b*]indole in place of carbazole. A white powder was obtained in an 87% yield. ^{1}H NMR (300 MHz, CD_2Cl_2) δ (ppm): 8.13 (d, *J* = 1.1 Hz, 1H), 8.02 (d, *J* = 5.2 Hz, 1H), 7.96 (dd, J = 7.8, 1.2 Hz, 1H), 7.76 (dd, *J* = 5.2, 1.1 Hz, 1H), 7.72–7.61 (m, 2H), 7.44 (d, *J* = 7.8 Hz, 4H), 7.37 (s, 2H), 7.16 (dd, J = 8.3, 7.0 Hz, 1H), 6.93 (dd, J = 7.9, 7.0 Hz, 1H), 6.77 (d, *J* = 8.3 Hz, 1H), 2.71 (hept, *J* = 7.0 Hz, 4H), 1.38 (*d*, J = 6.9 Hz, 12H), 1.28 (d, *J* = 6.9 Hz, 12H). ^{13}C{^{1}H} NMR (126 MHz, CD_2Cl_2) δ (ppm): 178.30, 150.74, 146.68,

146.33, 146.03, 139.57, 137.41, 137.39, 135.87, 135.85, 134.77, 131.31, 131.25, 128.43, 126.27, 124.85, 124.05, 123.86, 122.26, 121.24, 117.05, 115.31, 114.16, 29.53, 29.36, 24.78, 24.72, 24.43, 24.29. HR MS (FAB$^+$): Calcd for $C_{38}H_{43}AuN_4$, 752.32; Found: 753.3237 $[M+H]^+$.

Synthesis of Au(^{Dipp}Im)(γCb). Au(^{Dipp}Im)(γCb) was synthesized following the protocols identical to the synthesis of Au(^{Dipp}Im)(Cz), except using 5*H*-pyrido[4,3-*b*]indole in place of carbazole. A white powder was obtained in a 90% yield. ^{1}H NMR (300 MHz, CD_2Cl_2) δ (ppm): 9.04 (s, 1H), 8.04 (d, *J* = 5.8 Hz, 1H), 7.94 (d, *J* = 7.7 Hz, 1H), 7.65 (t, *J* = 7.8 Hz, 2H), 7.43 (d, *J* = 7.8 Hz, 4H), 7.37 (s, 2H), 7.16–7.05 (m, 1H), 7.03–6.92 (m, 1H), 6.75 (dt, *J* = 8.0, 0.9 Hz, 1H), 6.53 (d, *J* = 5.8 Hz, 1H), 2.70 (d, *J* = 6.9 Hz, 4H), 1.37 (d, *J* = 6.9 Hz, 12H), 1.28 (d, *J* = 6.9 Hz, 12H). ^{13}C{^{1}H} NMR (126 MHz, CD_2Cl_2) δ (ppm): 178.19, 153.27, 149.98, 146.70, 146.33, 142.98, 142.30, 134.76, 131.29, 125.06, 124.83, 124.43, 124.07, 122.82, 121.35, 120.01, 118.05, 114.48, 109.05, 29.52, 29.36, 24.76, 24.43, 24.29. HR MS (FAB$^+$): Calcd for $C_{38}H_{43}AuN_4$, 752.32; Found: 753.3231. Anal. Calcd for $C_{41}H_{42}AuN_5$: C, 60.63; H, 5.76; N, 7.44. Found: C, 60.93; H, 5.74; N, 7.37%.

Synthesis of Au(^{Dipp}Im)(δCb). Au(^{Dipp}Im)(δCb) was synthesized following the protocols identical to the synthesis of Au(^{Dipp}Im)(Cz), except using 5*H*-pyrido[3,2-*b*]indole in place of carbazole. A white powder was obtained in an 89% yield. ^{1}H NMR (300 MHz, CD_2Cl_2) δ (ppm): 8.18 (dd, *J* = 4.4, 1.7 Hz, 1H), 8.09 (dd, *J* = 7.7, 1.3 Hz, 1H), 7.71–7.60 (m, 2H), 7.43 (d, *J* = 7.8 Hz, 4H), 7.36 (s, 2H), 7.13 (dd, *J* = 8.3, 7.0 Hz, 1H), 7.02–6.87 (m, 3H), 6.74 (d, *J* = 8.2 Hz, 1H), 2.70 (hept, *J* = 7.0 Hz, 4H), 1.37 (d, *J* = 6.9 Hz, 12H), 1.28 (d, *J* = 6.9 Hz, 12H). ^{13}C{^{1}H} NMR (126 MHz, CD_2Cl_2) δ (ppm): 178.56, 150.67, 146.71, 143.10, 142.69, 139.05, 134.80, 131.23, 125.78, 124.81, 124.01, 123.21, 120.04, 119.91, 118.68, 117.11, 114.98, 29.51, 24.75, 24.43. HR MS (FAB$^+$): Calcd for $C_{38}H_{43}AuN_4$, 752.32; Found: 753.3228 $[M+H]^+$. Anal. Calcd for $C_{38}H_{43}AuN_4$: C, 60.63; H, 5.76; N, 7.44. Found: C, 60.79; H, 5.73; N, 7.37 %.

Synthesis of Au(^{Dipp}BZI)(CNCz). Au(^{Dipp}BZI)(CNCz) was synthesized following the protocols identical to the synthesis of Au(^{Dipp}Im)(CNCz), except using Au(^{Dipp}BZI)Cl in place of Au(^{Dipp}Im)Cl. A white powder was obtained in a 47% yield. ^{1}H NMR (300 MHz, CD_2Cl_2) δ (ppm): 8.25 (d, *J* = 0.9 Hz, 2H), 7.78 (t, *J* = 7.8 Hz, 2H), 7.56–7.51 (m, 6H), 7.39–7.35 (dd, *J* = 6.9, 1.5 Hz, 2H), 7.29–7.26 (d, *J* = 3.3 Hz, 2H), 6.69 (d, 2H), 1.23 (d, *J* = 6.9 Hz, 24H). ^{13}C{^{1}H} NMR (126 MHz, CD_2Cl_2) δ (ppm): 152.58, 147.66, 135.39, 131.98, 131.74, 128.46, 126.31, 125.49, 125.34, 125.25, 123.69, 121.59, 115.17, 112.67, 100.13, 29.65, 29.48, 24.92, 24.36, 24.16.

Synthesis of Au(^{Dipp}BZI)(Cz_3). Au(^{Dipp}BZI)(Cz_3) was synthesized following the protocols identical to the synthesis of Au(^{Dipp}Im)(Cz_3), except using Au(^{Dipp}BZI)Cl in place of Au(^{Dipp}Im)Cl. A brown powder was obtained in a 47% yield. ^{1}H NMR (300 MHz, CD_2Cl_2) δ (ppm): 8.14 (*d*, J = 0.6 Hz, 4H), 8.03 (d, *J* = 1.8 Hz, 2H), 7.71–7.73 (m, 3H), 7.51–7.57 (m, 6H), 7.20–7.38 (m, 15H), 6.94 (d, *J* =

8.1 Hz, 2H), 2.63 (m, 4H), 1.50 (d, J = 6.9 Hz, 24H). $^{13}C\{^{1}H\}$ NMR (126 MHz, CD_2Cl_2) δ (ppm): 185.10, 149.96, 147.68, 142.76, 135.51, 132.16, 131.65, 126.82, 126.42, 126.14, 126.09, 125.32, 124.73, 124.26, 123.28, 120.70, 120.48, 120.24, 120.17, 119.66, 119.29, 115.21, 112.61, 110.53, 110.28, 68.31, 54.43, 54.21, 53.99, 53.78, 53.57, 29.73, 26.13, 25.02, 24.39.

X-Ray Single Crystallography. Single crystal of Au(^{Dipp}Im)(Cz) was coated with Parabar 10312 (Hampton Research Inc.) to be mounted on a micro-loop. Data collections were carried out on a Bruker SMART APEX II and Rigaku Rapid Auto CCD diffractometer equipped with a monochromator in the Mo K_α (λ = 0.71073 Å) incident beam. The CCD data were integrated and scaled using the Bruker-SAINT or Rigaku Rapid Auto software package, and the structure was solved and refined using SHELXTL V 6.12, SHELXT-2018/2, and SHELXXL-2018/3.[4-5] All non-hydrogen atoms were refined with anisotropic thermal parameters. The crystallographic data for Au(^{Dipp}Im)(Cz) is listed in Table S1 and Tables S2–S3 list the selected bond distances and angles. Crystal data for Au(^{Dipp}Im)(Cz): $C_{39}H_{44}AuN_3$, Monoclinic, $P2_1/n$, Z = 4, a = 10.378(2), b = 14.847(3), c = 22.544(5) Å, β = 96.85(3)°, V = 3449.0(12) Å^3, μ = 4.295 mm^{-1}, ρ_{calcd} = 1.448 g/cm^3, R_1 = 0.0580, wR_2 = 0.1247 for 6226 unique reflections, 417 variables. CCDC-2463745 for Au(^{Dipp}Im)(Cz) contains the supplementary crystallographic data for this paper. These data can be obtained free of charge via www.ccdc.cam.ac.uk/data_request/cif (or from the Cambridge Crystallographic Data Centre, 12, Union Road, Cambridge CB2 1EZ, UK; fax: (+44) 1223-336-033; or deposit@ccdc.cam.ac.uk).

Steady-State UV–Vis Absorption Measurements. UV−Vis absorption spectra were collected on an Agilent, Cary 300 spectrophotometer at 298 K. Sample solutions were prepared prior to measurements to a concentration of 10 μM, unless otherwise stated. The solution was delivered into a quartz cell (Hellma, beam path length = 1.0 cm) for the measurement.

Steady-State Photoluminescence Measurements. Photoluminescence spectra were obtained at 298 K using a Photon Technology International, Quanta Master 400 scanning spectrofluorometer. Sample solutions were prepared prior to measurements to a concentration of 10 μM. All the solutions were deaerated by bubbling Ar for 20 min prior to the measurements. A quartz cell (Hellma, beam path length = 1.0 cm) was used for solution samples. The excitation wavelength was 300 nm.

Determination of Photoluminescence Lifetime. Photoluminescence decay traces were acquired on the basis of time-correlated single-photon counting (TCSPC) techniques, using a PicoQuant, FluoTime 200 instrument after 377 nm pulsed laser excitation (pulse duration = 10 ns, unless otherwise stated). A picosecond pulsed diode laser that produced 377 nm (PicoQuant, LDH375) was driven by a PDL800-D driver (PicoQuant). Transient photon signals were collected

at the peak emission wavelength for Au(^{Dipp}Im)(Cz) through an automated motorized monochromator. The photon acquisition was terminated when the accumulated photon count reached 10^4. Photoluminescence decay traces were fitted to exponential decay models embedded in the OriginLab, OriginPro 2023b software to yield a weighted average photoluminescence lifetime (τ_{obs}).

Determination of Φ_{PL}. The photoluminescence quantum yield (Φ_{PL}) was determined for 10 μM Au(^{Dipp}Im)(Cz) through the equation $\Phi_{PL} = \Phi_{PL,ref} \times (I / I_{ref}) \times (A_{ref} / A) \times (n / n_{ref})^2$, where A, I, and n are the absorbance at the excitation wavelength, the integrated photoluminescence intensity, and the refractive index of the solvent, respectively. 9,10-Diphenylanthracene ($\Phi_{PL,ref}$ = 1.00, toluene; λ_{ex} = 373 nm) was used as the reference.[6] Photoluminescence spectra were collected at 298 K in the emission range 320–580 nm and were integrated using the OriginLab, OriginPro 2023b software. The radiative rate constant (k_r) and the non-radiative rate constant (k_{nr}) were determined using the following relationship:

$$k_r = \frac{\Phi_{\mathrm{PL}}}{\tau_{obs}} \quad (1)$$

$$k_{nr} = \frac{1 - \Phi_{\mathrm{PL}}}{\tau_{obs}} \quad (2)$$

Photoluminescence Quenching Experiments. Photoluminescence spectra were obtained at 298 K using a Photon Technology International, Quanta Master 400 scanning spectrofluorometer. Stock solutions of Au(^{Dipp}Im)(Cz) (100 μM) and **1a** (1 mM, 10 mM, and 100 mM) were prepared in DMSO. 3.0 mL of Au(^{Dipp}Im)(Cz) solution was added into a quartz cell (Hellma, beam path length = 1.0 cm). Photoluminescence spectra of Au(^{Dipp}Im)(Cz) were recorded under photoexcitation at a wavelength of 300 nm, with increasing the concentration of **1a**. The final concentration of **1a** was 1.5 mM.

Electrochemical Characterization. Cyclic and differential pulse voltammetry experiments were conducted using a CH Instruments, CHI630 B potentiostat with a three-electrode cell assembly. A Pt wire and a glassy carbon were used as the counter and working electrodes, respectively. An Ag/$AgNO_3$ couple was used as the pseudo-reference electrode. Measurements were carried out in Ar-saturated CH_3CN (3.0 mL) with 0.10 M tetrabutylammonium hexafluorophosphate ($TBAPF_6$) as the supporting electrolyte at scan rates of 100 mV s^{-1} (cyclic voltammetry) and 4.0 mV s^{-1} (differential pulse voltammetry). A ferrocenium/ferrocene redox couple was employed as the external reference. No reduction process was observed within the solvent window. Thus, the reduction potential (E_{red}) value was estimated using the following relationship:

$$E_{red} = E_{\mathrm{ox}} - \Delta E_g \quad (3)$$

In this equation, ΔE_g is the optical bandgap energy determined from the onset wavelength of UV−Vis absorption spectrum (3.26 eV). The excited-state oxidation (E_{ox}*) and reduction (E_{red}*) potentials were calculated based on the following equations:

$$E^*_{\mathrm{ox}} = E_{\mathrm{ox}} - \Delta E_{T_1} (4)$$

$$E^*_{\mathrm{red}} = E_{\mathrm{red}} + \Delta E_{T_1} (5)$$

In equations 4 and 5, ΔE_{T1} was the triplet state energy determined from the peak wavelength of the phosphorescence spectrum (2.87 eV). The E_{ox} of styrene was reported to be 1.42 V vs standard calomel electrode (SCE; CH_3CN).[7]

Determination of $\Phi_{[2+2]}$. The quantum yield for [2+2] cycloaddition of **1a** ($\Phi_{[2+2]}$) was determined using the standard ferrioxalate actinometry.[8] A 6.0 mM ferrioxalate in a glass vial (1.5 cm diameter) was photoilluminated with the 365 nm light for 30 s. The same volume of 1 wt % 1,10-phenanthroline in sodium acetate buffer was added and stored in the dark for 1 h. The absorbance changes at 510 nm (ΔAbs(510 nm)) was measured by UV−Vis spectrophotometer. Inserting the value to the following equation returned the photon flux (I_0) of 3.90 × 10^{-8} einstein s^{-1}:

Photon flux (I_0, einstein s^{-1}) = (ΔAbs(510 nm) × V) / (Φ × 11000 M^{-1} cm^{-1} × l × Δt) (6)

where, V, Φ, l , and Δt are the volume (L), the quantum yield (1.1) of the ferrioxalate actinometer, the beam pass length (cm), and the photoirradiation time (s), respectively. Finally, the $\Phi_{[2+2]}$was calculated from the following equation:

$$\Phi_{[2+2]} = \frac{[\mathbf{2a}]}{I_0 \times \Delta t} (7)$$

where, [**2a**] is the molar concentration of the [2+2] cycloaddition product (**2a**) quantified with ^{1}H NMR spectroscopy, and Δt (s) is the photoirradiation time.

Quantum Chemical Calculations. Geometry optimization was performed using the PBE0 hybrid exchange-correlation functional with the density-dependent dispersion correction (dDsC) at the TZ2P basis set level, employing the *J*-fitting scheme for Coulomb integration (PBE0-dDsC/TZ2P-J), as implemented in the AMS program package. Time-dependent density functional theory (TD−DFT) calculations were carried out for the optimized geometries, with scalar relativistic effects included via the zero-order regular approximation (ZORA) Hamiltonian.

Nanosecond Transient Absorption Measurements. An Ar-saturated DMSO containing 100 μM Au(^{Dipp}Im)(Cz) in a 1 cm × 1 cm quartz cell was excited by a Nd:YAG laser (Continuum, SLII-10; 355 nm and 5 mJ $pulse^{-1}$) in the absence and presence of 1.5 mM 1a. Time courses of the transient absorption signals were measured using a photomultiplier tube (visible region) and an InGaAs-PIN photodiode (Hamamatsu 2949) (NIR region). The output from the photomultiplier tube and photodiode was recorded with a digitized oscilloscope (Tektronix, TDS3032; 300 MHz). All

experiments were performed at 298 K.

Determination of Φ_{ISC}. The quantum yields for intersystem crossing (Φ_{ISC}) were determined based on actinometry, employing $[Ru(bpy)_3]Cl_2$ in H_2O as a reference system (Φ_{ISC} = 100%)[9] and naphthalene as a triplet acceptor[10]. Nanosecond transition absorption spectral measurements were performed for solutions of Au(^{Dipp}Im)(Cz) containing 50 mM naphthalene in various solvents (DMSO, DMF, THF, EtOAc, CH_3CN). In these experiments, differences in solvent refractive indices were neglected. The solutions of the Au(^{Dipp}Im)(Cz):naphthalene complexes and the reference $[Ru(bpy)_3]Cl_2$ solution in H_2O without additives were adjusted to an identical optical density of 0.85 at the excitation wavelength of 355 nm. Under these conditions, excitation with the transient absorption set-up ensures that comparable amounts of photosensitizers are initially populated in their singlet excited states. Time-resolved absorption experiments were then used to extract maximum or minimum Δ*OD* values immediately after the excitation pulses. These values allowed the calculation of the concentrations of the reference or acceptor molecules in their respective triplet excited states.

$$c_{3naph} = \frac{\Delta OD_{max}}{\varepsilon_{3naph} \times d} \quad (8)$$

$$c_{3Ru} = \frac{\Delta OD_{min}}{\Delta\varepsilon_{455nm} \times d} \quad (9)$$

The known change in molar extinction coefficient ($\Delta\varepsilon_r$) for the ground-state MLCT bleach of excited $[Ru(bpy)_3]Cl_2$ at 455 nm ($\Delta\varepsilon_{455nm}$ = −10100 M^{-1} cm^{-1})[11] and the molar extinction coefficient of triplet naphthalene at 420 nm (ε_{3naph} = 13200 M^{-1} cm^{-1})[12] were used in these calculations, with *d* denoting the path length of the optical cuvette (*d* = 1.0 cm). Given that the intersystem crossing of $[Ru(bpy)_3]^{2+}$ is quantitative, the Φ_{ISC} values of the complexes could be estimated according to the equation:

$$\phi_{isc} = \frac{c_{3naph}}{c_{3Ru}} \quad (10)$$

Femtosecond Transient Absorption Measurements. Femtosecond transient absorption spectroscopic experiments were performed at Korea Basic Science Institute (KBSI), Seoul Center. An Ar-saturated DMSO containing 10 mM Au(^{Dipp}Im)(Cz) in a 1 cm × 1 mm quartz cell was excited by a Yb:KGW femtosecond amplifier system (Light Conversion, 200 kHz, 20 W). The sample was excited with a femtosecond pulsed laser at 375 nm (7 μW), and the transient absorption spectra were recorded using a broadband white-light probe in the 500–750 nm range. The data were collected with a time resolution sufficient to capture ultrafast processes over a 0–6000 ps window. To analyze ultrafast dynamics, we performed global analyses over a 540–640 nm probe window

in Surface Xplorer (Ultrafast Systems). The dataset was converted to the Ultrafast Systems binary format (.ufs) using a Python script. A time-independent background was removed by subtracting the average of 10 points at negative delay, after which dispersion and time-zero corrections were applied. Singular value decomposition (SVD) guided the selection of 15 components; we retained three signal-bearing kinetic components and 12 dummy (noise) components. Global fitting was first performed on an early window (≤500 ps) and a late window (0.5–6 ns) to refine initial parameters, followed by a final fit over the full temporal range. The final model used a biexponential decay with a constant offset (A_∞), and the fit converged.

^{1}H NMR Titration Experiments. ^{1}H NMR (400 MHz) titration experiments were conducted for 1.0 mM Au(^{Dipp}Im)(Cz) in CD_2Cl_2, with the addition of DMSO-d_6. Stock solutions of Au(^{Dipp}Im)(Cz) (50 mM in CD_2Cl_2) and DMSO-d_6 (50 mM in CD_2Cl_2) were prepared prior to the experiments. The method of continuous variations was applied to determine the binding stoichiometry between Au(^{Dipp}Im)(Cz) and DMSO. The total volume and the total molar concentration were kept to 3.0 mL and 50 mM, respectively.

Photocatalytic [2+2] Cycloaddition Reactions. An oven-dried reusable tube equipped with a magnetic stir bar was charged with 5 mol% of Au(^{Dipp}Im)(Cz), the alkene substrate **1** (1.0 equiv), and DMSO (0.5 M) under an Ar atmosphere. The tube was then placed under 365 nm LED irradiation (18 W) at room temperature. The reaction progress was monitored by thin-layer chromatography or gas chromatography (GC). Upon completion, the reaction mixture was diluted with ethyl acetate and washed with brine. The layers were separated, and the organic layer was dried with $MgSO_4$, filtered, and concentrated in vacuo to afford a crude residue that was purified by silica gel column chromatography to give the corresponding [2+2] cycloaddition product, **2**.

Analytic Data for [2+2] Cycloaddition Reaction Products

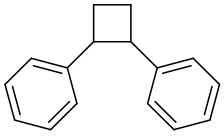

1,2-Diphenylcyclobutane (diastereoisomers, *trans*:*cis* = 3.4:1), **2a**[13]: colourless oil; ^{1}H NMR (400 MHz, $CDCl_3$) δ 7.30 (dd, *J* = 7.1, 6.9 Hz, 4H, *trans*), 7.24 (d, *J* = 6.9 Hz, 4H, *trans*), 7.19 (t, *J* = 7.1 Hz, 2H, *trans*), 7.09 (dd, *J* = 7.3, 7.3 Hz, 4H, *cis*), 7.01 (t, *J* = 7.3 Hz, 2H, *cis*), 6.94 (d, *J* = 7.3 Hz, 4H, *cis*), 4.06 – 3.99 (m, 2H, *cis*), 3.64 – 3.52 (m, 2H, *trans*), 2.52 – 2.43 (m, 4H, *cis*), 2.40 – 2.26 (m, 2H, *trans*), 2.21 – 2.08 (m, 2H, *trans*); ^{13}C{^{1}H} NMR (101 MHz, $CDCl_3$) δ 144.8, 141.7, 128.5, 128.1, 127.8, 126.8, 126.3, 125.7, 48.1, 45.5, 26.1, 24.4; FT–IR (neat): ν = 3026, 2972, 2941 cm^{-1}; R_f = 0.85 (hexane:EtOAc = 6:1, v/v).

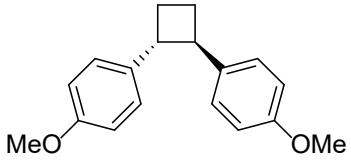

(1*R*,2*R*)-1,2-Bis(4-methoxyphenyl)cyclobutane, ***trans*-2b**[14]: colorless oil; ^{1}H NMR (400 MHz, $CDCl_3$) δ 7.15 (d, *J* = 8.6 Hz, 4H), 6.84 (d, *J* = 8.6 Hz, 4H), 3.79 (s, 6H), 3.50 – 3.39 (m, 2H), 2.32 – 2.22 (m, 2H), 2.13 – 2.01 (m, 2H); ^{13}C{^{1}H} NMR (101 MHz, $CDCl_3$) δ 158.2, 137.1, 127.8, 113.9, 55.5, 48.0, 26.2; FT–IR (neat): ν = 2955, 2937, 2908, 1246 cm^{-1}; R_f = 0.52 (hexane:EtOAc = 6:1, v/v).

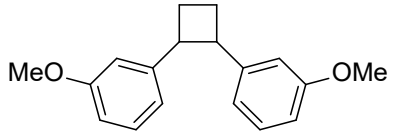

1,2-Bis(3-methoxyphenyl)cyclobutane (diastereoisomers, *trans*:*cis* = 8.3:1), **2c**[15]: yellow oil; ^{1}H NMR (400 MHz, $CDCl_3$) δ 7.21 (dd, *J* = 8.2, 7.6 Hz, 2H, *trans*), 7.03 (dd, *J* = 8.0, 7.4 Hz, 2H, *cis*), 6.84 (d, *J* = 7.6 Hz, 2H, *trans*), 6.79 (s, 2H, *trans*), 6.74 (d, *J* = 8.2 Hz, 2H, *trans*), 6.59 (d, *J* = 7.4 Hz, 2H, *cis*), 6.59 (d, *J* = 8.0 Hz, 2H, *cis*), 6.48 (s, 2H, *cis*), 4.04 – 3.93 (m, 2H, *cis*), 3.79 (s, 6H, *trans*), 3.63 (s, 6H, *cis*), 3.60 – 3.49 (m, 2H, *trans*), 2.49 – 2.39 (m, 4H, *cis*), 2.38 – 2.25 (m, 2H, *trans*), 2.21 – 2.03 (m, 2H, *trans*); ^{13}C{^{1}H} NMR (101 MHz, $CDCl_3$) δ 159.9, 159.4, 146.5, 143.4, 129.5, 128.8, 120.7, 119.3, 113.8, 112.7, 111.6, 111.5, 55.4, 55.3, 48.1, 45.5, 26.0, 24.6; FT–IR (neat): ν = 2969, 2941, 2865, 1260 cm^{-1}; R_f = 0.71 (hexane:EtOAc = 4:1, v/v).

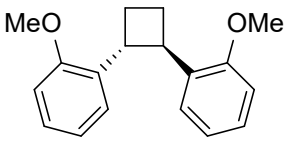

(1*R*,2*R*)-1,2-Bis(2-methoxyphenyl)cyclobutane, ***trans*-2d**: colourless oil; ^{1}H NMR (400 MHz, $CDCl_3$) δ 7.30 (dd, *J* = 7.5, 1.7 Hz, 2H), 7.15 (ddd, *J* = 8.1, 7.4, 1.7 Hz, 2H), 6.90 (ddd, *J* = 7.5, 7.4, 1.2 Hz, 2H), 6.81 (dd, *J* = 8.1, 1.2 Hz, 2H), 4.01 – 3.90 (m, 2H), 3.77 (s, 6H), 2.39 – 2.32 (m, 2H), 1.98 – 1.92 (m, 2H); ^{13}C{^{1}H} NMR (101 MHz, $CDCl_3$) δ 157.5, 133.2, 127.4, 127.0, 120.6, 110.2, 55.4, 40.5, 27.3; FT–IR (neat): ν = 2969, 2938, 2866, 1244 cm^{-1}; HRMS *m*/*z* (EI) calc. for $C_{18}H_{20}O_2$ [M$^+$] 268.1463, found 268.1460; R_f = 0.58 (hexane:EtOAc = 6:1, v/v).

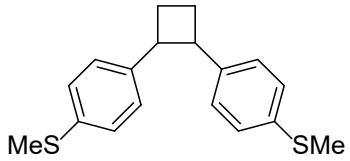

1,2-Bis(4-(methylthio)phenyl)cyclobutane (diastereoisomers, *trans*:*cis* = 5.3:1), **2e**: yellowish oil; ^{1}H NMR (400 MHz, $CDCl_3$) δ 7.20 (d, *J* = 8.4 Hz, 4H, *trans*), 7.14 (d, *J* = 8.4 Hz, 4H, *trans*), 7.02 (d, *J* = 8.3 Hz, 4H, *cis*), 6.86 (d, *J* = 8.3 Hz, 4H, *cis*), 3.99 – 3.92 (m, 2H, *cis*), 3.53 – 3.37 (m, 2H, *trans*), 2.46 (s, 6H, *trans*), 2.40 (s, 6H, *cis*), 2.38 – 2.33 (m, 2H, *cis*), 2.33 – 2.25 (m, 2H, *trans*), 2.14 – 2.06 (m, 2H, *trans*), 2.05 – 1.99 (m, 2H, *cis*); ^{13}C{^{1}H} NMR (101 MHz, $CDCl_3$) δ 141.8, 138.8, 135.9, 135.2, 128.7, 127.4, 127.3, 126.7, 48.0, 45.0, 26.0, 24.6, 16.5, 16.4; FT–IR (neat): ν = 2971, 2940, 2919, 1494 cm^{-1}; HRMS *m*/*z* (EI) calc. for $C_{18}H_{20}S_2$ [M$^+$] 300.1006, found 300.1003; R_f = 0.77 (hexane:EtOAc = 4:1, v/v).

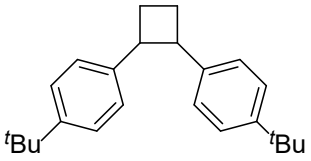

1,2-Bis(4-(*tert*-butyl)phenyl)cyclobutane (diastereoisomers, *trans*:*cis* = 2.9:1), **2f**[16]: colourless solid; ^{1}H NMR (400 MHz, $CDCl_3$) δ 7.31 (d, *J* = 8.0 Hz, 4H, *trans*), 7.18 (d, *J* = 8.0 Hz, 4H, *trans*), 7.07 (d, *J* = 8.0 Hz, 4H, *cis*), 6.82 (d, *J* = 8.0 Hz, 4H, *cis*), 3.99 – 3.91 (m, 2H, *cis*), 3.62 – 3.49 (m, 2H, *trans*), 2.47 – 2.39 (m, 4H, *cis*), 2.36 – 2.25 (m, 2H, *trans*), 2.16 – 2.04 (m, 2H, *trans*), 1.31 (s, 18H, *trans*), 1.20 (s, 18H, *cis*); ^{13}C{^{1}H} NMR (101 MHz, $CDCl_3$) δ 149.0, 148.4, 141.9, 138.7, 127.8, 126.5, 125.3, 124.5, 47.5, 45.2, 31.6, 31.5, 26.3, 24.2; FT–IR (neat): ν = 2961, 2904, 2867 cm^{-1}; R_f = 0.88 (hexane:EtOAc = 6:1, v/v).

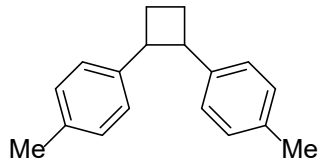

1,2-Di-*p*-tolylcyclobutane (diastereoisomers, *trans*:*cis* = 2.9:1), **2g**[16]: colourless solid; ^{1}H NMR (400 MHz, $CDCl_3$) δ 7.13 (d, *J* = 8.4 Hz, 4H, *trans*), 7.10 (d, *J* = 8.4 Hz, 4H, *trans*), 6.91 (d, *J* = 7.9 Hz, 4H, *cis*), 6.84 (d, *J* = 7.9 Hz, 4H, *cis*), 3.98 – 3.92 (m, 2H, *cis*), 3.56 – 3.46 (m, 2H, *trans*), 2.47 – 2.35 (m, 4H, *cis*), 2.32 (s, 6H, *trans*), 2.31 – 2.26 (m, 2H, *trans*), 2.22 (s, 6H, *cis*), 2.14 – 2.04 (m, 2H, *trans*); ^{13}C{^{1}H} NMR (101 MHz, $CDCl_3$) δ 141.9, 138.9, 135.7, 135.0, 129.2, 128.6, 128.0, 126.7, 47.9, 45.1, 26.2, 24.8, 21.24, 21.18; FT–IR (neat): ν = 2970, 2940, 2921 cm^{-1}; R_f = 0.30 (hexane:EtOAc = 6:1, v/v).

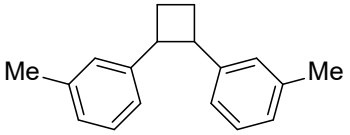

1,2-Di-*m*-tolylcyclobutane (diastereoisomers, *trans*:*cis* = 3.0:1), **2h**[16]: colourless oil; ^{1}H NMR (400 MHz, $CDCl_3$) δ 7.18 (dd, *J* = 7.5 Hz, 2H, *trans*), 7.07 – 6.97 (m, 6H, *trans*), 6.96 (d, *J* = 7.5 Hz, 2H, *cis*), 6.82 (d, *J* = 7.5 Hz, 2H, *cis*), 6.76 – 6.72 (m, 4H, *cis*), 3.98 – 3.93 (m, 2H, *cis*), 3.60 – 3.49 (m, 2H, *trans*), 2.46 – 2.40 (m, 4H, *cis*), 2.33 (s, 6H, *trans*), 2.33 – 2.25 (m, 2H, *trans*), 2.18

(s, 6H, *cis*), 2.13 – 2.07 (m, 2H, *trans*); $^{13}C\{^{1}H\}$ NMR (101 MHz, $CDCl_3$) δ 144.9, 141.7, 138.0, 137.2, 129.1, 128.4, 127.7, 127.6, 127.0, 126.44, 126.39, 125.2, 123.9, 47.8, 45.4, 26.3, 24.5, 21.7, 21.6; FT–IR (neat): ν = 2970, 2940, 2923 cm^{-1}; R_f = 0.36 (hexane:EtOAc = 6:1, v/v).

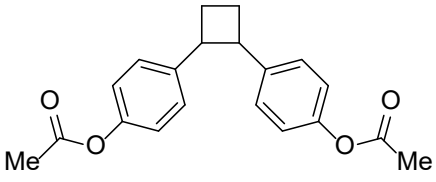

Cyclobutane-1,2-diylbis(4,1-phenylene) diacetate (diastereoisomers, *trans*:*cis* = 2.9:1), **2i**: yellowish oil; ^{1}H NMR (400 MHz, $CDCl_3$) δ 7.22 (d, J = 8.6 Hz, 4H, *trans*), 7.00 (d, J = 8.6 Hz, 4H, *trans*), 6.92 (d, J = 8.6 Hz, 4H, *cis*), 6.83 (d, J = 8.6 Hz, 4H, *cis*), 4.03 – 3.97 (m, 2H, *cis*), 3.63 – 3.43 (m, 2H, *trans*), 2.50 – 2.44 (m, 2H, *cis*), 2.43 – 2.37 (m, 2H, *cis*), 2.34 – 2.30 (m, 2H, *trans*), 2.29 (s, 6H, *trans*), 2.23 (s, 6H, *cis*), 2.14 – 2.06 (m, 2H, *trans*); $^{13}C\{^{1}H\}$ NMR (101 MHz, $CDCl_3$) δ 169.9, 169.7, 149.2, 148.8, 142.1, 139.0, 129.0, 127.8, 121.5, 120.9, 47.6, 44.9, 26.2, 24.5, 21.34, 21.32; FT–IR (neat): ν = 2970, 2943, 1755 cm^{-1}; HRMS *m*/*z* (EI) calc. for $C_{20}H_{20}O_4$ [M^+] 324.1362, found 324.1365; R_f = 0.43 (hexane:EtOAc = 4:1, v/v).

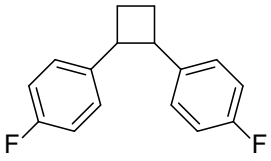

1,2-Bis(4-fluorophenyl)cyclobutane (diastereoisomers, *trans*:*cis* = 2.9:1), **2j**[16]: colourless oil; ^{1}H NMR (400 MHz, $CDCl_3$) δ 7.16 (dd, J = 8.6 Hz, $J_{H\text{-}F}$ = 5.5 Hz, 4H, *trans*), 6.97 (dd, $J_{H\text{-}F}$ = 8.7 Hz, J = 8.6 Hz, 4H, *trans*), 6.86 (dd, J = 8.7 Hz, $J_{H\text{-}F}$ = 5.6 Hz, 4H, *cis*), 6.78 (dd, $J_{H\text{-}F}$ = 8.8 Hz, J = 8.7 Hz, 4H, *cis*), 4.02 – 3.91 (m, 2H, *cis*), 3.53 – 3.38 (m, 2H, *trans*), 2.51 – 2.35 (m, 4H, *cis*), 2.34 – 2.25 (m, 2H, *trans*), 2.14 – 2.03 (m, 2H, *trans*); $^{13}C\{^{1}H\}$ NMR (101 MHz, $CDCl_3$) δ 162.0 (d, $J_{C\text{-}F}$ = 231.3 Hz), 161.6 (d, $J_{C\text{-}F}$ = 243.8 Hz), 140.1 (d, $J_{C\text{-}F}$ = 3.0 Hz), 129.4 (d, $J_{C\text{-}F}$ = 7.8 Hz), 128.2 (d, $J_{C\text{-}F}$ = 7.6 Hz), 115.3 (d, $J_{C\text{-}F}$ = 21.1 Hz), 114.7 (d, $J_{C\text{-}F}$ = 21.1 Hz), 47.9, 44.7, 26.2, 24.4; ^{19}F NMR (376 MHz, $CDCl_3$) δ –117.1, –117.6; FT–IR (neat): ν = 2970, 2943, 2867 cm^{-1}; R_f = 0.73 (hexane:EtOAc = 6:1, v/v).

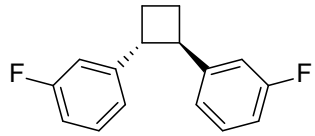

(1*R*,2*R*)-1,2-Bis(3-fluorophenyl)cyclobutane, ***trans*-2k**: colorless oil; ^{1}H NMR (400 MHz, $CDCl_3$) δ 7.25 (ddd, J = 8.2, 7.7, 6.0 Hz, 2H), 6.98 (d, J = 7.7 Hz, 2H), 6.94 – 6.86 (m, 4H), 3.61 – 3.46 (m, 2H), 2.38 – 2.29 (m, 2H), 2.20 – 2.04 (m, 2H); $^{13}C\{^{1}H\}$ NMR (101 MHz, $CDCl_3$) δ 163.2 (d, $J_{C\text{-}F}$ = 246.0 Hz), 147.0 (d, $J_{C\text{-}F}$ = 6.9 Hz), 130.0 (d, $J_{C\text{-}F}$ = 8.4 Hz), 122.5 (d, $J_{C\text{-}F}$ = 2.7 Hz), 113.6 (d, $J_{C\text{-}F}$ = 21.0 Hz), 113.3 (d, $J_{C\text{-}F}$ = 21.1 Hz), 47.8 (d, $J_{C\text{-}F}$ = 1.8 Hz), 26.0; ^{19}F NMR (376 MHz, $CDCl_3$) δ –113.4; FT–IR (neat): ν = 2970, 2945, 2868 cm^{-1}; HRMS m/z (EI) calc. for $C_{16}H_{14}F_2$ [M^+] 244.1064, found 244.1061; R_f = 0.73 (hexane:EtOAc = 4:1, v/v).

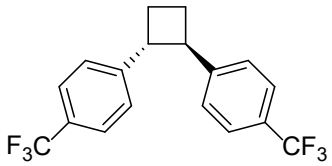

(1*R*,2*R*)-1,2-bis(4-(trifluoromethyl)phenyl)cyclobutane, ***trans*-2l**[16]: colorless oil; ^{1}H NMR (400 MHz, $CDCl_3$) δ 7.56 (d, J = 8.1 Hz, 4H), 7.31 (d, J = 8.0 Hz, 4H), 3.69 – 3.58 (m, 2H), 2.47 – 2.31 (m, 2H), 2.28 – 2.12 (m, 2H); ^{13}C{^{1}H} NMR (101 MHz, $CDCl_3$) δ 148.0, 129.0 (q, $J_{C\text{-}F}$ = 31.8 Hz), 127.1, 125.6 (q, $J_{C\text{-}F}$ = 3.6 Hz), 124.5 (q, $J_{C\text{-}F}$ = 272.7 Hz), 47.8, 26.0; ^{19}F NMR (376 MHz, $CDCl_3$) δ –62.4; FT–IR (neat): ν = 2970, 2947 cm^{-1}; R_f = 0.86 (hexane:EtOAc = 4:1, v/v).

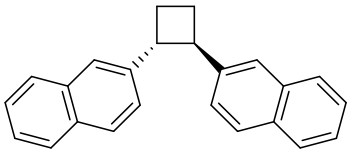

(1*R*,2*R*)-1,2-di(naphthalen-2-yl)cyclobutane, ***trans*-2m**[17]: white solid; ^{1}H NMR (400 MHz, $CDCl_3$) δ 7.84 – 7.75 (m, 6H), 7.70 (s, 2H), 7.48 – 7.39 (m, 6H), 3.92 – 3.79 (m, 2H), 2.51 – 2.42 (m, 2H), 2.38 – 2.29 (m, 2H); ^{13}C{^{1}H} NMR (101 MHz, $CDCl_3$) δ 142.2, 133.7, 132.4, 128.2, 127.9, 127.8, 126.2, 125.7, 125.5, 124.9, 48.4, 26.1; FT–IR (neat): ν = 3051, 2970, 2939 cm^{-1}; R_f = 0.86 (hexane:EtOAc = 4:1, v/v).

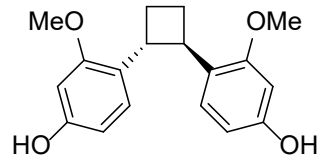

4,4'-((1*R*,2*R*)-cyclobutane-1,2-diyl)bis(3-methoxyphenol), ***trans*-2n**: orange oil; ^{1}H NMR (400 MHz, $CDCl_3$) δ 6.85 (d, J = 8.0 Hz, 2H), 6.74 (dd, J = 8.0, 2.0 Hz, 2H), 6.71 (d, J = 2.0 Hz, 2H), 5.49 (bs, 2H), 3.85 (s, 6H), 3.45 – 3.36 (m, 2H), 2.35 – 2.21 (m, 2H), 2.14 – 1.98 (m, 2H); ^{13}C{^{1}H} NMR (101 MHz, $CDCl_3$) δ 146.5, 144.1, 136.9, 119.4, 114.3, 109.4, 56.1, 48.6, 26.0; FT–IR (neat): ν = 3437, 2939, 2847, 1264 cm^{-1}; HRMS *m*/*z* (EI) calc. for $C_{18}H_{20}O_4$ [M$^+$] 300.1362, found 300.1363; R_f = 0.17 (hexane:EtOAc = 4:1, v/v).

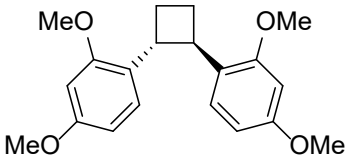

(1*R*,2*R*)-1,2-bis(2,4-dimethoxyphenyl)cyclobutane, ***trans*-2o**[18]: yellow oil; ^{1}H NMR (400 MHz, $CDCl_3$) δ 6.81 (d, J = 8.2 Hz, 2H), 6.78 (dd, J = 8.2, 1.9 Hz, 2H), 6.73 (d, J = 1.9 Hz, 2H), 3.86 (s, 6H), 3.84 (s, 6H), 3.49 – 3.39 (m, 2H), 2.34 – 2.20 (m, 2H), 2.15 – 2.04 (m, 2H); ^{13}C{^{1}H} NMR (101 MHz, $CDCl_3$) δ 149.0, 147.6, 137.6, 118.6, 111.3, 110.1, 56.1, 56.0, 48.4, 26.0; FT–IR (neat): ν = 2935, 2857, 2834, 1260 cm^{-1}; R_f = 0.23 (hexane:EtOAc = 4:1, v/v).

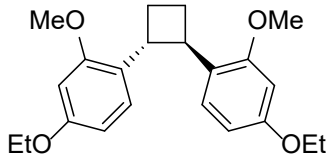

(1*R*,2*R*)-1,2-bis(4-ethoxy-2-methoxyphenyl)cyclobutane, ***trans*-2p**: yellow oil; ^{1}H NMR (400 MHz, $CDCl_3$) δ 6.81 (d, J = 8.1 Hz, 2H), 6.77 – 6.73 (m, 4H), 4.07 (q, J = 7.0 Hz, 4H), 3.83 (s, 6H), 3.50 – 3.35 (m, 2H), 2.31 – 2.22 (m, 2H), 2.18 – 2.07 (m, 2H), 1.44 (t, J = 7.0 Hz, 6H); ^{13}C{^{1}H} NMR (101 MHz, $CDCl_3$) δ 149.4, 146.9, 137.7, 118.7, 113.1, 110.6, 64.7, 56.1, 48.4, 25.9, 15.1; FT–IR (neat): ν = 3004, 2971, 1261 cm^{-1}; HRMS *m*/*z* (EI) calc. for $C_{22}H_{28}O_4$ [M$^+$] 356.1988, found 355.0675; R_f = 0.43 (hexane:EtOAc = 4:1, v/v).

Table S1 | Crystallographic data for Au(^{Dipp}Im)(Cz) grown in DMF

	Au(^{Dipp}Im)(Cz)
Empirical formula	$C_{39}H_{44}AuN_3$
Formula weight	751.74
Temperature (K)	173(2)
Wavelength (Å)	0.71073
Crystal system/space group	Monoclinic, $P2_1/n$
Unit cell dimensions	
a (Å)	10.378(2)
b (Å)	14.847(3)
c (Å)	22.544(5)
α (°)	90
β (°)	96.85(3)
γ (°)	90
Volume (Å^3)	3449.0(12)
Z	4
Calculated density (g cm^{-3})	1.448
Absorption coefficient (mm^{-1})	4.295
Reflections collected	26054
Independent reflections [*R*(int)]	6226 [0.1037]
Refinement method	Full-matrix least-squares on F^2
Data/restraints/parameters	6226/12/417
Goodness-of-fit on F^2	1.077
Final *R* indices [$I > 2\text{sigma}(I)$]	R_1 = 0.0580, wR_2 = 0.1247
R indices (all data)	R_1 = 0.0885, wR_2 = 0.1390

Table S2 | Selected bond distances (Å) of the Au(^{Dipp}Im)(Cz) crystal structure grown in DMF

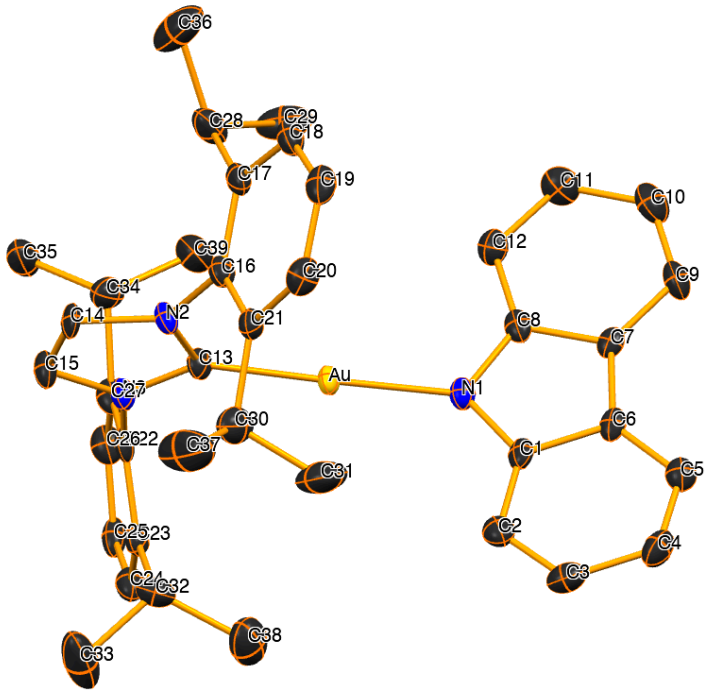

bond distances (Å)					
Au(1)	C(13)	1.970(8)	C(16)	C(21)	1.385(13)
Au(1)	N(1)	2.006(7)	C(16)	C(17)	1.390(13)
N(1)	C(8)	1.384(11)	C(17)	C(18)	1.407(13)
N(1)	C(1)	1.395(12)	C(17)	C(28)	1.510(15)
N(2)	C(13)	1.353(11)	C(18)	C(19)	1.346(15)
N(2)	C(14)	1.398(10)	C(19)	C(20)	1.375(14)
N(2)	C(16)	1.473(10)	C(20)	C(21)	1.420(12)
N(3)	C(13)	1.358(10)	C(21)	C(30)	1.512(15)
N(3)	C(15)	1.367(10)	C(22)	C(27)	1.380(14)
N(3)	C(22)	1.463(11)	C(22)	C(23)	1.398(13)
C(1)	C(2)	1.394(14)	C(23)	C(24)	1.414(13)
C(1)	C(6)	1.420(12)	C(23)	C(32)	1.496(14)
C(2)	C(3)	1.365(14)	C(24)	C(25)	1.377(14)
C(3)	C(4)	1.408(14)	C(25)	C(26)	1.361(14)

C(4)	C(5)	1.357(15)	C(26)	C(27)	1.390(12)
C(5)	C(6)	1.410(13)	C(27)	C(34)	1.521(14)
C(6)	C(7)	1.424(13)	C(28)	C(29)	1.490(15)
C(7)	C(9)	1.390(13)	C(28)	C(36)	1.539(18)
C(7)	C(8)	1.413(12)	C(30)	C(31)	1.483(16)
C(8)	C(12)	1.392(14)	C(30)	C(37)	1.514(18)
C(9)	C(10)	1.366(16)	C(32)	C(33)	1.514(15)
C(10)	C(11)	1.389(15)	C(32)	C(38)	1.538(16)
C(11)	C(12)	1.389(14)	C(34)	C(35)	1.498(14)
C(14)	C(15)	1.337(13)	C(34)	C(39)	1.539(15)

X-ray crystal structure of Au(^{Dipp}Im)(Cz) (dark-gray, C; blue, N; yellow, Au) with thermal ellipsoids drawn at the 30% probability level. Hydrogen atoms have been omitted for clarity. Only the major occupancy component of the disordered metal center is shown.

Table S3 | Selected bond angles (°) of the Au(^{Dipp}Im)(Cz) crystal structure grown in DMF

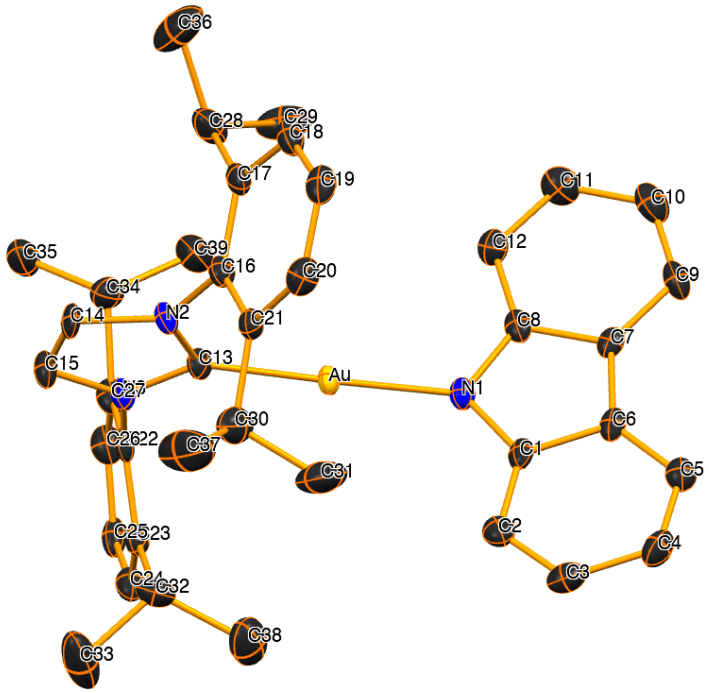

bond angles (°)					
C(13)	Au(1)	N(1)	176.3(3)	C(21) C(16) N(2)	116.7(8)
C(8)	N(1)	C(1)	105.4(7)	C(17) C(16) N(2)	117.4(9)
C(8)	N(1)	Au(1)	125.2(6)	C(16) C(17) C(18)	114.8(10)
C(1)	N(1)	Au(1)	125.0(6)	C(16) C(17) C(28)	123.8(9)
C(13)	N(2)	C(14)	111.7(7)	C(18) C(17) C(28)	121.3(9)
C(13)	N(2)	C(16)	125.2(7)	C(19) C(18) C(17)	122.5(10)
C(14)	N(2)	C(16)	123.0(7)	C(18) C(19) C(20)	120.9(9)
C(13)	N(3)	C(15)	112.3(7)	C(19) C(20) C(21)	120.8(9)
C(13)	N(3)	C(22)	123.2(7)	C(16) C(21) C(20)	115.2(9)
C(15)	N(3)	C(22)	124.5(7)	C(16) C(21) C(30)	125.0(8)
C(2)	C(1)	N(1)	128.4(8)	C(20) C(21) C(30)	119.8(9)
C(2)	C(1)	C(6)	120.6(9)	C(27) C(22) C(23)	123.2(8)
N(1)	C(1)	C(6)	110.9(8)	C(27) C(22) N(3)	117.6(8)
C(3)	C(2)	C(1)	119.1(9)	C(23) C(22) N(3)	119.2(8)

C(2)	C(3)	C(4)	121.1(10)	C(22)	C(23)	C(24)	115.3(9)
C(5)	C(4)	C(3)	120.6(10)	C(22)	C(23)	C(32)	123.6(8)
C(4)	C(5)	C(6)	120.0(9)	C(24)	C(23)	C(32)	121.0(9)
C(5)	C(6)	C(1)	118.6(9)	C(25)	C(24)	C(23)	122.2(10)
C(5)	C(6)	C(7)	135.3(8)	C(26)	C(25)	C(24)	119.6(9)
C(1)	C(6)	C(7)	106.0(8)	C(25)	C(26)	C(27)	121.2(10)
C(9)	C(7)	C(8)	119.6(9)	C(22)	C(27)	C(26)	118.2(10)
C(9)	C(7)	C(6)	134.1(9)	C(22)	C(27)	C(34)	122.2(8)
C(8)	C(7)	C(6)	106.2(8)	C(26)	C(27)	C(34)	119.5(10)
N(1)	C(8)	C(12)	128.4(8)	C(29)	C(28)	C(17)	111.3(10)
N(1)	C(8)	C(7)	111.4(9)	C(29)	C(28)	C(36)	109.7(10)
C(12)	C(8)	C(7)	120.1(8)	C(17)	C(28)	C(36)	112.3(10)
C(10)	C(9)	C(7)	120.4(9)	C(31)	C(30)	C(21)	111.3(10)
C(9)	C(10)	C(11)	120.0(10)	C(31)	C(30)	C(37)	109.3(12)
C(12)	C(11)	C(10)	121.4(11)	C(21)	C(30)	C(37)	113.6(10)
C(11)	C(12)	C(8)	118.6(9)	C(23)	C(32)	C(33)	112.0(9)
N(2)	C(13)	N(3)	103.0(7)	C(23)	C(32)	C(38)	110.7(9)
N(2)	C(13)	Au(1)	127.0(6)	C(33)	C(32)	C(38)	110.3(11)
N(3)	C(13)	Au(1)	130.0(6)	C(35)	C(34)	C(27)	112.8(8)
C(15)	C(14)	N(2)	105.8(8)	C(35)	C(34)	C(39)	111.4(10)
C(14)	C(15)	N(3)	107.2(8)	C(27)	C(34)	C(39)	110.1(9)
C(21)	C(16)	C(17)	125.9(8)				

X-ray crystal structure of Au(^{Dipp}Im)(Cz) (dark-gray, C; blue, N; yellow, Au) with thermal ellipsoids drawn at the 30% probability level. Hydrogen atoms have been omitted for clarity. Only the major occupancy component of the disordered metal center is shown.

Table S4 | A summary of τ_{obs}, Φ_{PL}, k_r, and k_{nr} values of Au(^{Dipp}Im)(Cz) (10 μM) determined in various solvents after Ar saturation

solvent	τ_{obs} (μs)[a]	Φ_{PL}[b]	k_r (10^4 s^{-1})[c]	k_{nr} (10^4 s^{-1})[d]
EtOAc	0.30	0.009	3.1	330
CH_2Cl_2	0.30	0.012	4.1	330
THF	0.40	0.004	1.1	250
PhMe	0.70	0.032	4.6	140
CH_3CN	1.9	0.003	0.16	53
DMF	5.4	0.034	0.63	18
DMSO	12.1	0.019	0.16	8.1

[a]Photoluminescence lifetime determined through biexponential fits of the photoluminescence decay traces monitored after pulsed laser photoexcitation at 377 nm. [b]Photolumunescence quantum yields determined relatively using the 9,10-diphenylanthracene standard. [c]Radiative rate constant, $k_r = \Phi_{PL} / \tau_{obs}$. [d]Nonradiative rate constant, $k_{nr} = (1 - \Phi_{PL}) / \tau_{obs}$.

Table S5 | A summary of simulated electronic transitions, isosurface plots of participating molecular orbitals, and SOC matrix elements for the X-ray single crystal geometry of Au(^{Dipp}Im)(Cz) (i.e., C–Au–N bent angle = 176 degree)

state	energy (eV)	participating MO (expansion coefficient)	oscillator strength	transition rate (10^6 s^{-1})	transition character
S_1	2.79	189 → 190 (0.96)	0.0055	0.19	LLCT
S_2	3.10	189 → 191 (0.98)	0.0023	0.095	LLCT
S_3	3.24	189 → 192 (0.98)	0.0089	0.42	LLCT
S_4	3.36	189 → 193 (0.54) 189 → 194 (0.44)	0.014	0.69	LLCT
S_5	3.38	189 → 194 (0.50) 189 → 193 (0.39)	0.024	1.2	LLCT
S_6	3.38	188 → 190 (0.89)	0.021	1.4	LLCT

state	energy (eV)	participating MO (expansion coefficient)	transition character
T_1	2.73	189 → 190 (0.96)	LLCT
T_2	3.10	189 → 191 (0.99)	LLCT
T_3	3.24	189 → 192 (0.98)	LLCT
T_4	3.31	189 → 196 (0.93)	LLCT
T_5	3.36	189 → 193 (0.64) 189 → 194 (0.33)	LLCT
T_6	3.38	189 → 194 (0.60) 189 → 193 (0.32)	LE(Cz)

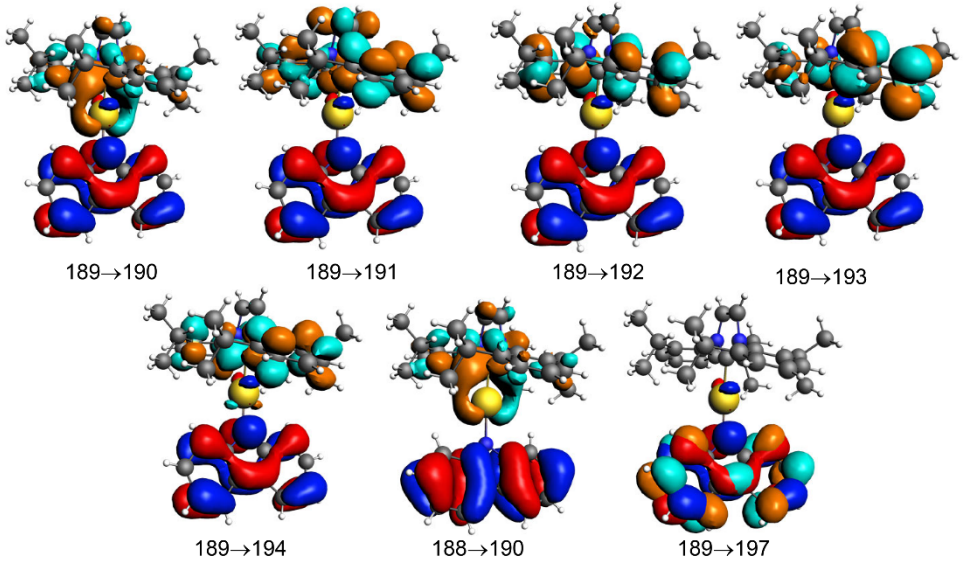

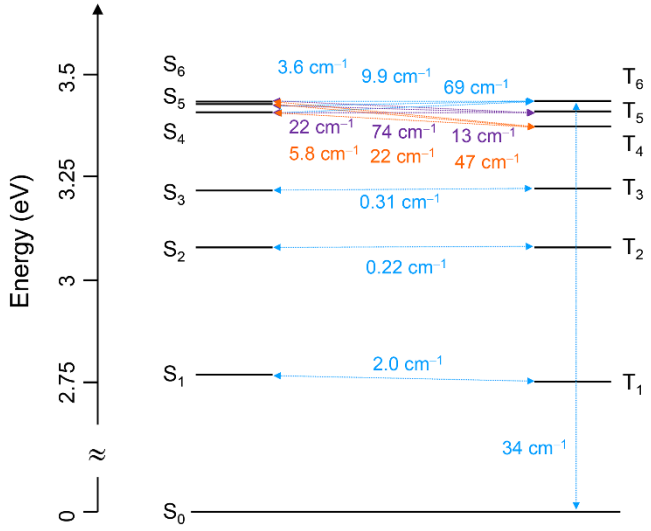

Table S6 | A summary of simulated electronic transitions and isosurface plots of participating molecular orbitals for the optimized S_0 geometry of Au(^{Dipp}Im)(Cz) (i.e., C–Au–N bent angle = 180 degree)

state	energy (eV)	participating MO (expansion coefficient)	oscillator strength	transition rate (10^6 s^{-1})	transition character
S_1	2.73	189 → 190 (0.96)	0.062	2.0	LLCT
S_2	3.00	189 → 191 (0.98)	0.0065	0.25	LLCT
S_3	3.04	189 → 192 (0.98)	0.0016	0.066	LLCT
S_4	3.16	189 → 193 (0.98)	0.011	0.49	LLCT
S_5	3.26	189 → 194 (0.96)	0.0058	0.27	LLCT
S_6	3.34	188 → 190 (0.98)	0.00051	0.25	LLCT

state	energy (eV)	participating MO (expansion coefficient)	transition character
T_1	2.72	189 → 190 (0.97)	LLCT
T_2	3.00	189 → 191 (0.98)	LLCT
T_3	3.04	189 → 192 (0.98)	LLCT
T_4	3.16	189 → 193 (0.98)	LLCT
T_5	3.25	189 → 194 (0.93)	LLCT
T_6	3.30	189 → 197 (0.94)	LE(Cz)

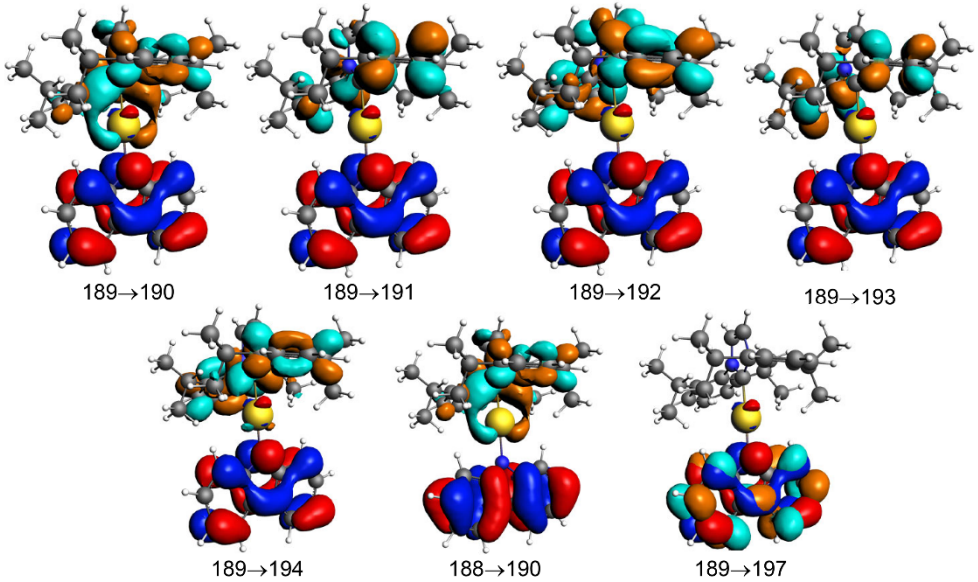

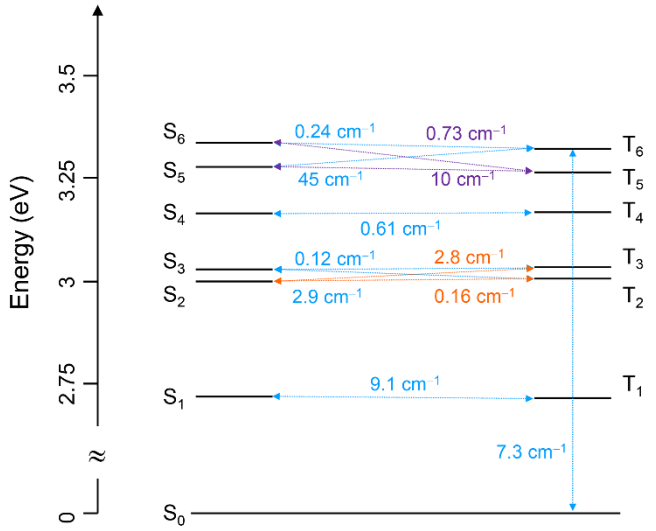

Table S7 | A summary of simulated electronic transitions, isosurface plots of participating molecular orbitals, and SOC matrix elements for Au(^{Dipp}Im)(Cz) with an C–Au–N bent angle of 170 degree

state	energy (eV)	participating MO (expansion coefficient)	oscillator strength	transition rate (10^6 s^{-1})	transition character
S_1	2.78	189 → 190 (0.95)	0.0026	0.089	LLCT
S_2	3.10	189 → 191 (0.97)	0.0021	0.082	LLCT
S_3	3.23	189 → 192 (0.95)	0.0073	0.32	LLCT
S_4	3.36	189 → 194 (0.50) 189 → 193 (0.47)	0.010	0.51	LLCT
S_5	3.37	189 → 194 (0.47) 189 → 193 (0.48)	0.038	1.9	LLCT
S_6	3.39	188 → 190 (0.96)	0.011	0.59	LLCT

state	energy (eV)	participating MO (expansion coefficient)	transition character
T_1	2.78	189 → 190 (0.95)	LLCT
T_2	3.10	189 → 191 (0.97)	LLCT
T_3	3.23	189 → 192 (0.95)	LLCT
T_4	3.30	189 → 196 (0.93)	LE(Cz)
T_5	3.35	189 → 193 (0.58)	LLCT
T_6	3.37	189 → 194 (0.55)	LLCT

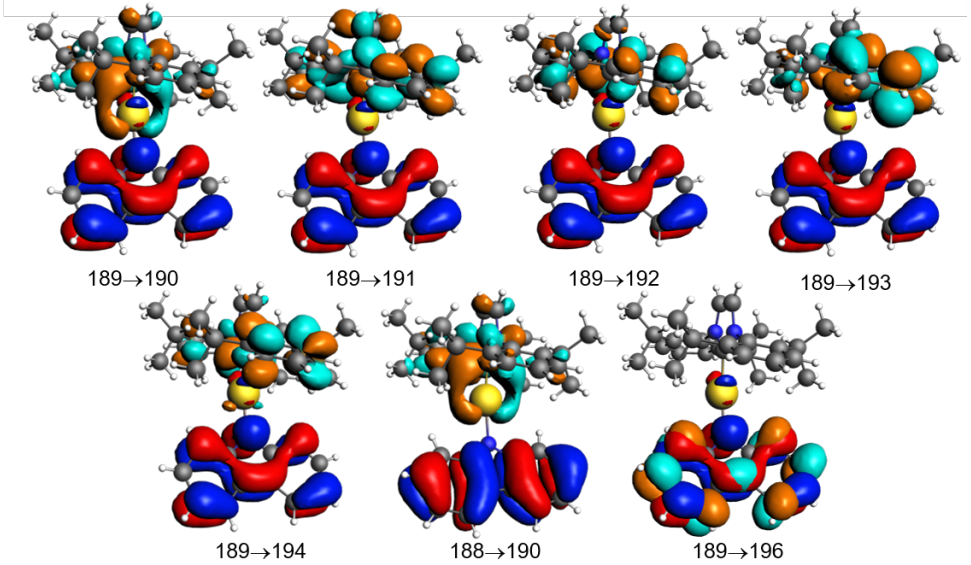

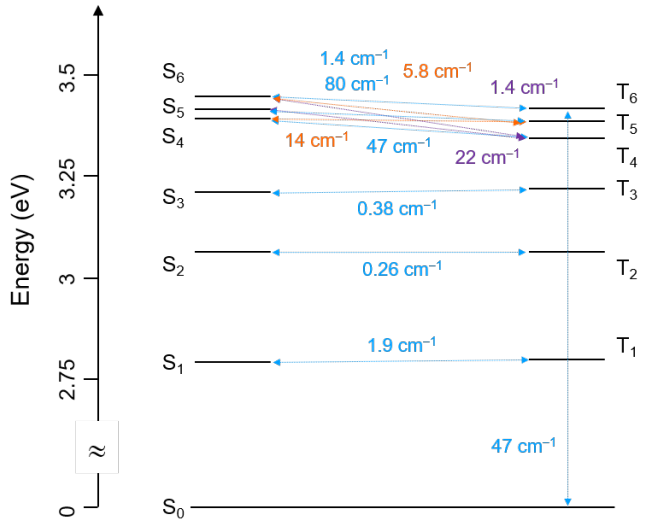

Table S8 | A summary of simulated electronic transitions, isosurface plots of participating molecular orbitals, and SOC matrix elements for Au(^{Dipp}Im)(Cz) with an C–Au–N bent angle of 172 degree

state	energy (eV)	participating MO (expansion coefficient)	oscillator strength	transition rate (10^6 s^{-1})	transition character
S_1	2.78	189 → 190 (0.95)	0.0033	0.11	LLCT
S_2	3.10	189 → 191 (0.98)	0.0021	0.091	LLCT
S_3	3.23	189 → 192 (0.96)	0.0075	0.34	LLCT
S_4	3.36	189 → 194 (0.44) 189 → 193 (0.49)	0.011	0.52	LLCT
S_5	3.38	189 → 194 (0.49) 189 → 193 (0.46)	0.034	0.16	LLCT
S_6	3.39	188 → 190 (0.95)	0.013	0.66	LLCT

state	energy (eV)	participating MO (expansion coefficient)	transition character
T_1	2.78	189 → 190 (0.95)	LLCT
T_2	3.10	189 → 191 (0.98)	LLCT
T_3	3.23	189 → 192 (0.96)	LLCT
T_4	3.30	189 → 196 (0.93)	LE(Cz)
T_5	3.36	189 → 193 (0.60)	LLCT
T_6	3.38	189 → 194 (0.57)	LLCT

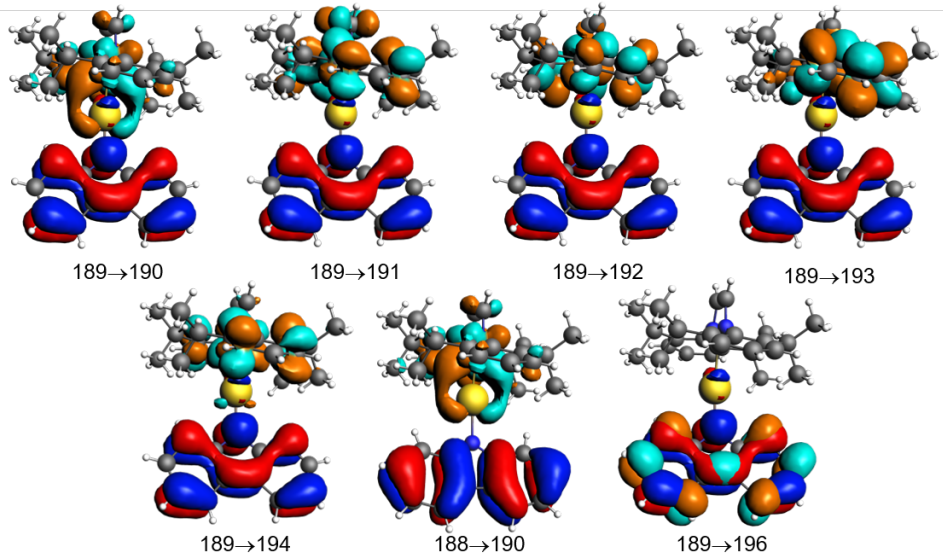

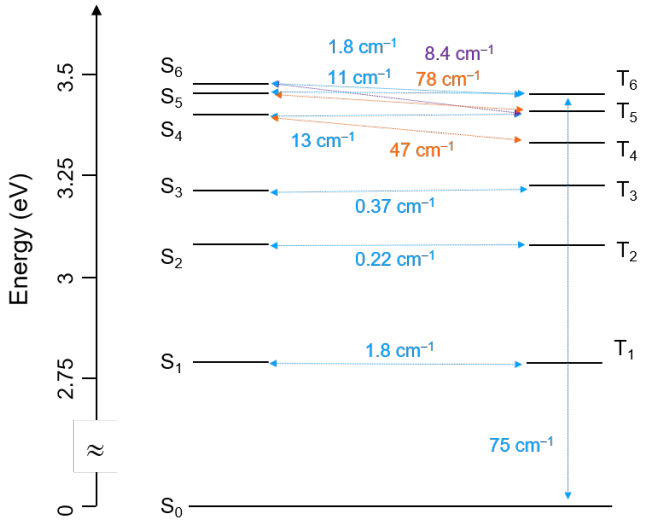

Table S9 | A summary of simulated electronic transitions, isosurface plots of participating molecular orbitals, and SOC matrix elements for Au(^{Dipp}Im)(Cz) with an C–Au–N bent angle of 174 degree

state	energy (eV)	participating MO (expansion coefficient)	oscillator strength	transition rate (10^6 s^{-1})	transition character
S_1	2.78	189 → 190 (0.95)	0.0033	0.11	LLCT
S_2	3.10	189 → 191 (0.98)	0.0021	0.091	LLCT
S_3	3.23	189 → 192 (0.96)	0.0075	0.34	LLCT
S_4	3.36	189 → 194 (0.44) 189 → 193 (0.49)	0.011	0.52	LLCT
S_5	3.38	189 → 194 (0.49) 189 → 193 (0.46)	0.034	0.16	LLCT
S_6	3.39	188 → 190 (0.95)	0.013	0.66	LLCT

state	energy (eV)	participating MO (expansion coefficient)	transition character
T_1	2.78	189 → 190 (0.95)	LLCT
T_2	3.10	189 → 191 (0.98)	LLCT
T_3	3.23	189 → 192 (0.96)	LLCT
T_4	3.30	189 → 196 (0.93)	LE(Cz)
T_5	3.36	189 → 193 (0.60)	LLCT
T_6	3.38	189 → 194 (0.57)	LLCT

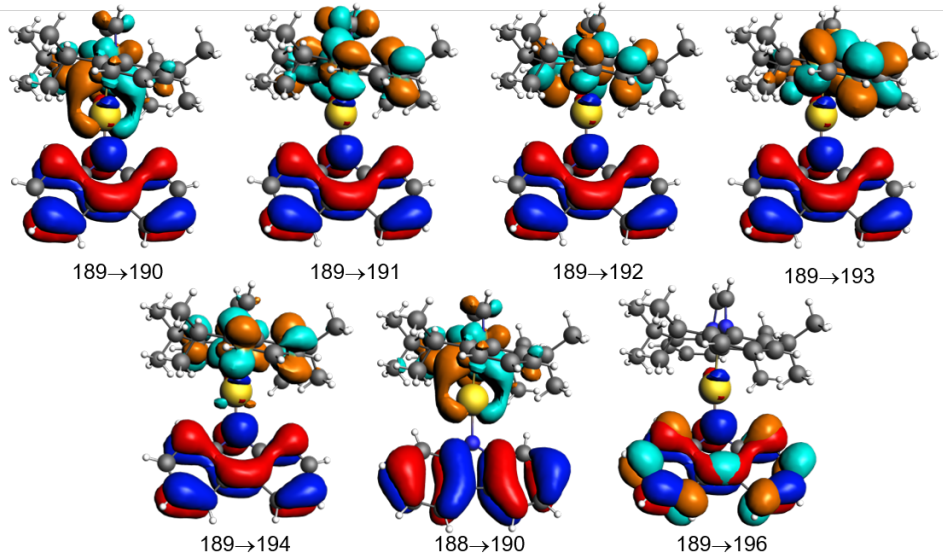

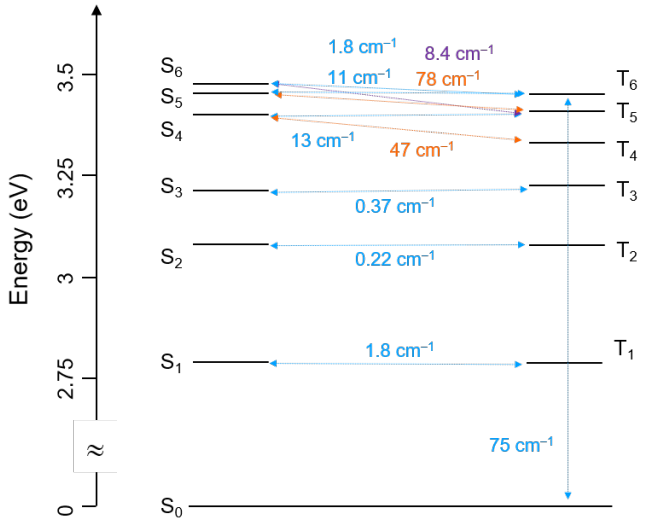

Table S10 | A summary of simulated electronic transitions, isosurface plots of participating molecular orbitals, and SOC matrix elements for Au(^{Dipp}Im)(Cz) with an C–Au–N bent angle of 178 degree

state	energy (eV)	participating MO (expansion coefficient)	oscillator strength	transition rate (10^6 s^{-1})	transition character
S_1	2.80	189 → 190 (0.96)	0.0067	0.23	LLCT
S_2	3.11	189 → 191 (0.99)	0.0024	0.10	LLCT
S_3	3.24	189 → 192 (0.98)	0.0097	0.44	LLCT
S_4	3.36	189 → 194 (0.42) 189 → 193 (0.55)	0.015	0.77	LLCT
S_5	3.38	189 → 194 (0.45) 189 → 193 (0.33)	0.018	0.91	LLCT
S_6	3.38	188 → 190 (0.78)	0.028	1.4	LLCT

state	energy (eV)	participating MO (expansion coefficient)	transition character
T_1	2.80	189 → 190 (0.96)	LLCT
T_2	3.11	189 → 191 (0.99)	LLCT
T_3	3.24	189 → 192 (0.98)	LLCT
T_4	3.31	189 → 196 (0.93)	LE(Cz)
T_5	3.36	189 → 193 (0.66)	LLCT
T_6	3.38	189 → 194 (0.58)	LLCT

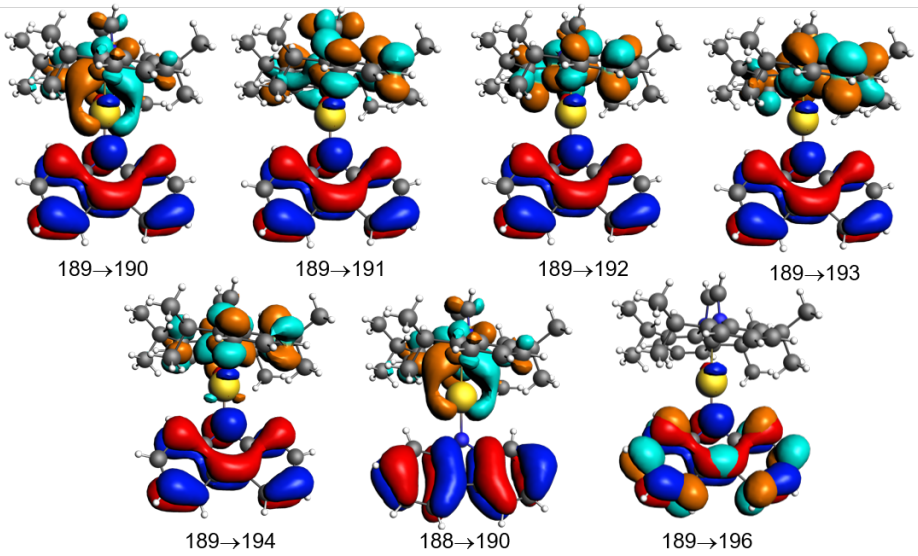

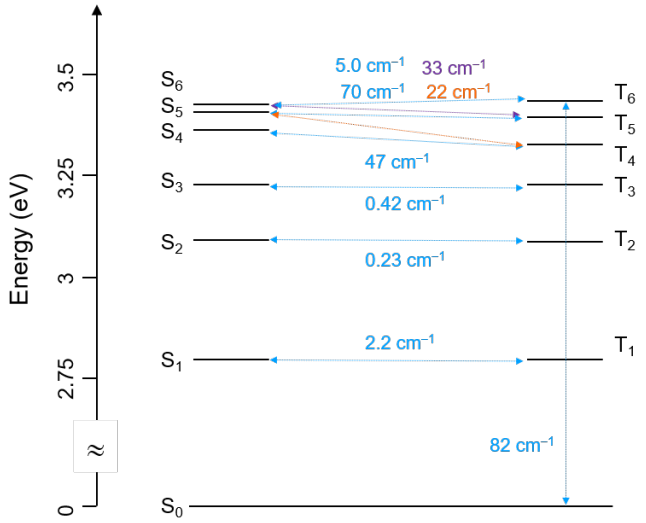

Table S11 | Optimization of reaction conditions[a,b]

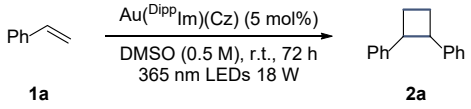

1a **2a**

entries	variations	yield
1	**-**	**68%**
2	w/o Au catalyst	n.d.
3	w/o light irradiation	n.d.
4	NMP	61%
5	DMF	61%
6	cyclohexane	23%
7	CH_3CN	37%
8	PhMe	17%
9	THF	57%
10	CH_2Cl_2	13%
11	EtOAc	53%
12	Au catalyst (1 mol%)	15%
13	Au catalyst (3 mol%)	55%
14	Au catalyst (10 mol%)	70%
15	DMSO (0.05 M)	32%
16	DMSO (0.1 M)	46%
17	DMSO (0.2 M)	49%
18	DMSO (1.0 M)	68%

[a]Reaction conditions: **1a** (0.1 mmol). [b]Yields were determined by ^{1}H NMR spectroscopy using dibromomethane as an internal standard.

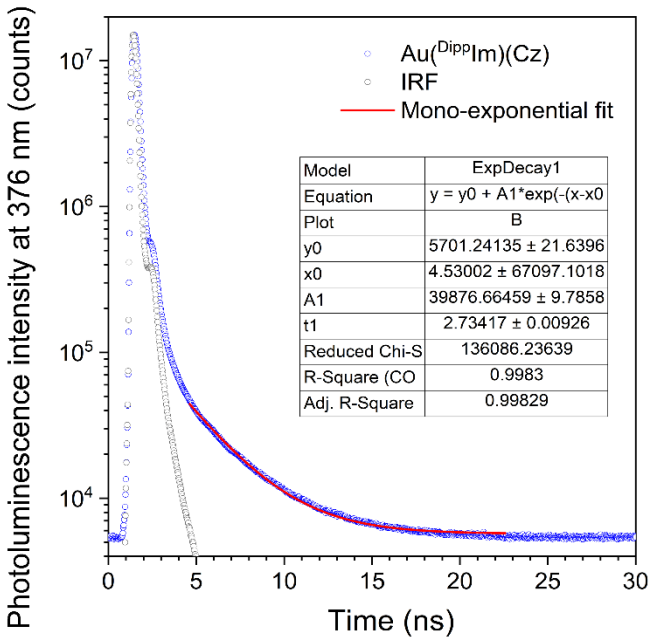

Fig. S1 | Photoluminescence decay traces of an Ar-saturated DMSO containing 100 μM Au(^{Dipp}Im)(Cz) recorded at a wavelength of 376 nm after picosecond pulsed laser photoexcitation at 377 nm (pulse duration = 25 ps). The grey symbols are the instrumental response function. The red curve is a monoexponential fit.

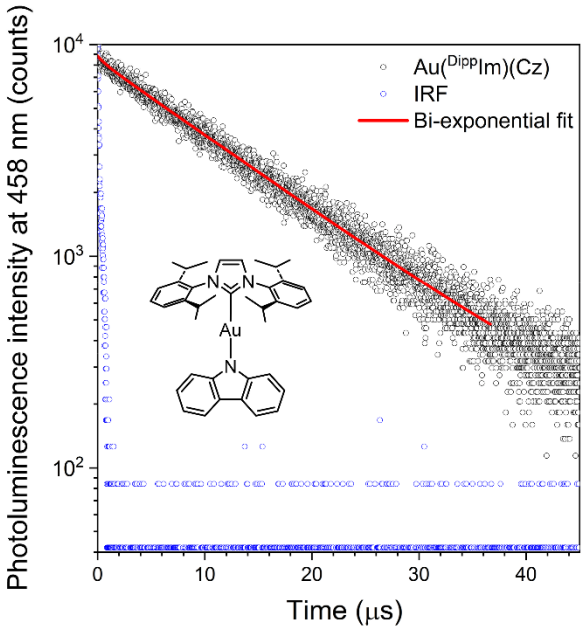

Equation	y0	x0	A1	t1 (ns)	A2	t2 (ns)	*R*-Square (COD)
y = y0 + A1*exp(-(x-x0)/t1) + A2*exp(-(x-x0)/t2)	0.00712	1168.20989	0.0086	788.60845	0.76127	12100.45135	0.98701

Fig. S2 | Nonlinear least-squares fit of photoluminescence decay traces of an Ar-saturated DMSO containing 10 μM Au(^{Dipp}Im)(Cz) recorded at a wavelength of 458 nm after nanosecond pulsed laser photoexcitation at 377 nm (pulse duration = 10 ns). The red curve is a nonlinear least-squares fit to a biexponential decay model. The bottom table lists the fit parameters.

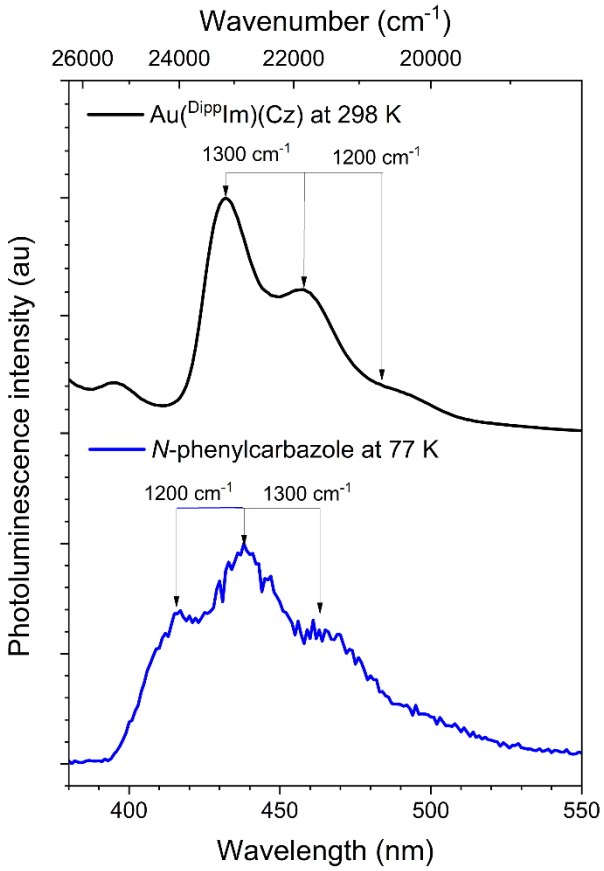

Fig. S3 | Vibronic progression analyses for the phosphorescence spectrum of 10 μM Au(^{Dipp}Im)(Cz) (298 K) and 10 μM *N*-phenylcarbazole (77 K) in Ar-saturated DMSO.

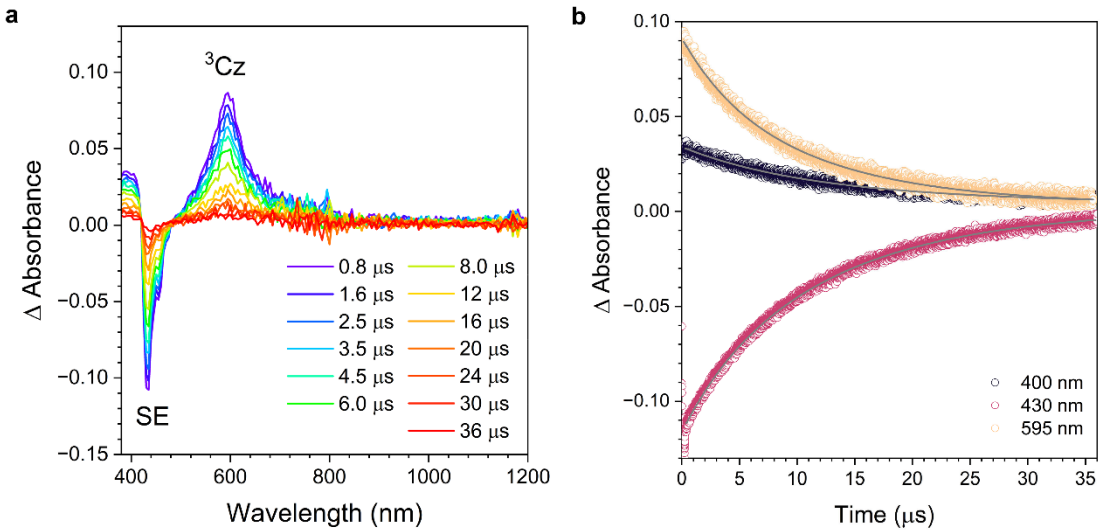

Fig. S4 | a, Selected transient absorption spectra of an Ar-saturated DMSO containing 100 μM Au(^{Dipp}Im)(Cz) recorded after nanosecond pulsed laser excitation at 355 nm. This graph is a copy of Fig. 1d of the main text. **b**, Time traces of the photoinduced signals recorded at 400, 430, and 595 nm. The grey curves are biexponential fits.

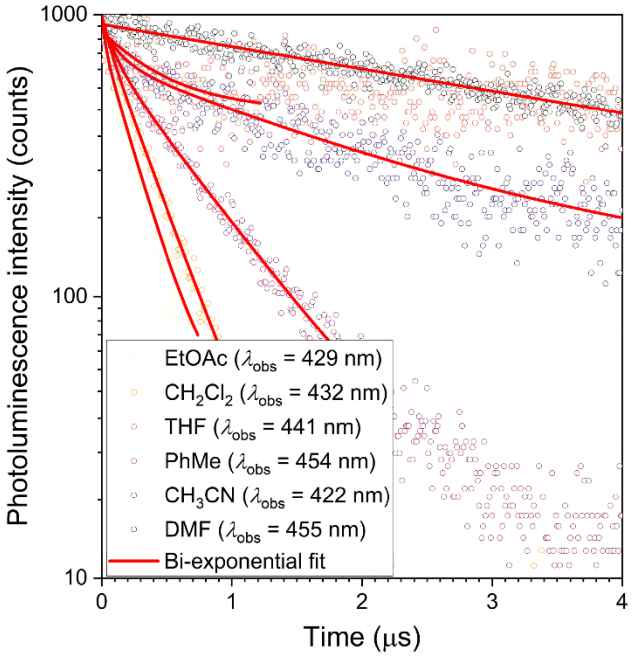

solvent	y0	x0	A1	t1 (ns)	A2	t2 (ns)	R-Square (COD)
EtOAc	0.0293	5.11303	0.15907	27.38992	0.75895	257.16343	0.98285
CH_2Cl_2	0.00258	16.41907	0.11652	75.9887	0.80749	349.71798	0.99687
THF	0.45629	-13.01847	0.29549	464.36146	0.13387	464.2929	0.48376
CH_3CN	0.11066	25.31303	0.18586	141.4343	0.56642	2024.54324	0.90639
DMF	0.01492	27.82358	0.45255	5379.50781	0.45227	5381.387	0.9836

y = y0 + A1*exp(-(x-x0)/t1) + A2*exp(-(x-x0)/t2)

Fig. S5 | Photoluminescence decay traces of Ar-saturated solutions containing 10 μM Au(^{Dipp}Im)(Cz) recorded at indicated wavelengths after nanosecond pulsed laser photoexcitation at 377 nm (pulse duration = 10 ns). Red curves are nonlinear least-squares fits to a biexponential model. The bottom table lists the fit parameters of the traces.

a

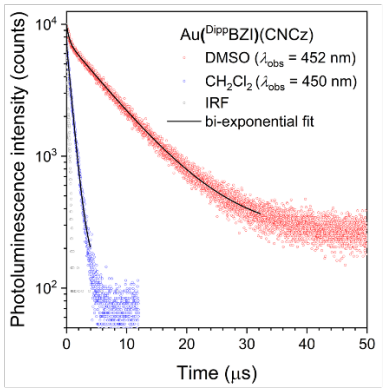

	y0	x0	A1	t1 (μs)	A2	t2 (μs)	R-Square
DMSO	258	67	2872	0.4	7269	7.7	0.99
CH_2Cl_2	133	91	129	0.03	6188	0.9	0.99

b

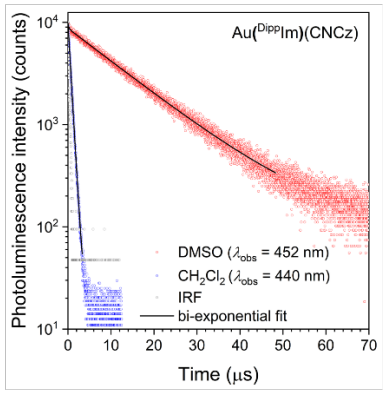

	y0	x0	A1	t1 (μs)	A2	t2 (μs)	R-Square
DMSO	105	1066	4.3	0.2	7977	13.3	0.99
CH_2Cl_2	14	70	128	0.09	8558	0.6	0.99

c

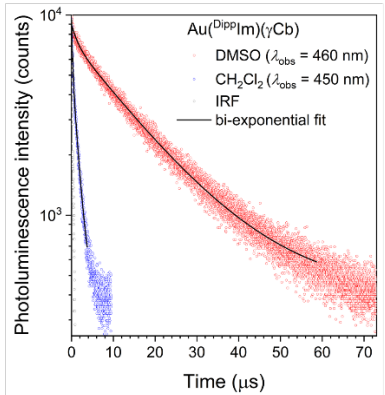

	y0	x0	A1	t1 (μs)	A2	t2 (μs)	R-Square
DMSO	411	209	1364	1.4	6864	15.9	0.99
CH_2Cl_2	345	8.2	3769	0.2	5542	1.4	0.99

d

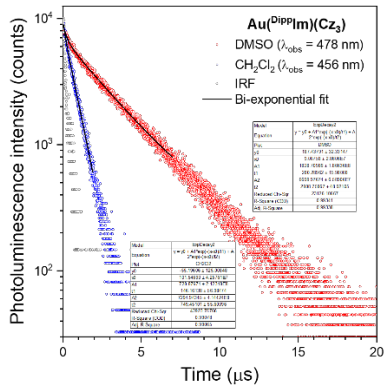

	y0	x0	A1	t1 (μs)	A2	t2 (μs)	R-Square
DMSO	187	9	1829	280	6700	2909	0.99
CH_2Cl_2	55	102	729	146	7295	749	0.99

e

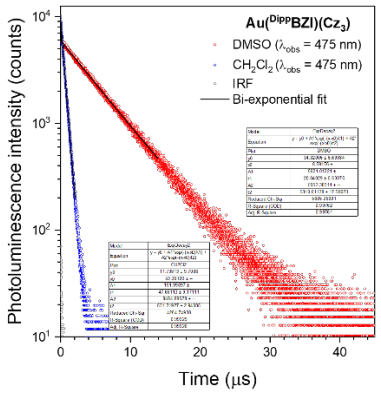

	y0	x0	A1	t1 (μs)	A2	t2 (μs)	R-Square
DMSO	34	9	5621	20	5953	5340	0.99
CH_2Cl_2	12	53	152	48	8485	531	0.99

f

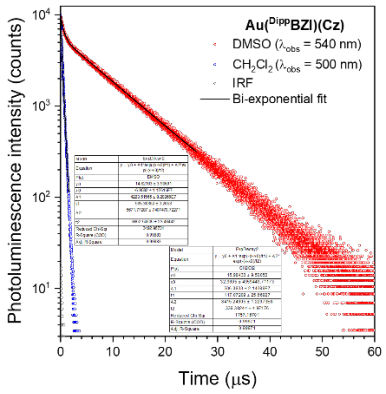

	y0	x0	A1	t1 (μs)	A2	t2 (μs)	R-Square
DMSO	15	7	4224	595	5672	8853	0.99
CH_2Cl_2	16	33	506	117	8415	339	0.99

g

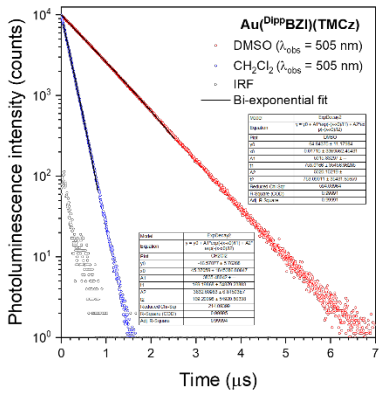

	y0	x0	A1	t1 (μs)	A2	t2 (μs)	R-Square
DMSO	65	0.017	5016	753	5020	753	0.99
CH_2Cl_2	17	45	3835	169	3833	169	0.99

h

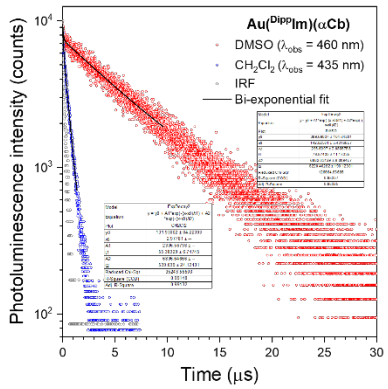

	y0	x0	A1	t1 (μs)	A2	t2 (μs)	R-Square
DMSO	390	143	296	77	6882	6220	0.95
CH_2Cl_2	132	3	2307	55	6897	539	0.99

i

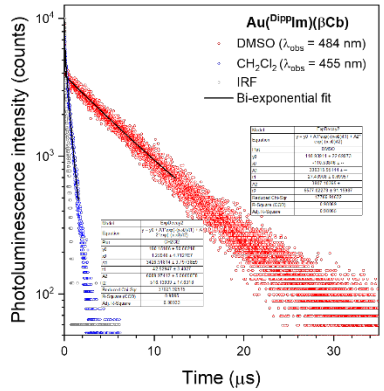

	y0	x0	A1	t1 (μs)	A2	t2 (μs)	R-Square
DMSO	119	111	336316	27	3807	6577	0.98
CH_2Cl_2	190	1	3427	43	6090	516	0.99

j

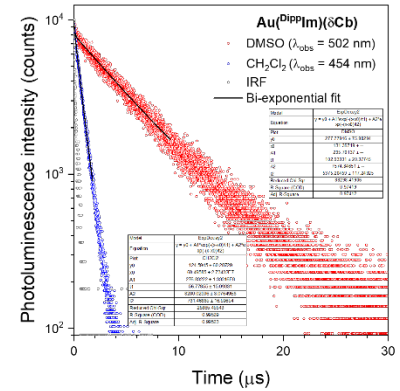

	y0	x0	A1	t1 (μs)	A2	t2 (μs)	R-Square
DMSO	278	131	296	103	7575	5375	0.97
CH_2Cl_2	125	60	277	57	8230	731	0.99

Fig. S6 | a–c, Photoluminescence decay traces of (**a**) 100 μM Au(^{Dipp}BZI)(CNCz), (**b**) 100 μM Au(^{Dipp}Im)(CNCz), (**c**) 100 μM Au(^{Dipp}Im)(γCb), (**d**) 100 μM Au(^{Dipp}Im)(Cz_3), (**e**) 100 μM Au(^{Dipp}BZI)(Cz_3), (**f**) 100 μM Au(^{Dipp}BZI)(Cz), (**g**) 100 μM Au(^{Dipp}BZI)(TMCz), (**h**) 100 μM Au(^{Dipp}Im)(αCb), (**i**) 100 μM Au(^{Dipp}Im)(αCb), and (**j**) 100 μM Au(^{Dipp}Im)(δCb) dissolved in Ar-saturated DMSO and CH_2Cl_2 recorded after nanosecond pulsed laser photoexcitation at 377 nm (pulse duration = 10 ns). The black curves are biexponential decay fits. The bottom tables list nonlinear least-squares fit results.

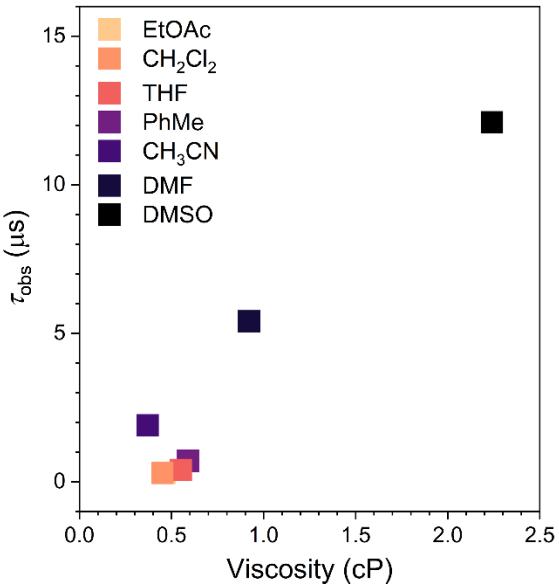

Fig. S7 | A plot of τ_{obs} as a function of solvent viscosity at 298 K.

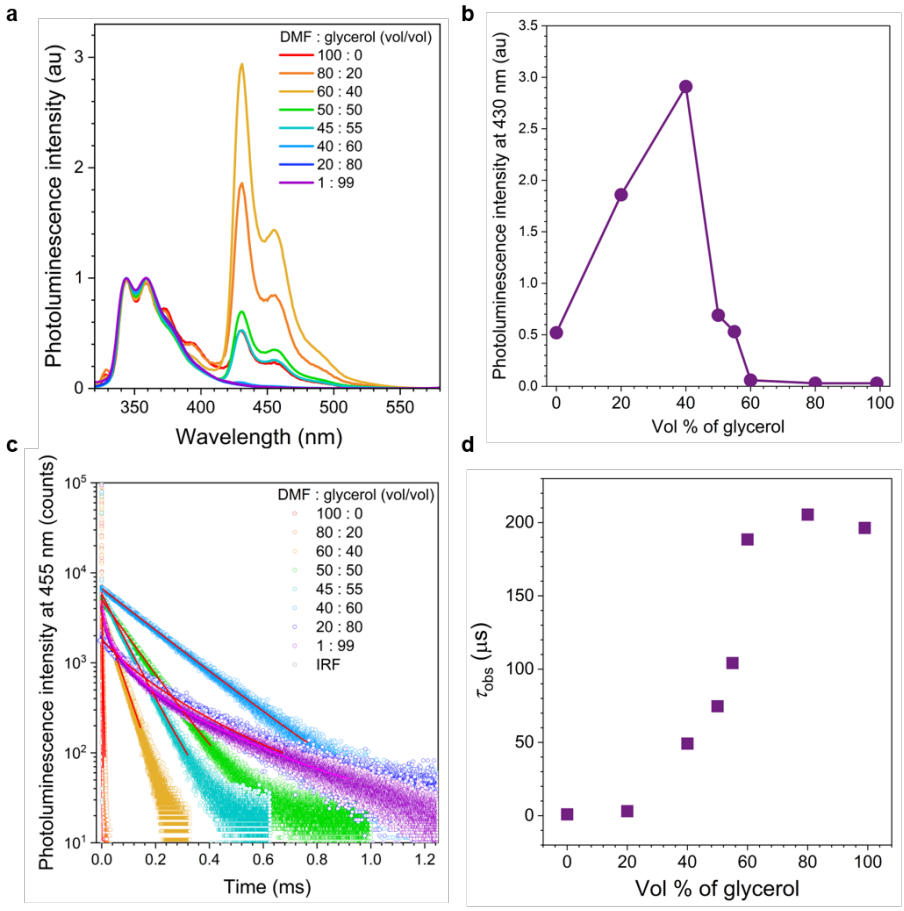

DMF:glycerol (vol/vol)	y0	x0	A1	t1 (ns)	A2	t2 (ns)	A3	t3 (ns)	R-Square
100 : 0	2.65828E-5	332.14325	0.00225	503	0.05102	997			0.99952
80 : 20	-6.45771E-5	695.79543	0.00102	556	0.04128	3089			0.99828
60 : 40	3.07632E-5	3952.5506	0.0045	41399	0.02805	50238			0.99618
50 : 50	1.77461E-4	15888.45061	4.2393E-4	34401	0.04245	104454			0.99885
45 : 55	1.37801E-4	8062.06551	0.00483	50415	0.0473	76363			0.99874
40 : 60	1.39812E-4	28432.93029	6.9371E-4	82775	0.0568	189016			0.99831
20 : 80	4.08601E-4	6674.16566	0.00569	70724	0.01125	226735			0.99377
1 : 99	2.23529E-4	-777.59892	0.02079	12025	0.01586	63049	0.00777	279082	0.99851

y = y0 + A1*exp(-(x-x0)/t1) + A2*exp(-(x-x0)/t2) (+ A3*exp(-(x-x0)/t3))

Fig. S8 | a, Photoluminescence spectra (λ_{ex} = 300 nm) of 10 μM Au(^{Dipp}Im)(Cz) dissolved in varying volumetric ratios of Ar-saturated DMF : glycerol at 298 K. **b**, Corresponding photoluminescence intensity at a wavelength of 430 nm as a function of the volume percent of glycerol. **c**, Photoluminescence decay traces of 100 μM Au(^{Dipp}Im)(Cz) dissolved in varying volumetric ratios of Ar-saturated DMF : glycerol recorded at 455 nm after nanosecond pulsed laser photoexcitation at 377 nm (pulse duration = 10 ns) at 298 K. The red curves are biexponential decay fits. A

triexponential decay model was applied to the traces recorded in a DMF:glycerol solution of 1:99 (v/v). **d**, Corresponding τ_{obs} as a function of the volume percent of glycerol. The bottom table lists the nonlinear least-squares fit results of the decay traces in **c**.

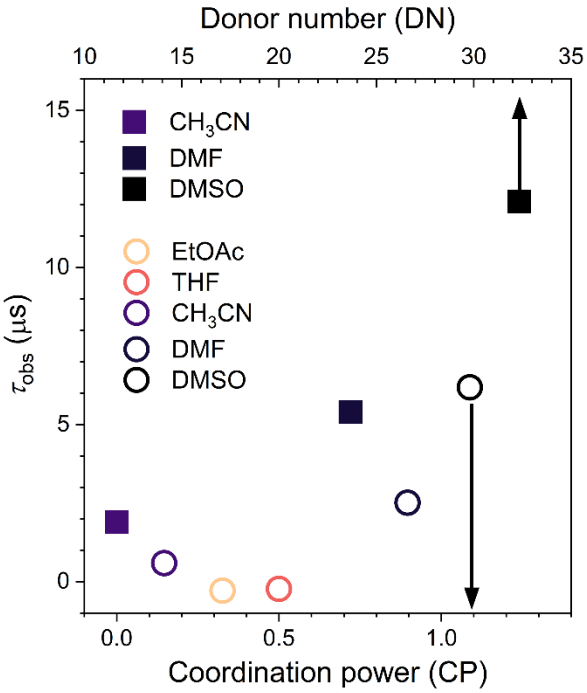

Fig. S9 | Plots of τ_{obs} as functions of Gutman's donor number (DN) and Munataka's coordination power (CP) of the solvent.

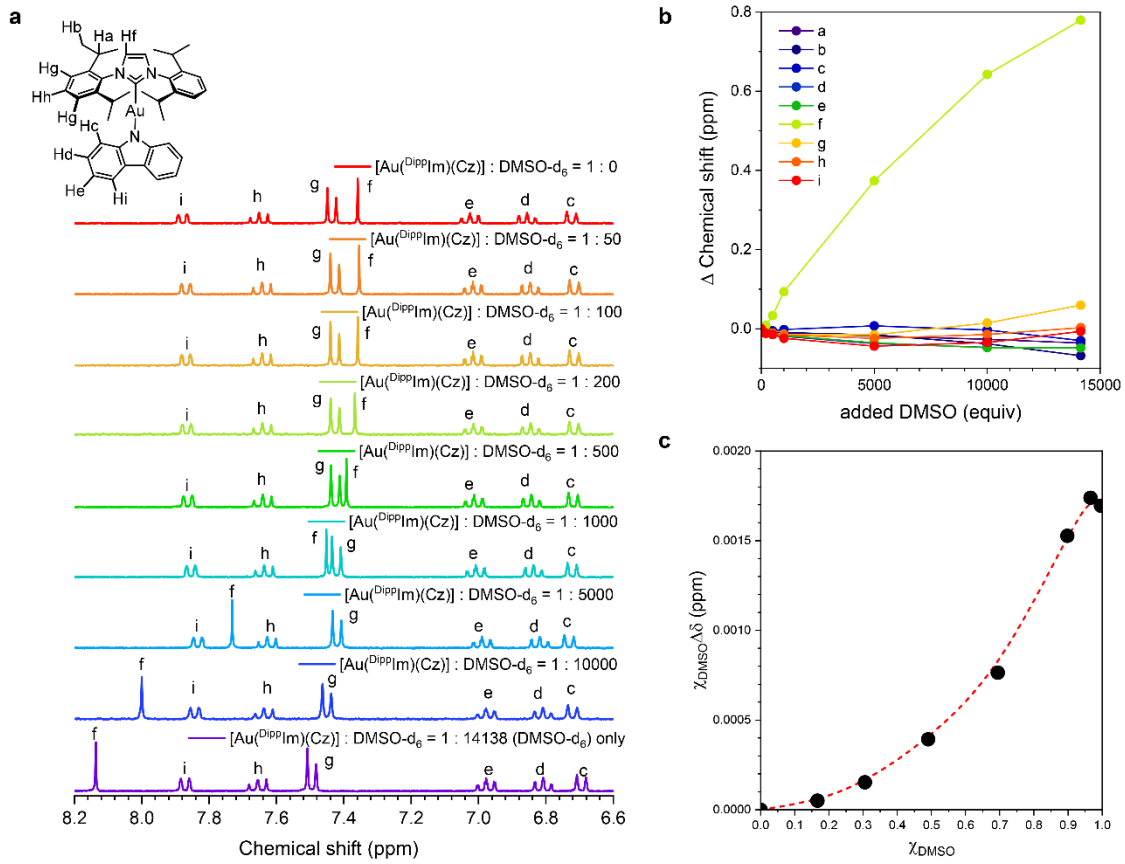

Fig. S10 | a, ^{1}H NMR (400 MHz) spectra of 1.0 mM Au(^{Dipp}Im)(Cz) in CD_2Cl_2 recorded with increased concentrations of DMSO-d_6 (0–10000 equiv). The ^{1}H NMR spectrum of 1.0 mM Au(^{Dipp}Im)(Cz) in DMSO-d_6 is included for comparison. **b**, Corresponding chemical shifts changes in the ^{1}H NMR peaks. **c**, Job plot obtained from ^{1}H NMR (300 MHz, CD_2Cl_2) spectroscopic measurements of the mixture of Au(^{Dipp}Im)(Cz) and DMSO-d_6 based on the method of continuous variations (total salt concentration = 50 mM).

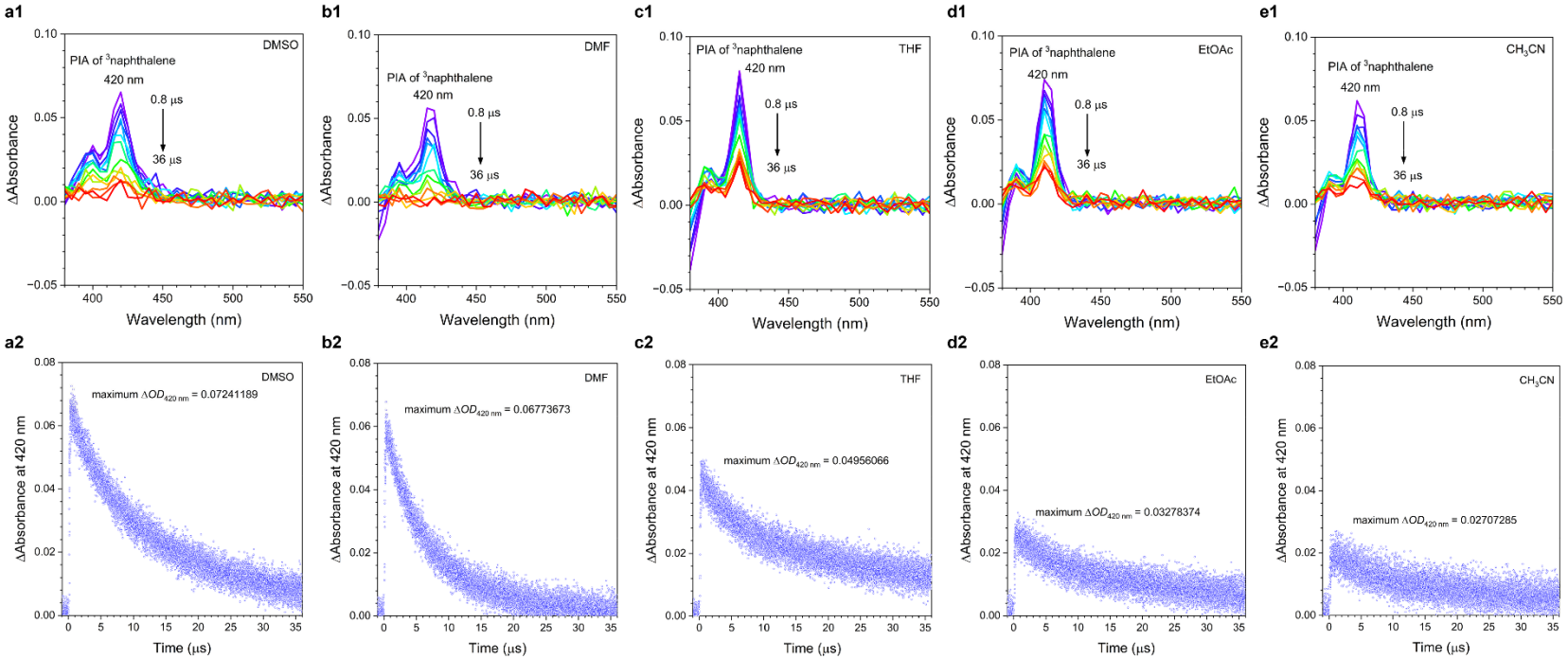

Fig. S11 | a1–e1, Selected transient absorption spectra for Ar-saturated solutions containing Au(^{Dipp}Im)(Cz) (*OD* at 355-nm pump laser (350 mW) = 0.85) and 50 mM naphthalene: **a1**, DMSO; **b1**, DMF; **c1**, THF; **d1**, EtOAc; **e1**, CH_3CN. The peak at 420 nm is due to triplet PIA of the triplet excited state of naphthalene (^{3}naphthalene) that is generated through triplet–triplet energy transfer from Au(^{Dipp}Im)(Cz). **a2–e2**, Corresponding decay traces recorded at a wavelength of 420 nm: **a2**, DMSO; **b2**, DMF; **c2**, THF; **d2**, EtOAc; **e2**, CH_3CN. The maximum ΔOD (ΔOD_{max}) value at 420 nm is used to calculate the molar concentration of ^{3}naphthalene (c_{3naph}), based on the equation $c_{3naph} = \Delta OD_{max} / (\varepsilon_{3naph} \times 1$ cm) where ε_{3naph} is 13200 M^{-1} cm^{-1}.[12] Recorded ΔOD_{max} values are shown in the panels. Calculated c_{3naph} values are 5.5 μM in DMSO, 5.1 μM in DMF, 3.8 μM in THF, 2.5 μM in EtOAC, and 2.1 μM in CH_3CN. Finally, Φ_{ISC} Au(^{Dipp}Im)(Cz) can be determined from the equation $\Phi_{ISC} = c_{3naph} / c_{3Ru}$, where c_{3Ru} (27 μM) is the molar concentration of the triplet excited state of 150 μM $[Ru(bpy)_3]Cl_2$ (*OD* at 355-nm pump laser

(350 mW) = 0.85) formed direct photoexcitation (Φ_{ISC} = 1.00) under the identical condition (see Fig. S12 for the details). Calculated Φ_{ISC} values of Au(^{Dipp}Im)(Cz) are 0.20 in DMSO, 0.19 in DMF, 0.14 in THF, 0.091 in EtOAC, and 0.075 in CH_3CN.

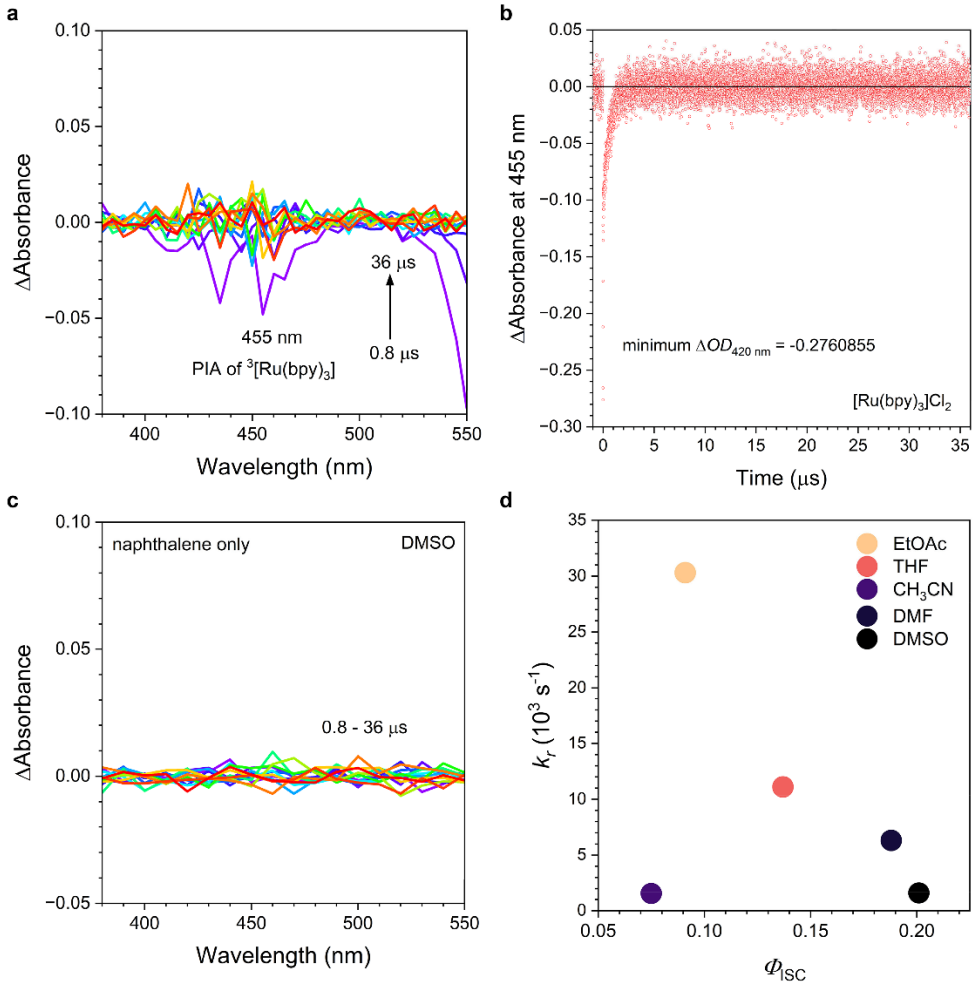

Fig. S12 | a, Selected transient absorption spectra for Ar-saturated H_2O containing 150 μM $[Ru(bpy)_3]Cl_2$ (*OD* at 355-nm pump laser (350 mW) = 0.85). The peak at 455 nm is due to photoinduced depletion of $[Ru(bpy)_3]Cl_2$ due to the formation of triplet excited state of $[Ru(bpy)_3]Cl_2$ ($^3[Ru(bpy)_3]$) upon direct photoexcitation (Φ_{ISC} = 1.00). **b**, Corresponding recovery traces recorded at a wavelength of 455 nm. The minimum ΔOD (ΔOD_{min}) value at 455 nm is used to calculate the molar concentration of $^3[Ru(bpy)_3]$ (c_{3Ru}), based on the equation $c_{3Ru} = \Delta OD_{min} / (\Delta\varepsilon_{455\ nm} \times 1\ cm)$ where $\Delta\varepsilon_{455\ nm}$ is 10100 M^{-1} cm^{-1}.[9] **c**, Selected transient absorption spectra for Ar-saturated DMSO containing 100 mM naphthalene. The spectral silence indicates the absence of the triplet excited-state of naphthalene upon direct photoexcitation. **d**, A plot of k_r values as a function of Φ_{ISC} of Au(^{Dipp}Im)(Cz). The weak correlation between k_r and Φ_{ISC} supports the claim that ISC alone cannot be the governing step of the phosphorescence emission of Au(^{Dipp}Im)(Cz).

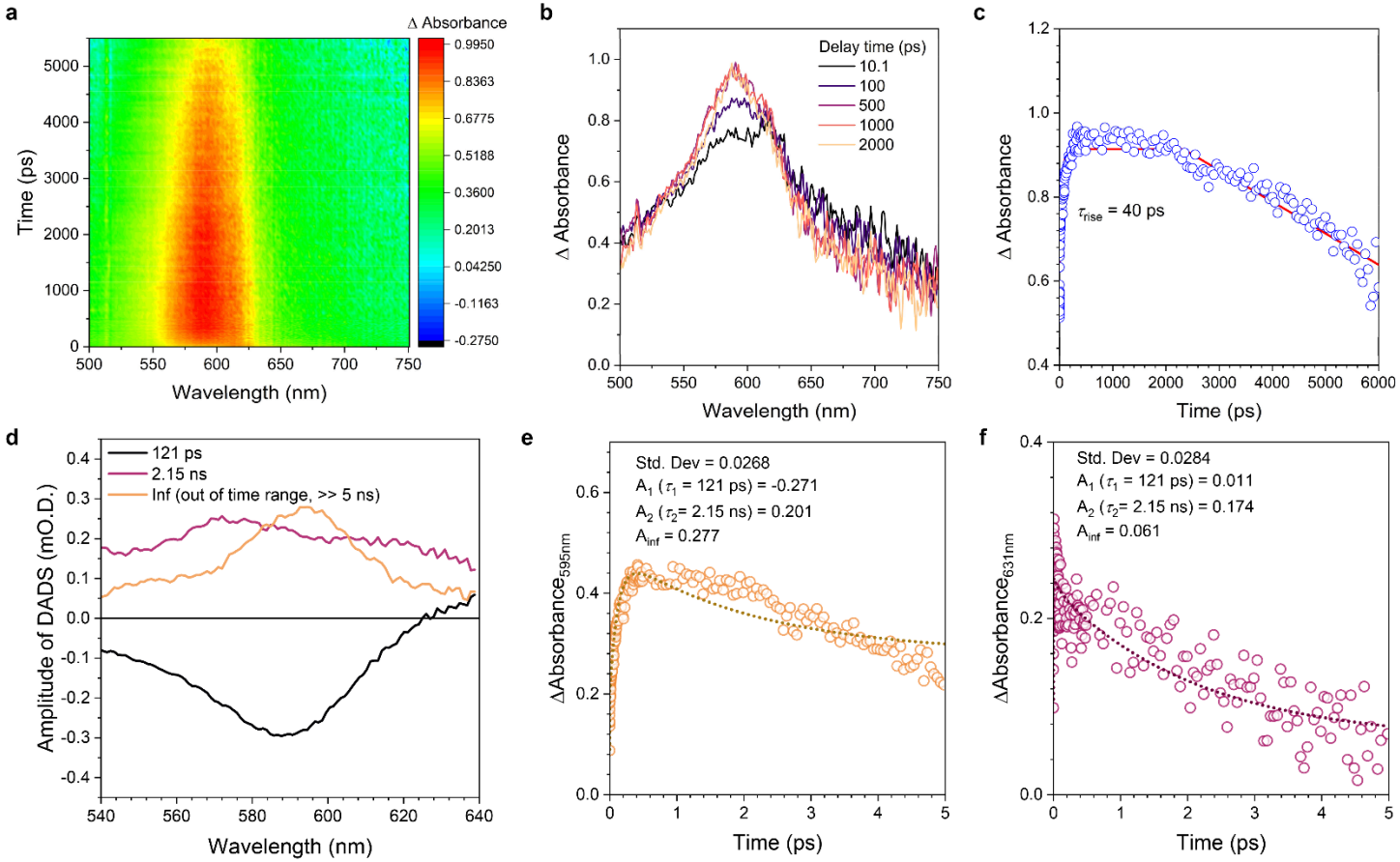

Fig. S13 | a, Heat map of transient absorption spectra of an Ar-saturated DMSO containing 10 mM Au(^{Dipp}Im)(Cz) recorded after femtosecond pulsed laser excitation at 375 nm. **b**, Selected transient absorption spectra. **c**, Time trace of the photoinduced signals recorded at 596 nm. The red curve is the fit to an exponential growth-decay model. **d**, Decay-associated difference spectra (DADS) obtained from global analyses using a biexponential decay model with a constant infinite offset (A_{Inf}). **e,f**, Representative kinetic traces at 595 nm (**e**) and 631 nm (**f**) overlaid with

biexponential decay fits with a constant infinite offset term using lifetimes fixed to the global values (τ_1 = 121 ps and τ_2 = 2.15 ns); amplitudes and offset parameters were optimized only.

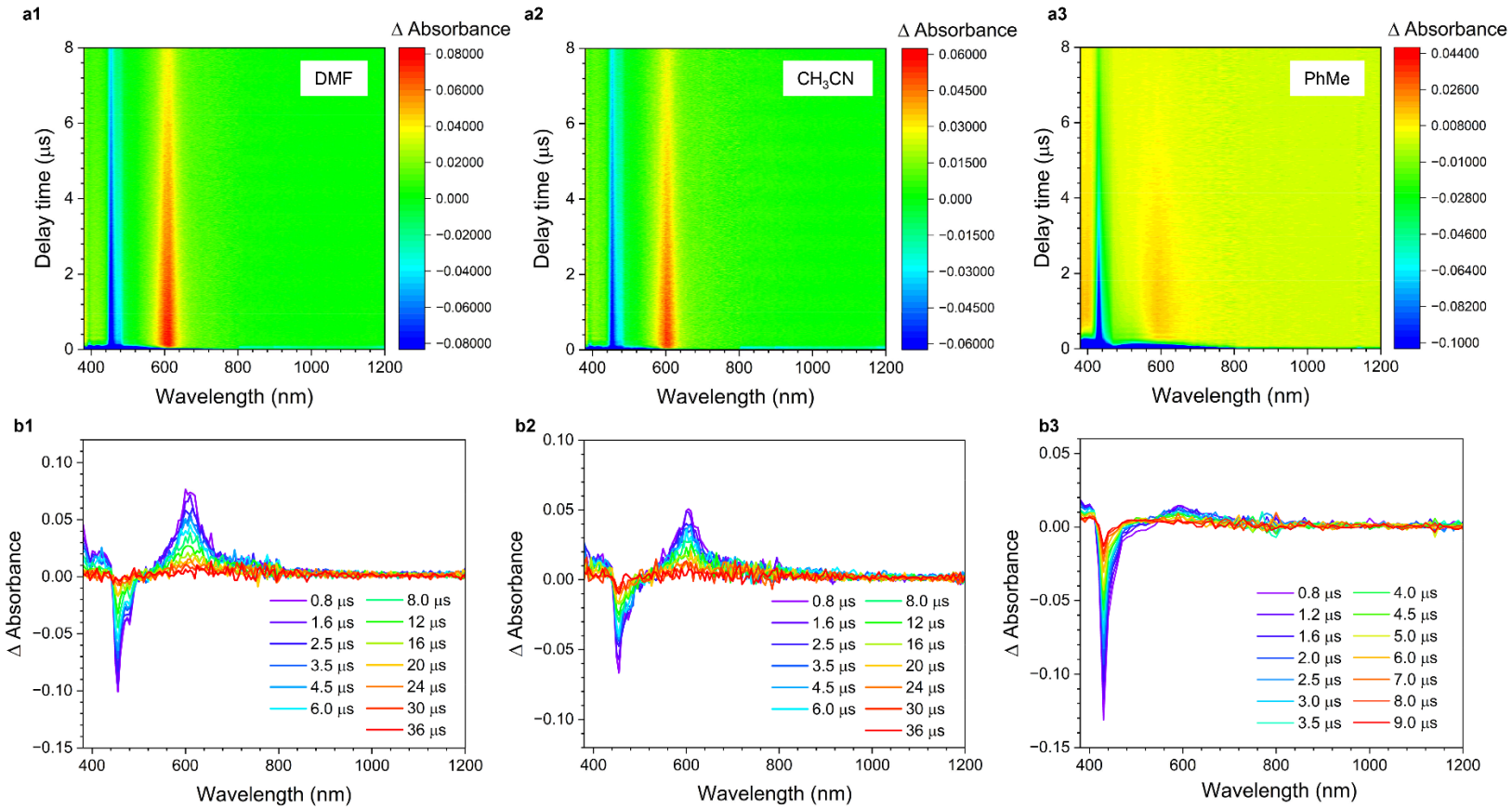
a1
DMF
Δ Absorbance
Delay time (μs)
Wavelength (nm)
a2
CH3CN
Δ Absorbance
Delay time (μs)
Wavelength (nm)
a3
PhMe
Δ Absorbance
Delay time (μs)
Wavelength (nm)
b1
Δ Absorbance
0.8 μs
1.6 μs
2.5 μs
3.5 μs
4.5 μs
6.0 μs
8.0 μs
12 μs
16 μs
20 μs
24 μs
30 μs
36 μs
Wavelength (nm)
b2
Δ Absorbance
0.8 μs
1.6 μs
2.5 μs
3.5 μs
4.5 μs
6.0 μs
8.0 μs
12 μs
16 μs
20 μs
24 μs
30 μs
36 μs
Wavelength (nm)
b3
Δ Absorbance
0.8 μs
1.2 μs
1.6 μs
2.0 μs
2.5 μs
3.0 μs
3.5 μs
4.0 μs
4.5 μs
5.0 μs
6.0 μs
7.0 μs
8.0 μs
9.0 μs
Wavelength (nm)

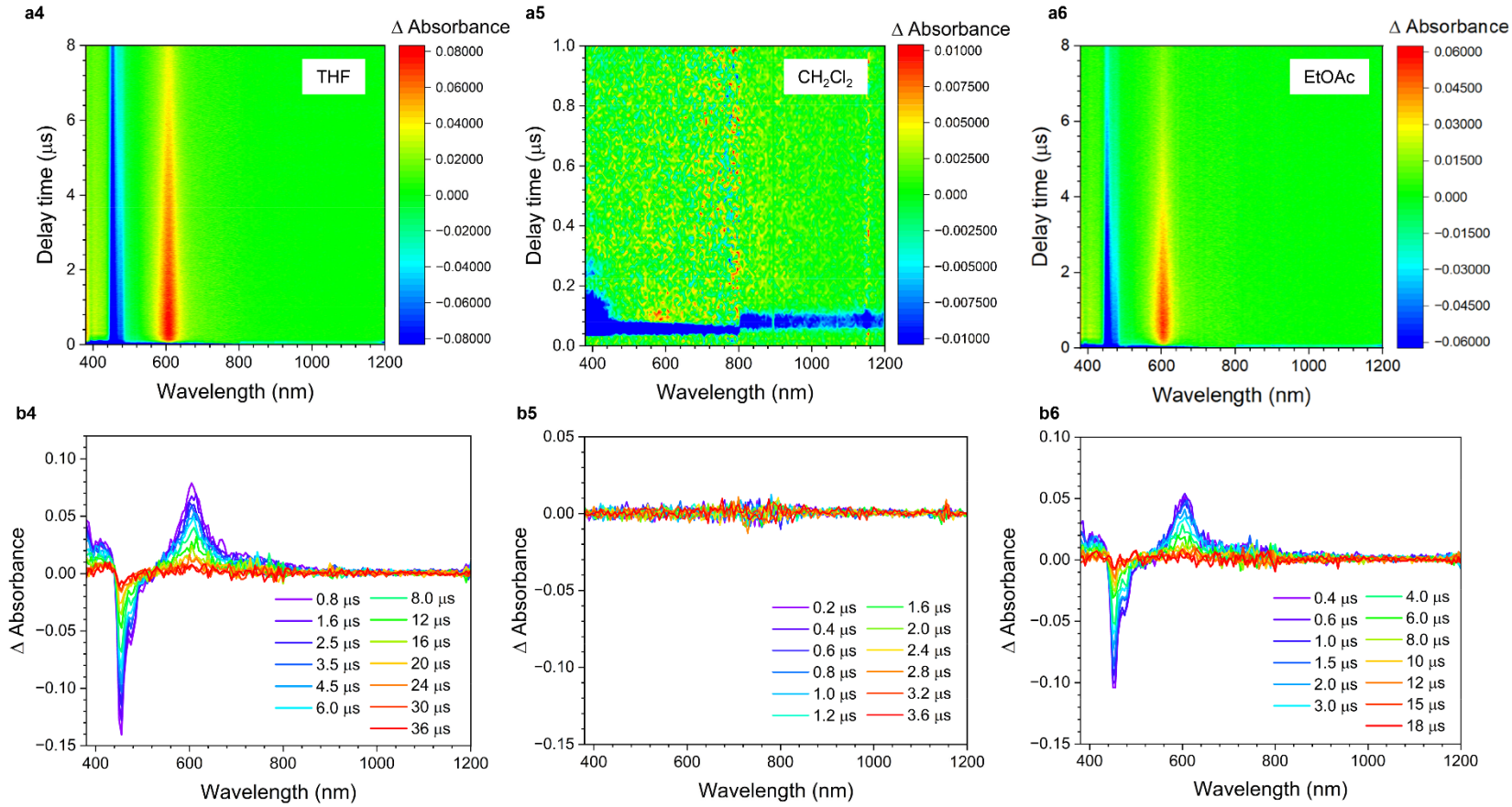

Fig. S14 | a1–6, Heat map of transient absorption spectra of 250 μM Au(^{Dipp}Im)(Cz) in Ar-saturated DMF (**a1**), CH_3CN (**a2**), PhMe (**a3**), THF (**a4**), CH_2Cl_2 (**a5**), and EtOAc (**a6**) recorded after nanosecond pulsed laser photoexcitation at 355 nm (350 mW). **b1–6**, Selected transient absorption spectra of 250 μM Au(^{Dipp}Im)(Cz) in Ar-saturated DMF (**b1**), CH_3CN (**b2**), PhMe (**b3**), THF (**b4**), CH_2Cl_2 (**b5**), and EtOAc (**b6**). Decay

traces are shown in Fig. S15.

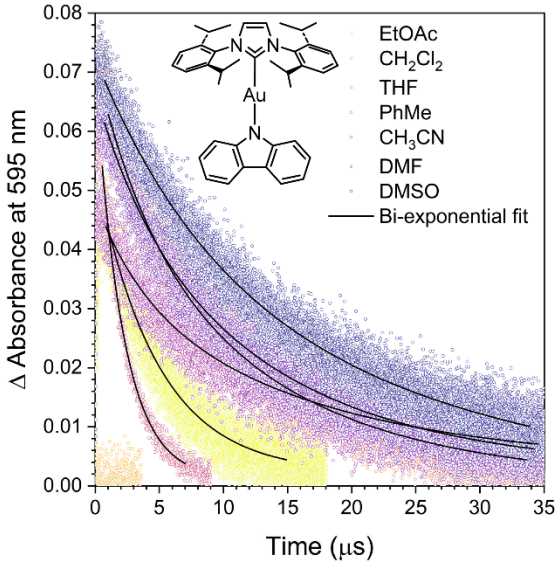

solvent	y0	x0	A1	t1 (μs)	A2	t2 (μs)	R-Square
EtOAc	0.00216	0.98179	0.02097	4.7	0.02073	4.8	0.92
THF	0.000622	1.2048	0.01854	4.2	0.04231	13	0.96
PhMe	0.00118	0.51516	0.0269	2.1	0.02685	2.1	0.99
CH_3CN	0.00361	1.21214	0.01014	3.6	0.02825	16	0.88
DMF	0.00262	1.13739	0.01184	3.9	0.04427	13	0.95
DMSO	-0.00581	1.45302	0.03689	9.5	0.03398	38	0.96

$y = y0 + A1*\exp(-(x-x0)/t1) + A2*\exp(-(x-x0)/t2)$

Fig. S15 | Transient absorption decay traces of the photoinduced signals recorded at 595 nm of 250 μM Au(^{Dipp}Im)(Cz) in Ar-saturated EtOAc, CH_2Cl_2, THF, PhMe, CH_3CN, DMF, and DMSO, shown in Fig. S14. The black curves are biexponential fits. The bottom table lists nonlinear least-squares fit results.

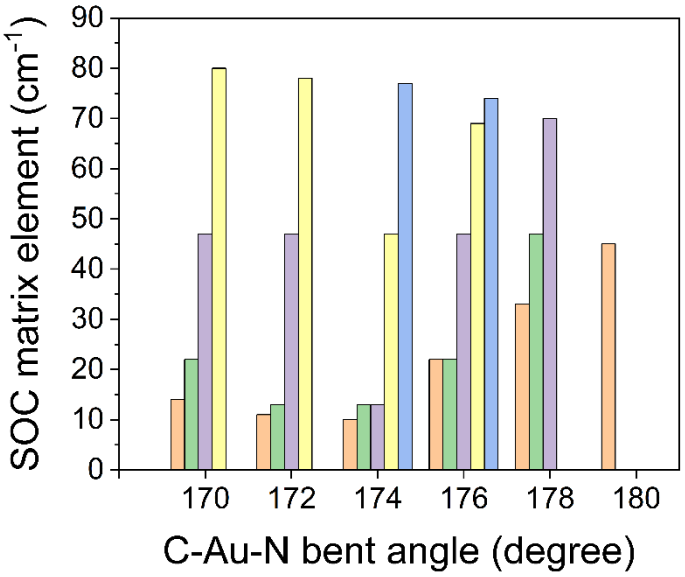

Fig. S16 | Plot of large-amplitude (> 10 cm^{-1}) SOCME values of Au(^{Dipp}Im)(Cz) at different C–Au–N bond angles.

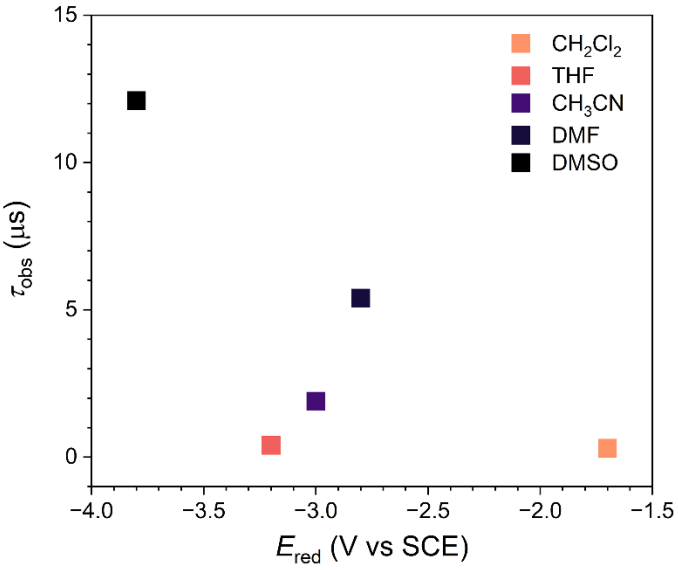

Fig. S17 | Plot of τ_{obs} as a function of the reduction potential (E_{red}, V vs SCE) of solvents.[19] The poor correlation between τ_{obs} and E_{red} can serve to exclude the formation of an exciplex as an intermediacy for solvatochronic behaviors.

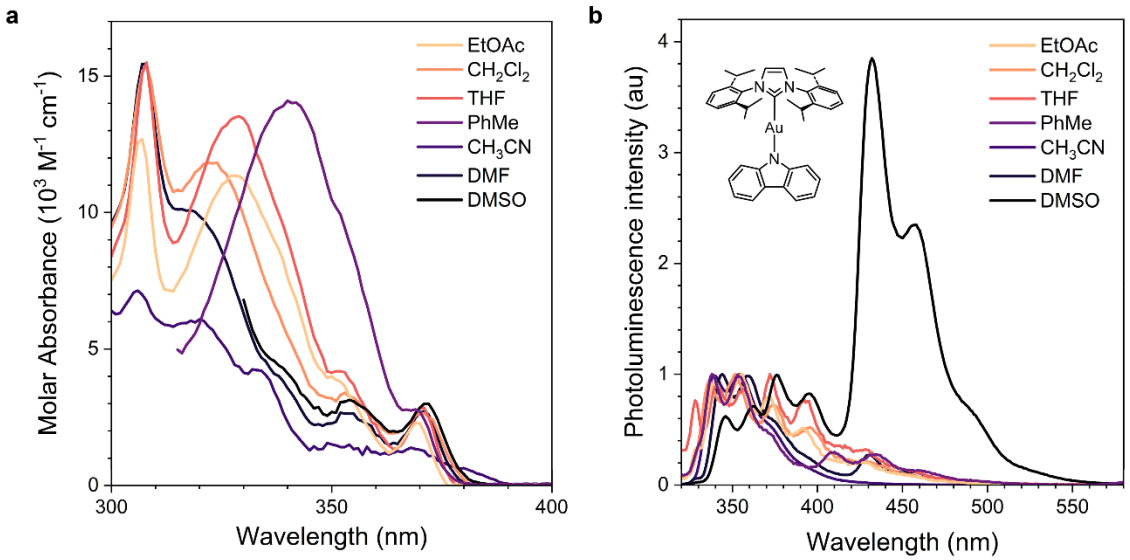

Fig. S18 | a, UV–vis absorption and **b**, photoluminescence spectra of 10 μM Au(^{Dipp}Im)(Cz) in various solvents (Ar-saturated).

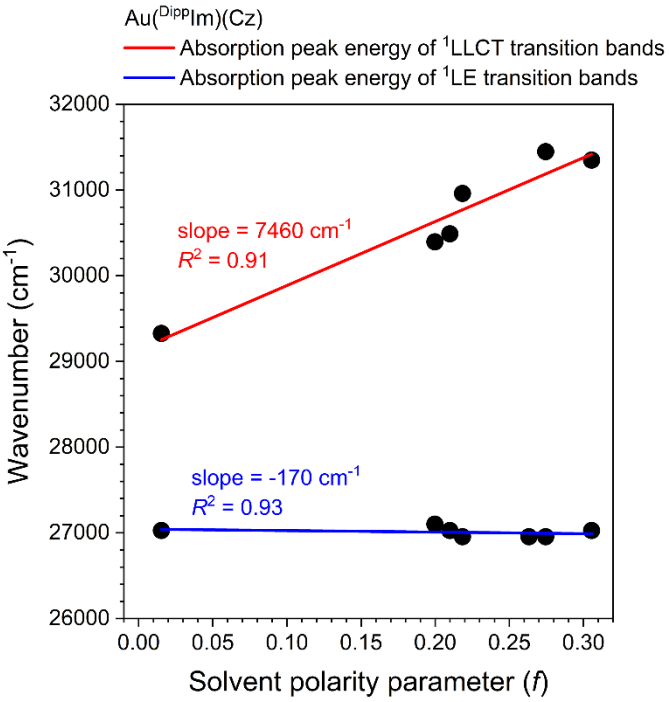

Fig. S19 | Lippert–Mataga plots of the peak absorption energies of the singlet ligand-to-ligand charge-transfer transition (^{1}LLCT, red) and the singlet local excitation centered within carbazolide (^{1}LE, blue) as functions of the solvent polarity parameter (*f*). The *f* value is calculated from the refractive index (*n*) and the dielectric constant (ε) through the relationship $f = (\varepsilon - 1)/(2\varepsilon + 1) - (n^2 - 1)/(2n^2 + 1)$.

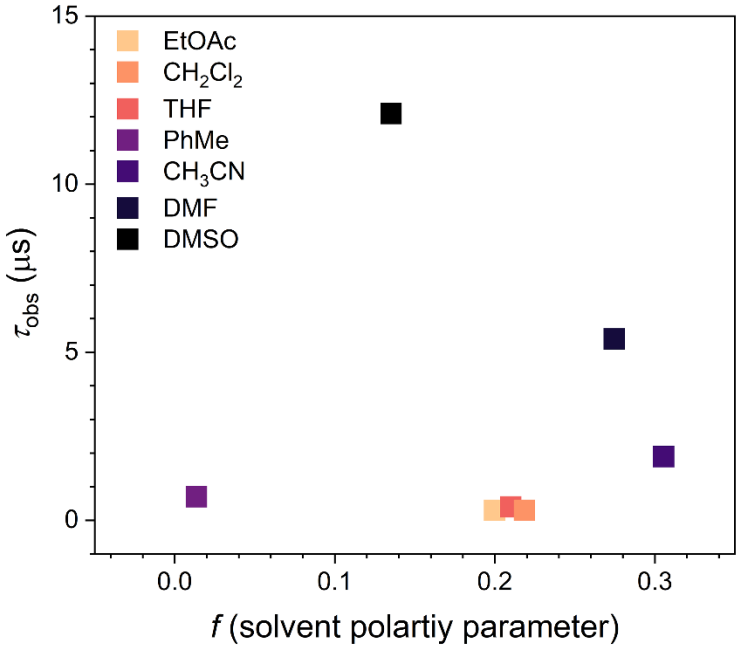

Fig. S20 | Plot of τ_{obs} as a function of the polarity parameter (*f*) of solvents.

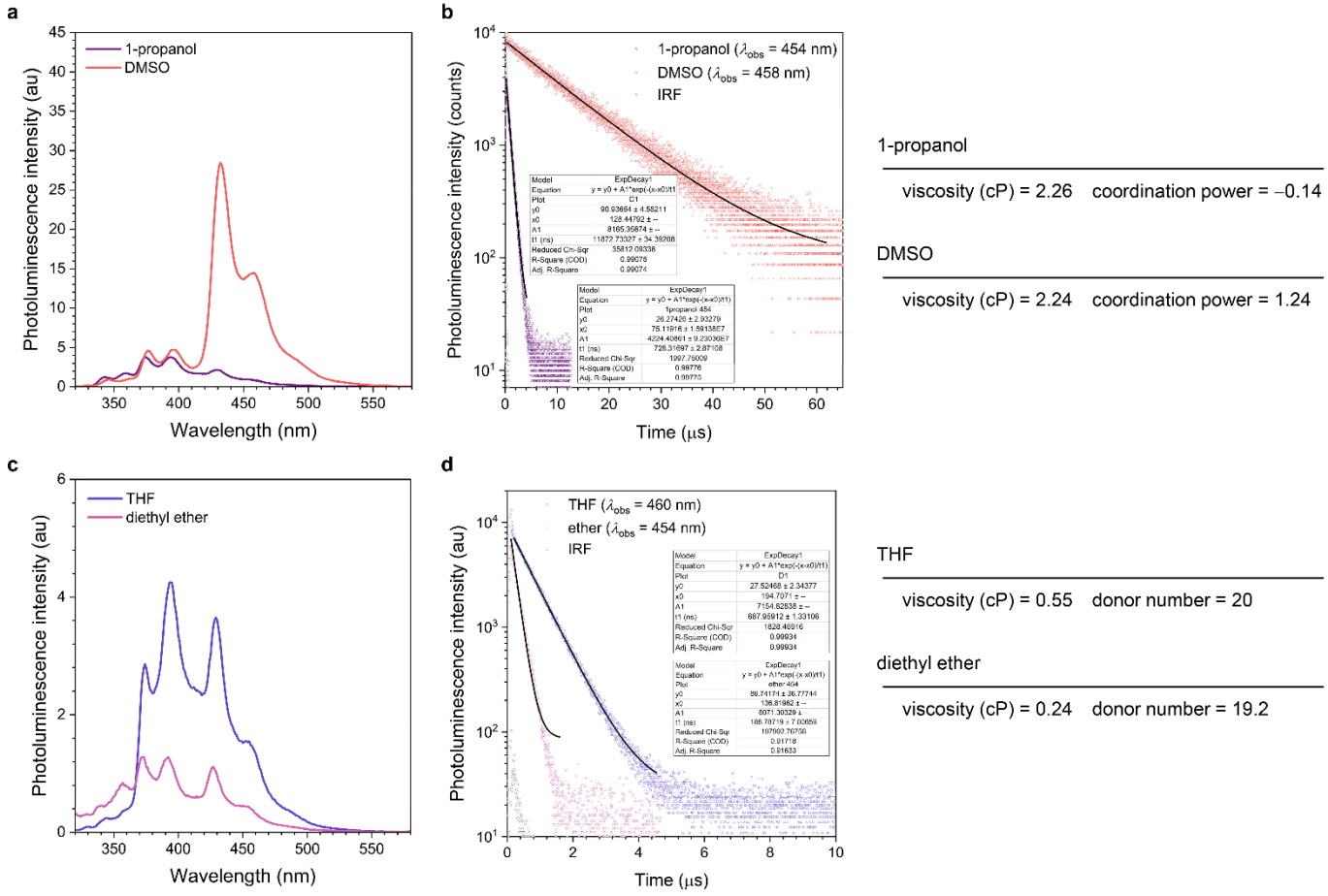

1-propanol

viscosity (cP) = 2.26 coordination power = –0.14

DMSO

viscosity (cP) = 2.24 coordination power = 1.24

THF

viscosity (cP) = 0.55 donor number = 20

diethyl ether

viscosity (cP) = 0.24 donor number = 19.2

Fig. S21 | a, Photoluminescence spectra (λ_{ex} = 300 nm) of 10 μM Au(^{Dipp}Im)(Cz) dissolved in Ar-saturated 1-propanol and DMSO. **b**, Photoluminescence decay traces of of 10 μM Au(^{Dipp}Im)(Cz) dissolved in Ar-saturated 1-propanol (λ_{obs} = 454 nm) and DMSO (λ_{obs} = 458 nm) recorded after nanosecond pulsed laser photoexcitation at 377 nm (pulse duration = 10 ns). The black curves are monoexponential decay fits.

c, Photoluminescence spectra (λ_{ex} = 300 nm) of 10 μM Au(^{Dipp}Im)(Cz) dissolved in Ar-saturated THF and diethyl ether. **d**, Photoluminescence decay traces of of 10 μM Au(^{Dipp}Im)(Cz) dissolved in Ar-saturated THF (λ_{obs} = 460 nm) and diethyl ether (λ_{obs} = 454 nm) recorded after nanosecond pulsed laser photoexcitation at 377 nm (pulse duration = 10 ns). The black curves are monoexponential decay fits. The viscosity and coordination power of solvents are shown on the right.

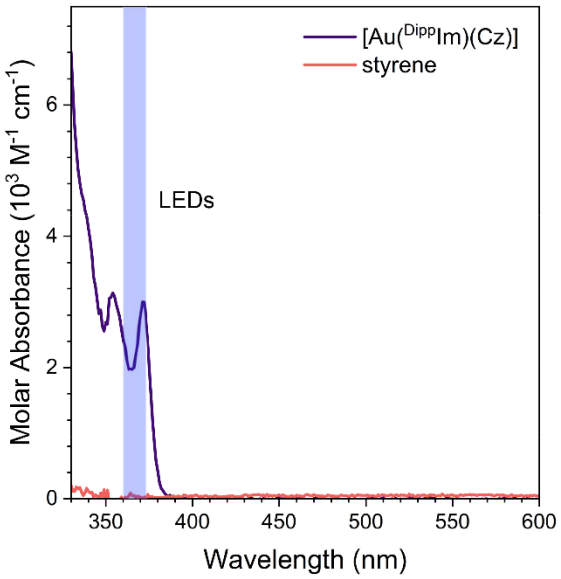

Fig. S22 | UV–Vis absorption spectra of 10 μM Au(^{Dipp}Im)(Cz) and 10 μM styrene (**1a**) in DMSO. The purple region indicates the emission wavelength range of LEDs used in our photocatalytic [2+2] cycloaddition reactions.

a

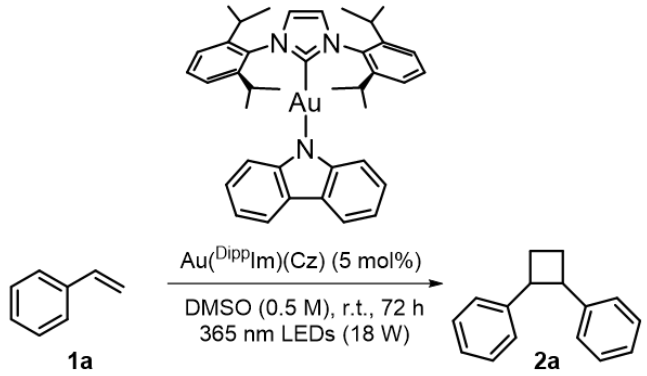

1a (mmol)	Au(DippIm)(Cz) (mmol)	**2a** (mmol)	yield (%)	TON	$\Phi_{[2+2]}$ (%)
0.01	0.005	0.00195	39	0.39	0.028
0.05	0.005	0.011	44	2.2	0.15
0.1	0.005	0.035	70	7	0.35
0.5	0.005	0.114	46	22.8	1.32
1	0.005	0.155	31	31	2.35

b

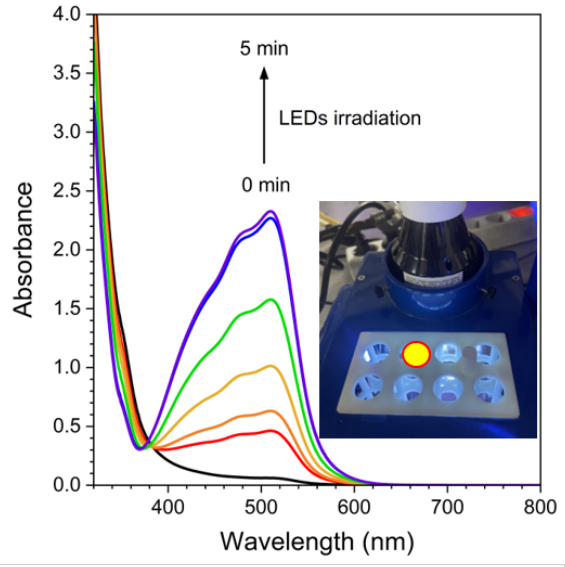

c

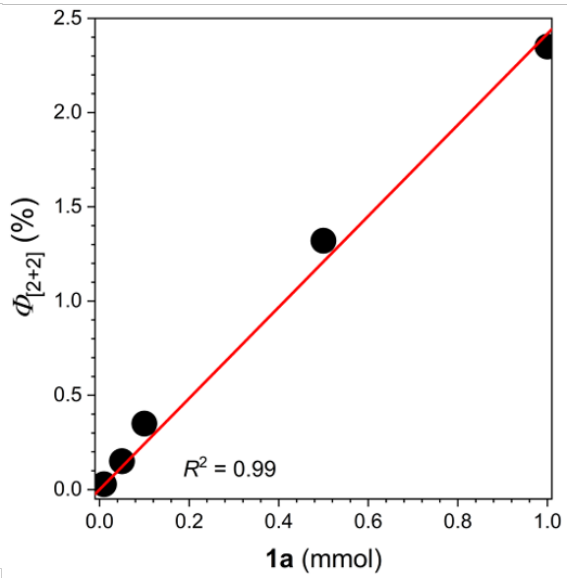

Fig. S23 | a, Determination of the turn-over numbers (TONs) and the quantum yields for the photocatalytic [2+2] cycloaddition reaction ($\Phi_{[2+2]}$s) with increased amounts of **1a**. The TON was computed with the equation TON = (mole of **2a**) / (mole of catalyst). The $\Phi_{[2+2]}$ was calculated with the equation $\Phi_{[2+2]}$ = (mole of **2a**) / (q × time), where q is the photon flux determined by the ferrioxalate ($K_3[Fe(C_2O_4)_3]$) actinometry (see below). The yield of the product was determined by

^{1}H NMR spectroscopy using dibromomethane as an internal standard. **b**, UV–Vis absorption spectra of 6.0 mM $K_3[Fe(C_2O_4)_3]\cdot 3H_2O$ photoirradiated using 365 nm LEDs for a period of 5 min. The photoirradiated solutions were treated with 1.0 M sodium acetate (aq) and 1.0 wt % 1.10-phenanthroline·H_2O under dark before the UV–Vis absorption measurements. The photon flux (q) from the LEDs was determined from the equation $q = [\Delta Abs_{510\ nm} \times V] / [\Phi \times \varepsilon_{510\ nm} \times l \times t]$, where $\Delta Abs_{510\ nm}$ is the absorbance change at a wavelength of 510 nm (0.95), V is the volume of the solution (1.5 mL), Φ is the quantum yield of the ferrioxalate actinometer (1.1), $\varepsilon_{510\ nm}$ is the molar absorbance of the photooxidized species of the actinometer at 510 nm (1.1×10^4 M^{-1} cm^{-1}), l is the beam pass length (0.1 cm), and t is the photoirradiation time (5 min). $q = 3.9 \times 10^{-8}$ einstein s^{-1}. **c**, A plot of $\Phi_{[2+2]}$ as a function of the amount of added **1a**.

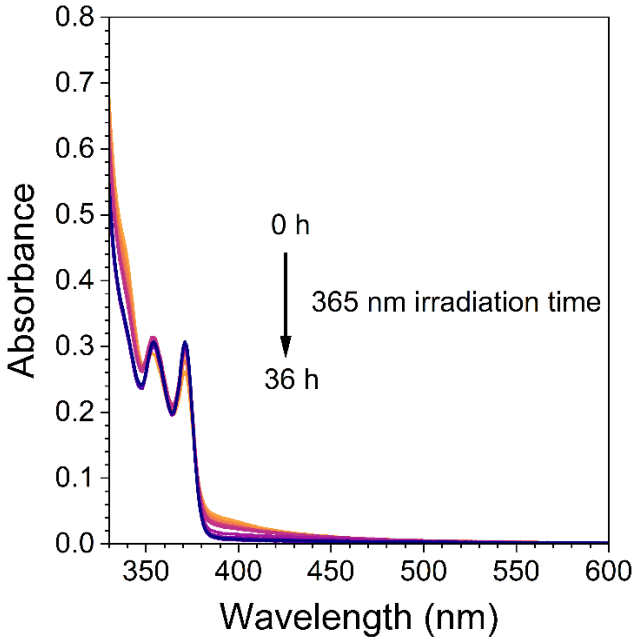

Fig. S24 | UV–Vis absorption spectra of 100 μM Au(^{Dipp}Im)(Cz) recorded during continuous photoirradiation at 365 nm (10 mW) in deaerated DMSO.

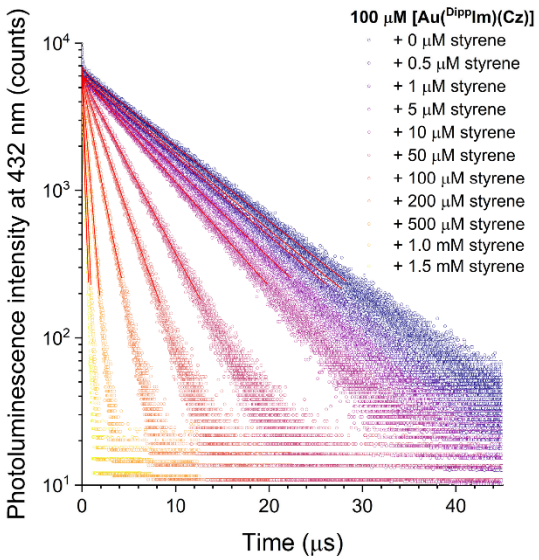

styrene (equiv)	y0	x0	A1	t1 (ns)	A2	t2 (ns)	*R*-Square (COD)
0	0.00151	1187.08221	0.00143	338.29464	0.56655	8413.9452	0.99827
0.005	9.40125E-4	1338.58041	2.67453E-4	241.62397	0.50379	7945.39594	0.99807
0.01	0.00147	1400.50846	9.79942E-4	380.01794	0.5179	8118.48298	0.99801
0.05	9.54952E-4	1057.41571	0.00176	313.59454	0.49668	7072.74639	0.99785
0.1	7.14498E-4	1068.27485	0.00158	301.1014	0.49287	6067.68721	0.99798
0.5	7.62844E-4	580.34266	0.01202	422.7918	0.49595	3609.35779	0.99788
1	0.00183	262.96102	0.02442	183.50952	0.51811	2298.4936	0.99817
2	0.00485	86.50558	0.06674	92.78553	0.53879	1271.36445	0.99761
5	1271.36445	46.69064	0.09267	60.62929	0.53295	557.99626	0.9977
10	-0.01676	23.28564	0.25338	101.60282	0.40223	389.55663	0.99744
15	0.00367	19.26665	0.20745	71.06179	0.40327	223.5671	0.99815

Fit equation: y = y0 + A1*exp(-(x-x0)/t1) + A2*exp(-(x-x0)/t2)

Fig. S25 | Nonlinear least-squares fit analyses for photoluminescence decay traces of 100 μM Au(^{Dipp}Im)(Cz) (Ar-saturated DMSO), recorded at a wavelength of 432 nm after nanosecond pulsed laser photoexcitation at 377 nm (pulse duration = 5 ns) with increasing the concentration of styrene (0–1.5 mM).

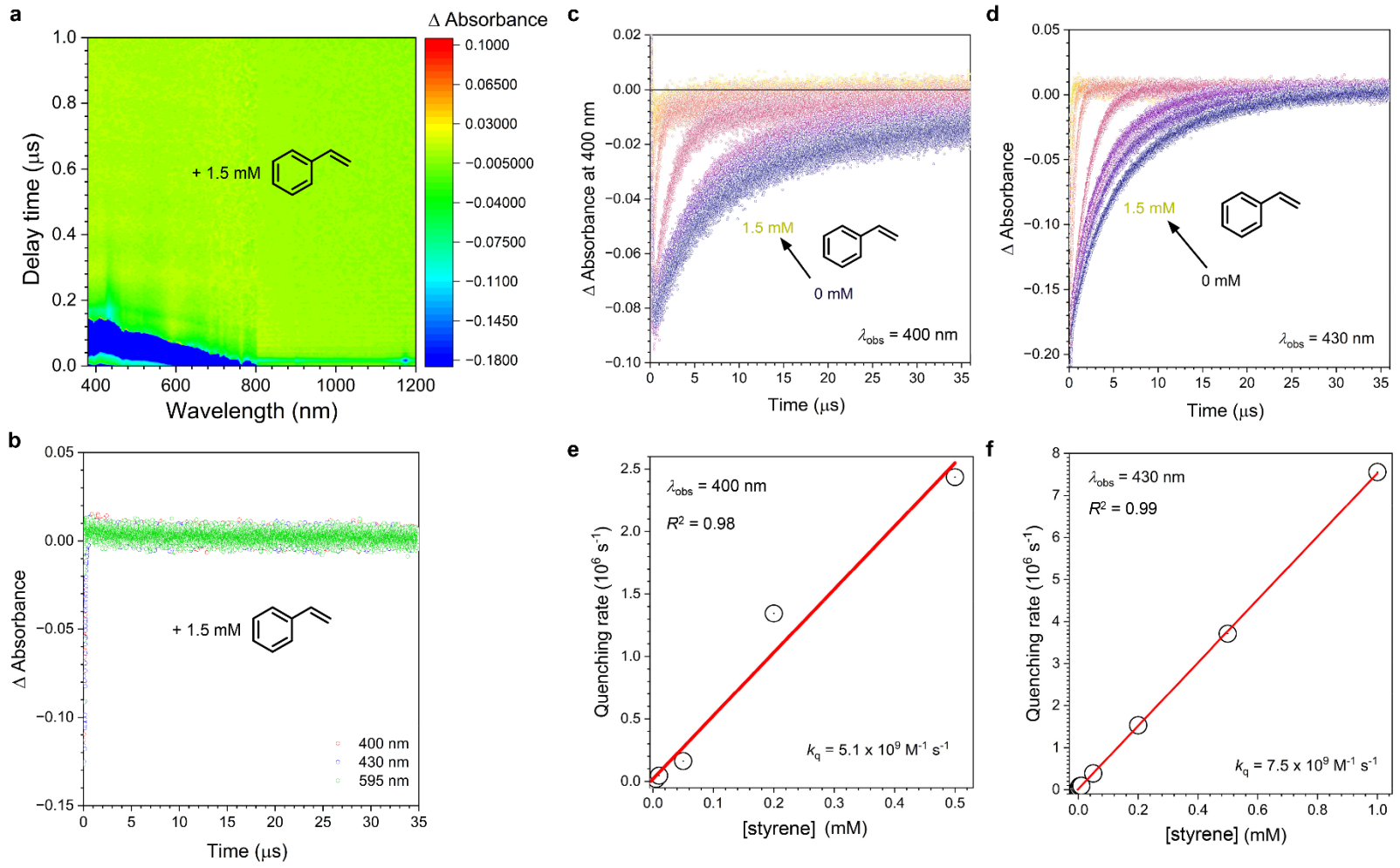

Fig. S26 | a, Heat map of transient absorption spectra of an Ar-saturated DMSO containing 100 μM Au(^{Dipp}Im)(Cz) and 1.5 mM **1a** recorded after nanosecond pulsed laser excitation at 355 nm. **b**, Time traces of the photoinduced absorption of 100 μM Au(^{Dipp}Im)(Cz) in the presence

of 1.5 mM **1a** (Ar-saturated DMSO), monitored at wavelengths of 400, 430, and 595 nm. **c,d**, Time traces of the photoinduced absorption of 100 μM Au(^{Dipp}Im)(Cz) with the increased concentration of **1a** (0–1.5 mM; Ar-saturated DMSO), monitored at wavelengths of 400 (**c**) and 430 nm (**d**). **e,f**, Corresponding pseudo-first-order kinetics analyses of the quenching rate recorded at wavelengths of 400 (**e**) and 430 nm (**f**) as a function of added **1a**. The quenching rate was calculated according to the relationship rate = $1/\tau_{obs}'$(**1a**)-$1/\tau_{obs}'$(0), where τ_{obs}'(**1a**) and τ_{obs}'(0) are the observed lifetime of the 400 nm or 430 nm signal of 100 μM Au(^{Dipp}Im)(Cz) in the presence and absence, respectively, of **1a**.

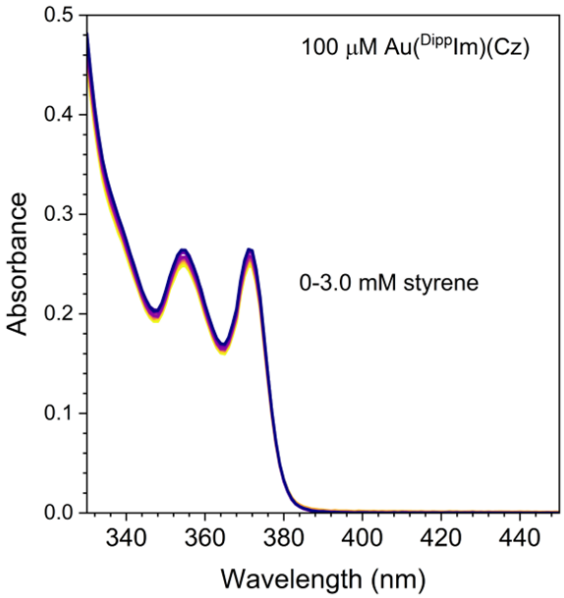

Fig. S27 | UV–Vis absorption spectra of 100 μM Au(^{Dipp}Im)(Cz) (DMSO) recorded with increased concentration of styrene (**1a**) (0–3.0 mM). The spectral invariance suggests the absence of a ground-state association between Au(^{Dipp}Im)(Cz) and **1a**.

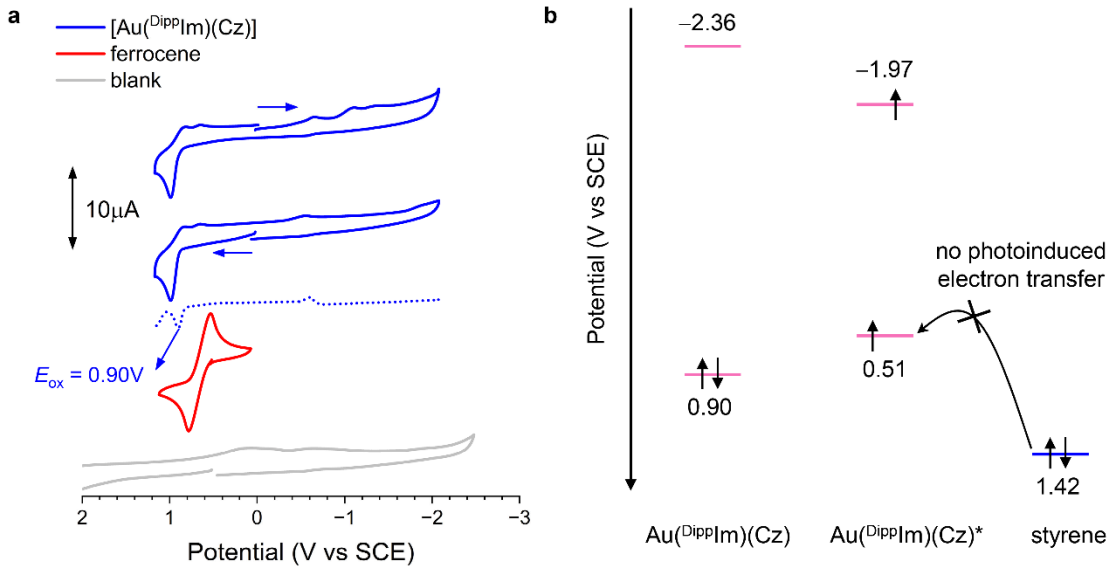

Fig. S28 | a, Cyclic (solid curves) and differential pulse (dotted curve) voltammograms of 2.0 mM Au(^{Dipp}Im)(Cz) dissolved in Ar-saturated CH_3CN containing 0.10 M $TBAPF_6$. A Pt working and a Pt counter electrodes, and an $Ag/AgNO_3$ pseudo reference electrode were employed. Scan rate = 0.10 V s^{-1} (cyclic voltammetry) and 0.004 V s^{-1} (differential pulse voltammetry). The potentials were calibrated based on the ferrocenium/ferrocene redox couple (red curve). The grey curve is the voltammogram obtained for the blank sample without the Au(I) complex. **b**, Comparisons of the electrochemical potentials of the ground and excited states of Au(^{Dipp}Im)(Cz) with the oxidation potential of styrene (**1a**).

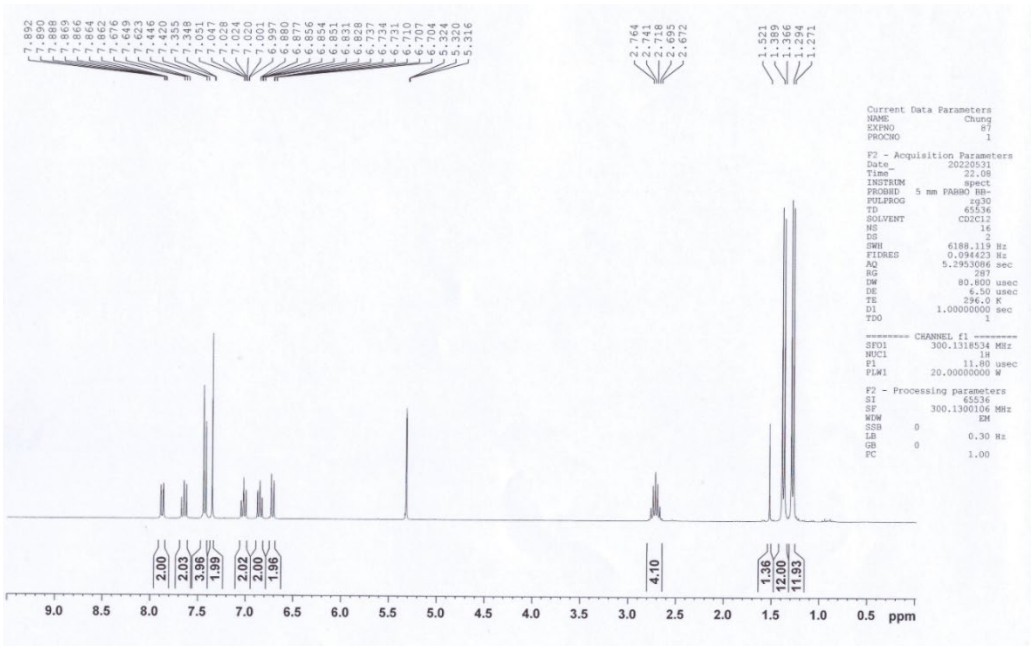

Fig. S29 | ^{1}H NMR (300 MHz, CD_2Cl_2) spectrum of Au(^{Dipp}Im)(Cz).

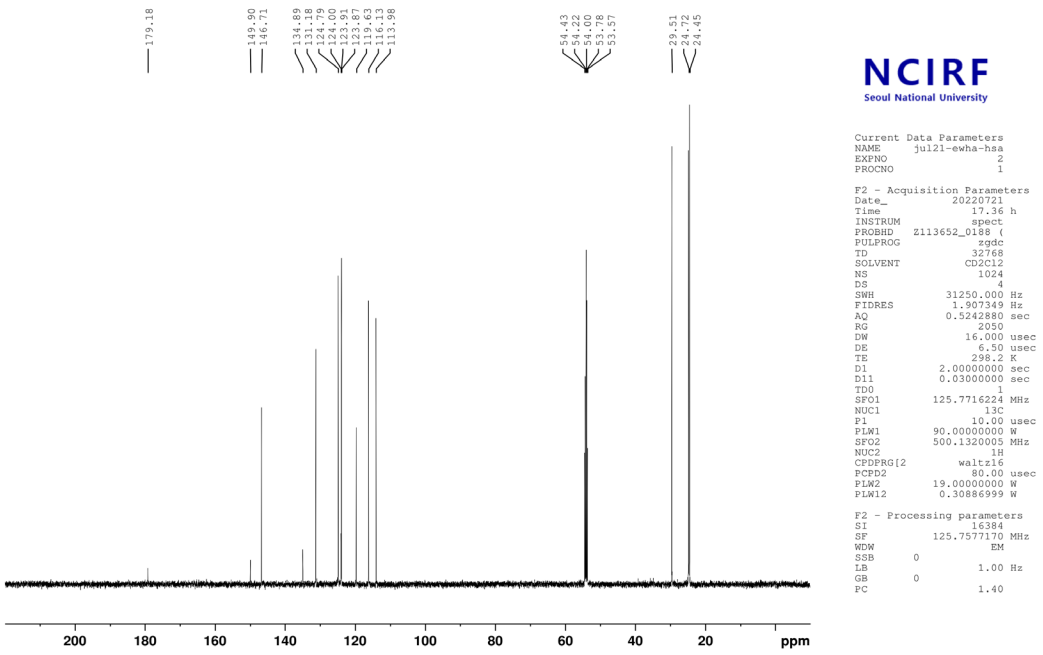

Fig. S30 | $^{13}C\{^{1}H\}$ NMR (126 MHz, CD_2Cl_2) spectrum of Au(^{Dipp}Im)(Cz).

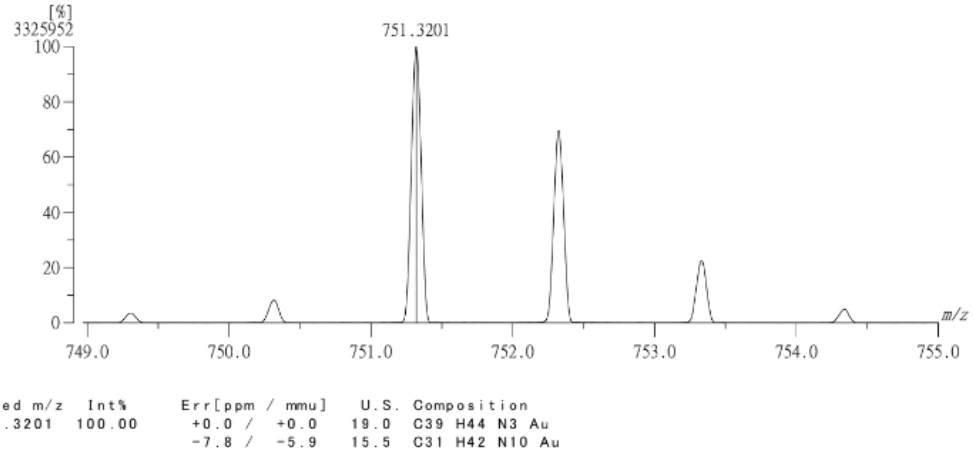

	Observed m/z	Int%	Err[ppm / mmu]	U.S.	Composition
1	751.3201	100.00	+0.0 / +0.0	19.0	C39 H44 N3 Au
2			-7.8 / -5.9	15.5	C31 H42 N10 Au

Fig. S31 | High-resolution mass spectrum (FAB, m-NBA, positive mode) of Au(^{Dipp}Im)(Cz).

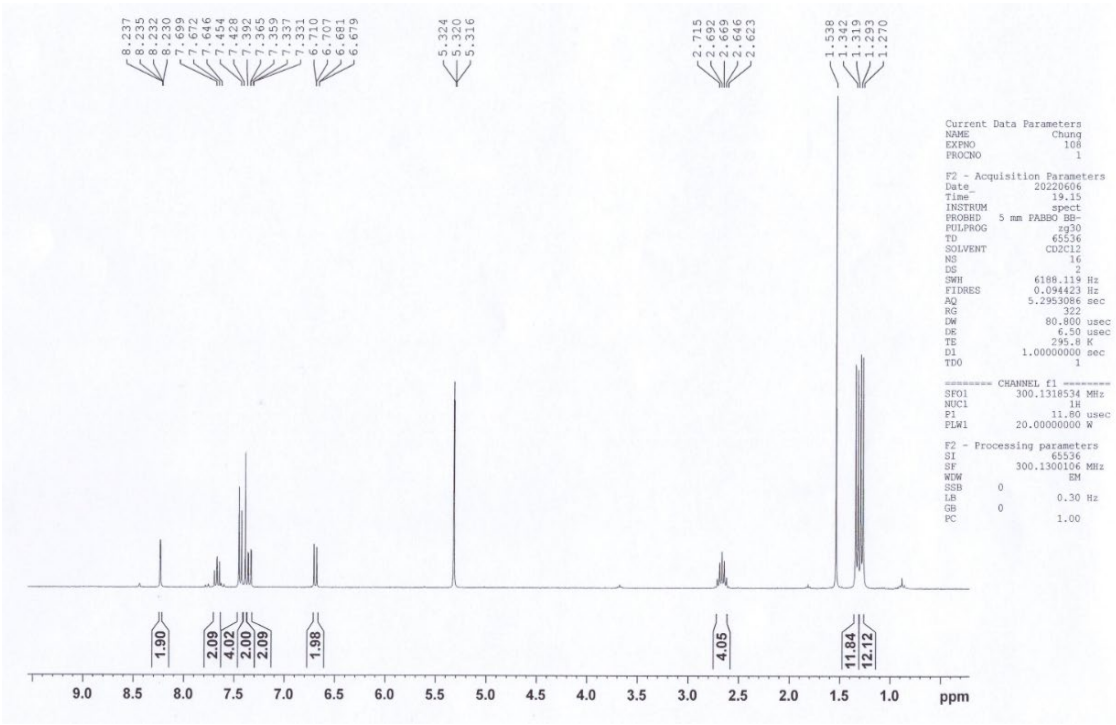

Fig. S32 | ^{1}H NMR (300 MHz, CD_2Cl_2) spectrum of Au(^{Dipp}Im)(CNCz).

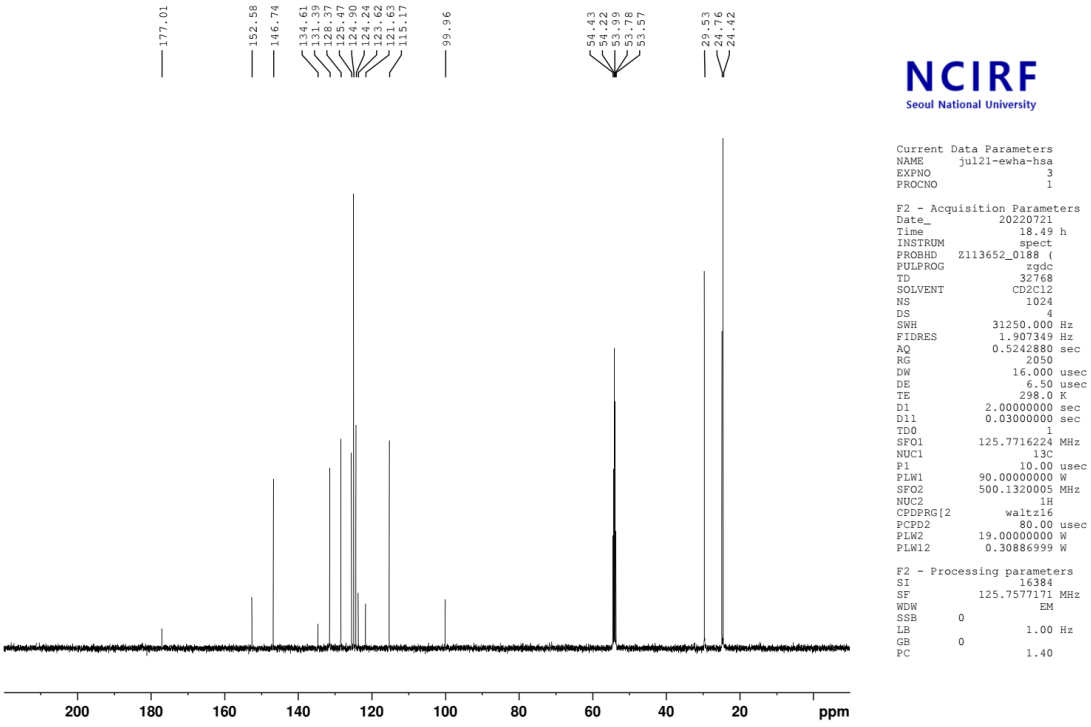

Fig. S33 | $^{13}C\{^{1}H\}$ NMR (126 MHz, CD_2Cl_2) spectrum of Au(^{Dipp}Im)(CNCz).

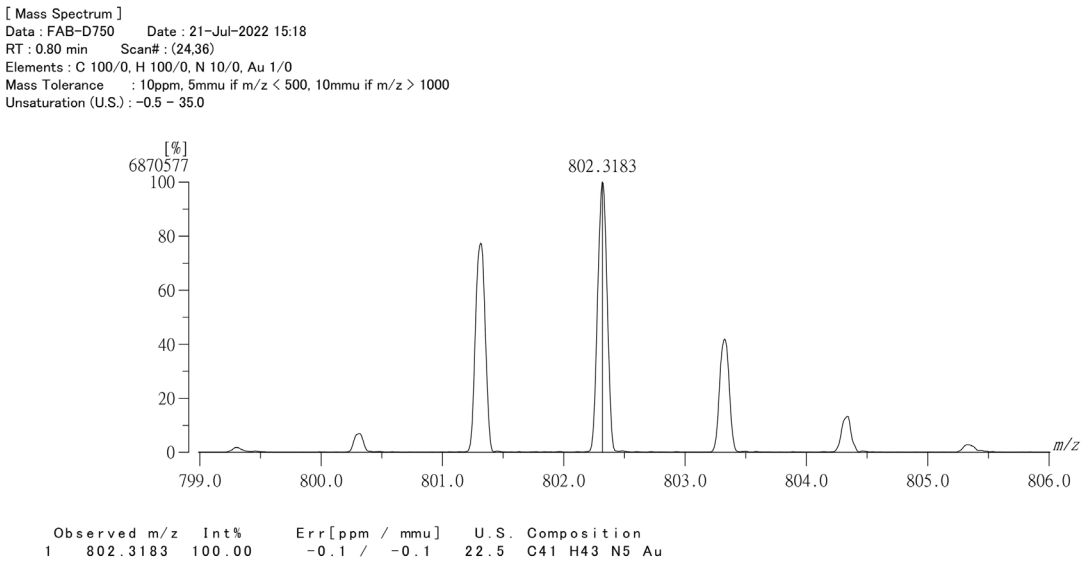

Fig. S34 | High-resolution mass spectrum (FAB, m-NBA, positive mode) of Au(^{Dipp}Im)(CNCz).

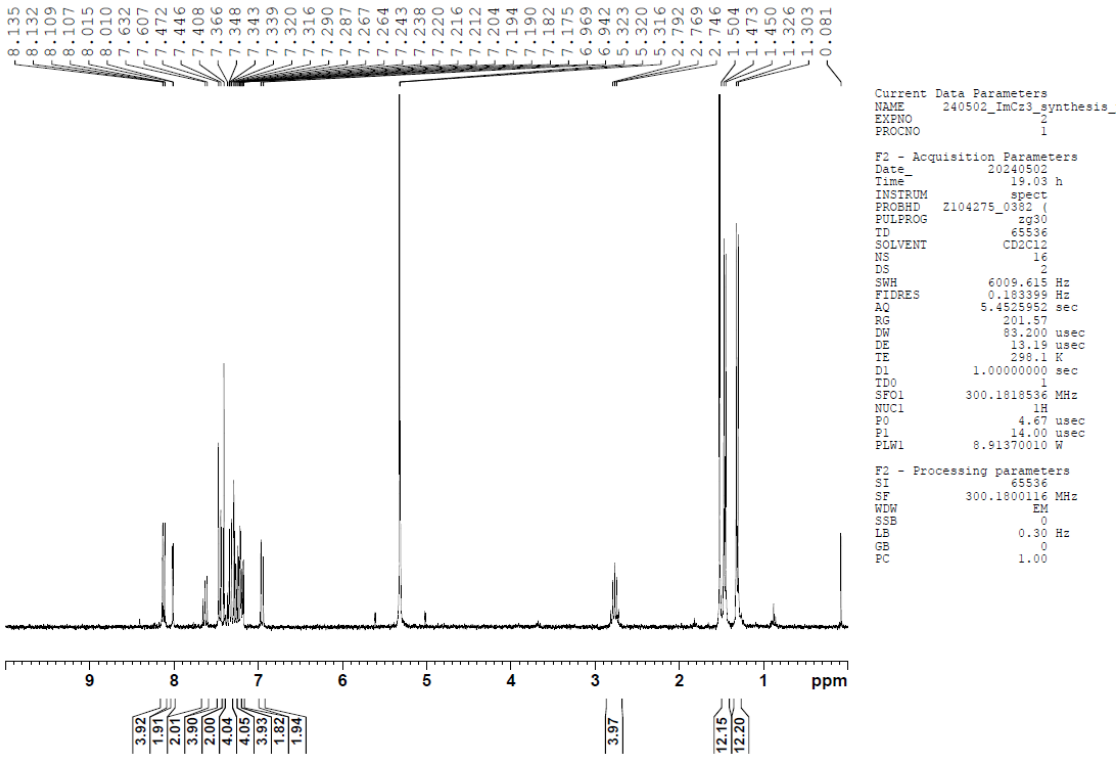

Fig. S35 | ^{1}H NMR (300 MHz, CD_2Cl_2) spectrum of Au(^{Dipp}Im)(Cz_3).

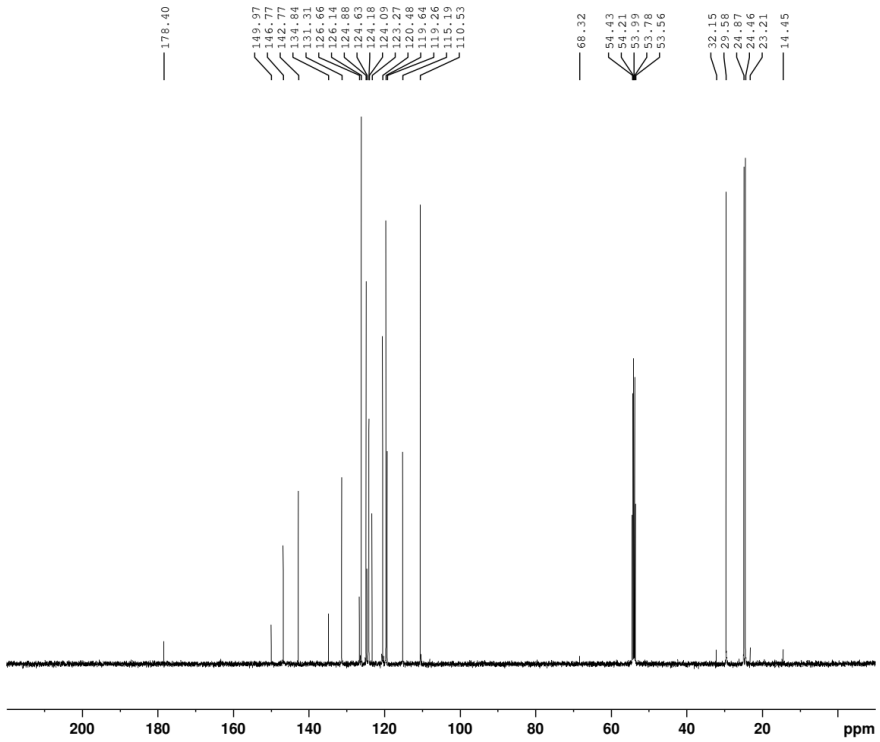

NCIRF
Seoul National University

```
Current Data Parameters
NAME      jul21-ewha-hsa
EXPNO                 1
PROCNO                1

F2 - Acquisition Parameters
Date_           20220722
Time               9.21 h
INSTRUM           spect
PROBHD   Z113652_0188 (
PULPROG           zgdc
TD               32768
SOLVENT          CD2Cl2
NS                2048
DS                   4
SWH          31250.000 Hz
FIDRES        1.907349 Hz
AQ           0.5242880 sec
RG                2050
DW              16.000 usec
DE               6.50 usec
TE              298.0 K
D1           2.00000000 sec
D11          0.03000000 sec
TD0                  1
SFO1       125.7716224 MHz
NUC1               13C
P1               10.00 usec
PLW1        90.00000000 W
SFO2       500.1320005 MHz
NUC2               1H
CPDPRG[2        waltz16
PCPD2            80.00 usec
PLW2        19.00000000 W
PLW12        0.30886999 W

F2 - Processing parameters
SI               16384
SF         125.7577178 MHz
WDW                EM
SSB       0
LB               1.00 Hz
GB        0
PC               1.40
```

Fig. S36 | $^{13}C\{^{1}H\}$ NMR (126 MHz, CD_2Cl_2) spectrum of Au(^{Dipp}Im)(Cz_3).

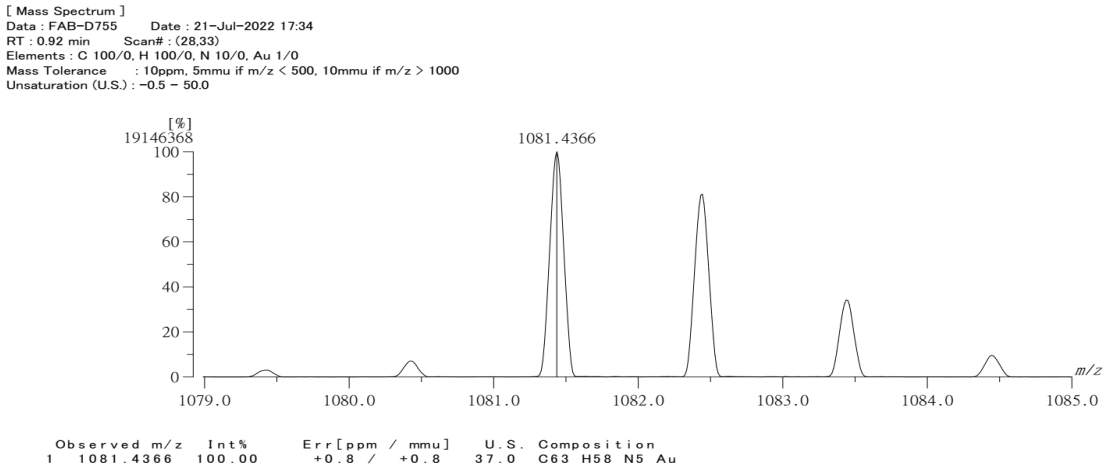

Fig. S37 | High-resolution mass spectrum (FAB, m-NBA, positive mode) of Au(^{Dipp}Im)(Cz_3).

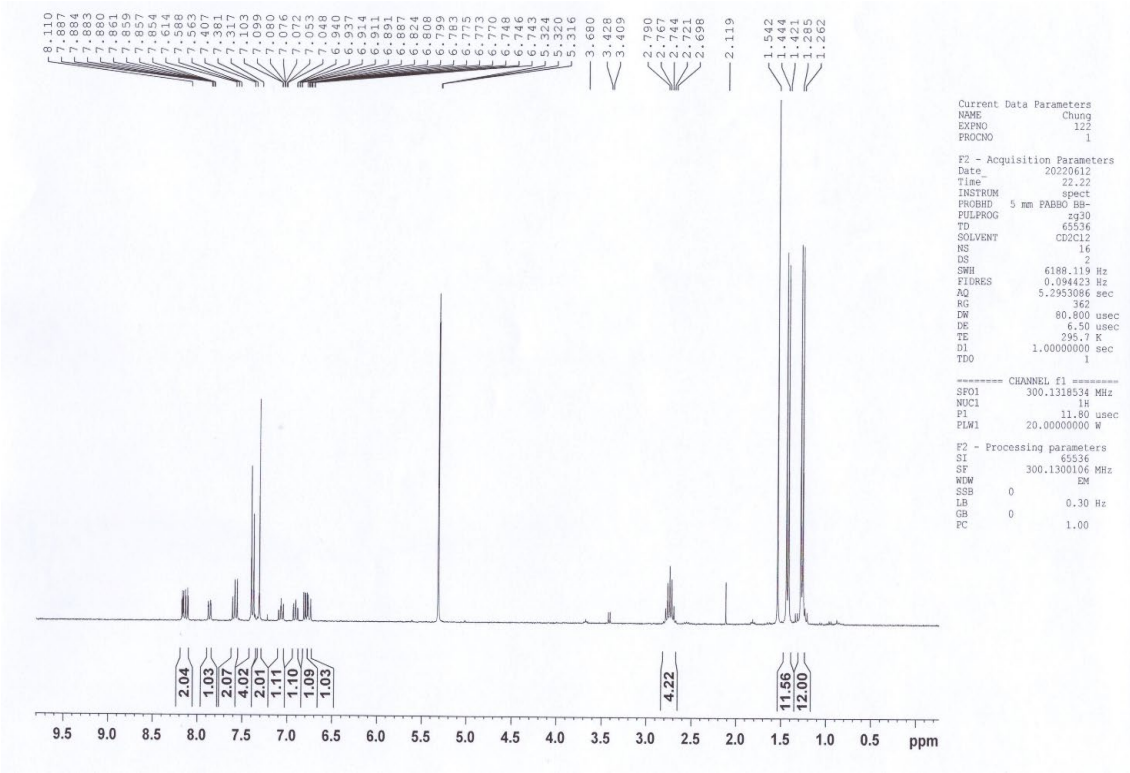

Fig. S38 | ^{1}H NMR (300 MHz, CD_2Cl_2) spectrum of Au(^{Dipp}Im)(αCb).

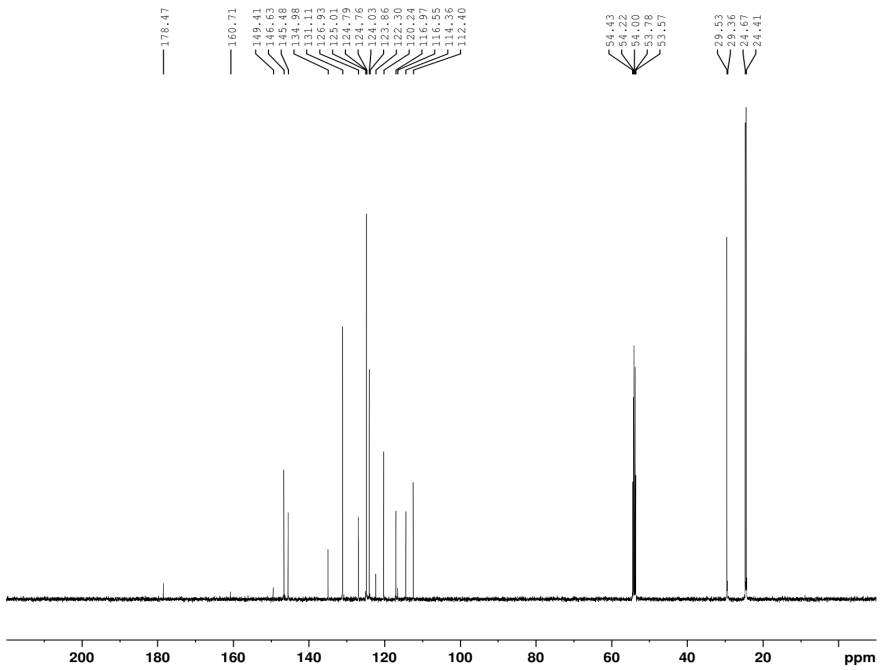

NCIRF
Seoul National University

```
Current Data Parameters
NAME      jul21-ewha-hsa
EXPNO                 4
PROCNO                1

F2 - Acquisition Parameters
Date_          20220722
Time              10.06 h
INSTRUM           spect
PROBHD   Z113652_0188 (
PULPROG           zgdc
TD               32768
SOLVENT          CD2Cl2
NS                1969
DS                   4
SWH          31250.000 Hz
FIDRES        1.907349 Hz
AQ            0.5242880 sec
RG                2050
DW              16.000 usec
DE               6.50 usec
TE              298.0 K
D1           2.00000000 sec
D11          0.03000000 sec
TD0                  1
SFO1       125.7716224 MHz
NUC1              13C
P1              10.00 usec
PLW1       90.00000000 W
SFO2       500.1320005 MHz
NUC2              1H
CPDPRG[2       waltz16
PCPD2            80.00 usec
PLW2       19.00000000 W
PLW12       0.30886999 W

F2 - Processing parameters
SI               16384
SF         125.7577173 MHz
WDW                EM
SSB       0
LB               1.00 Hz
GB        0
PC               1.40
```

Fig. S39 | $^{13}C\{^{1}H\}$ NMR (126 MHz, CD_2Cl_2) spectrum of Au(^{Dipp}Im)(αCb).

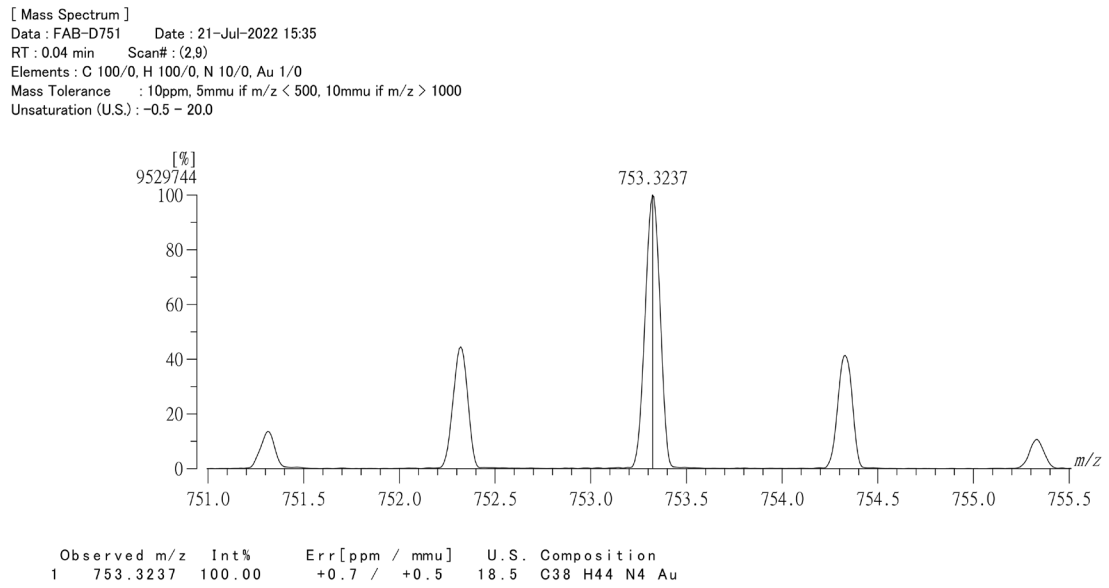

Fig. S40 | High-resolution mass spectrum (FAB, m-NBA, positive mode) of Au(^{Dipp}Im)(αCb).

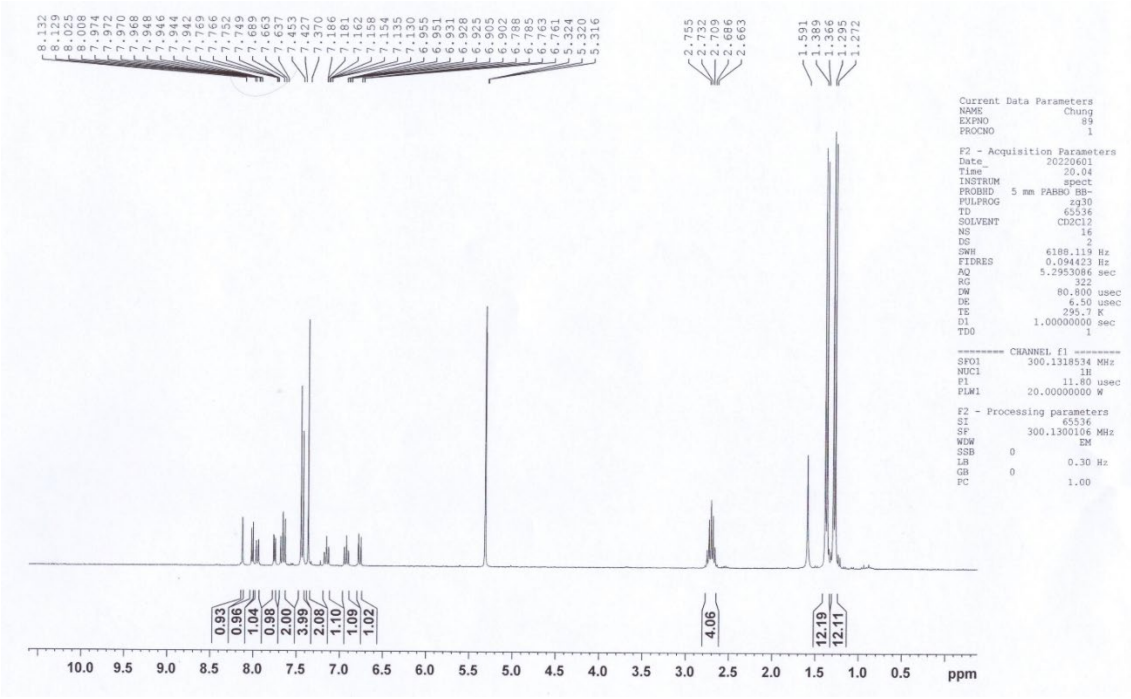

Fig. S41 | ^{1}H NMR (300 MHz, CD_2Cl_2) spectrum of Au(^{Dipp}Im)(βCb).

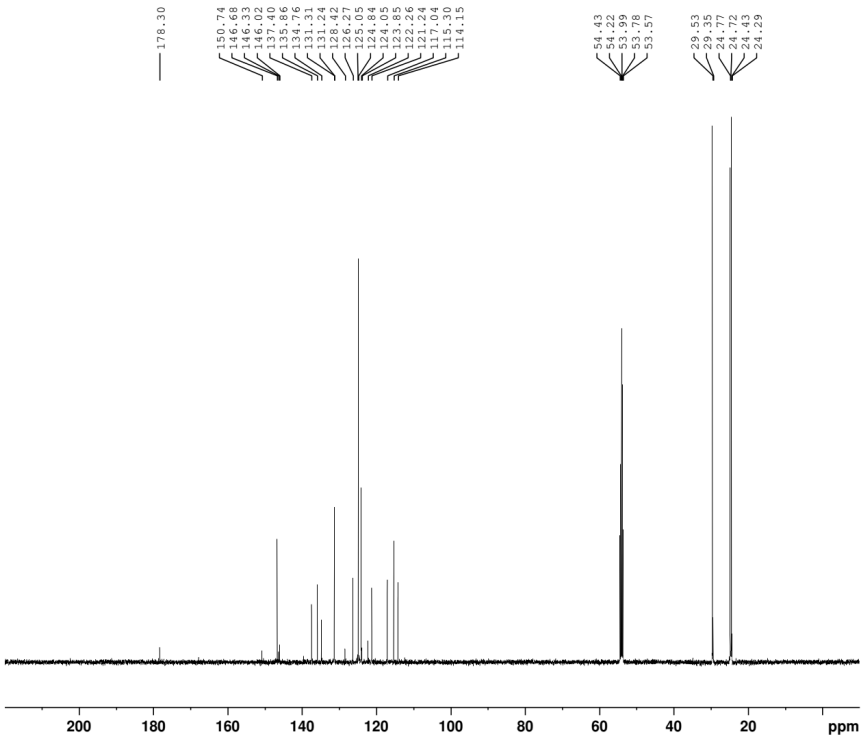

NCIRF
Seoul National University

```
Current Data Parameters
NAME      jul21-ewha-hsa
EXPNO                 5
PROCNO                1

F2 - Acquisition Parameters
Date_          20220722
Time              10.55 h
INSTRUM            spect
PROBHD   Z113652_0188 (
PULPROG            zgdc
TD                32768
SOLVENT          CD2Cl2
NS                 2048
DS                    4
SWH           31250.000 Hz
FIDRES         1.907349 Hz
AQ            0.5242880 sec
RG                 2050
DW               16.000 usec
DE                6.50 usec
TE                298.0 K
D1            2.00000000 sec
D11           0.03000000 sec
TD0                   1
SFO1         125.7716224 MHz
NUC1                 13C
P1                10.00 usec
PLW1         90.00000000 W
SFO2         500.1320005 MHz
NUC2                  1H
CPDPRG[2         waltz16
PCPD2             80.00 usec
PLW2         19.00000000 W
PLW12         0.30886999 W

F2 - Processing parameters
SI                16384
SF           125.7577171 MHz
WDW                  EM
SSB       0
LB                1.00 Hz
GB        0
PC                1.40
```

Fig. S42 | $^{13}C\{^{1}H\}$ NMR (126 MHz, CD_2Cl_2) spectrum of Au(^{Dipp}Im)(βCb).

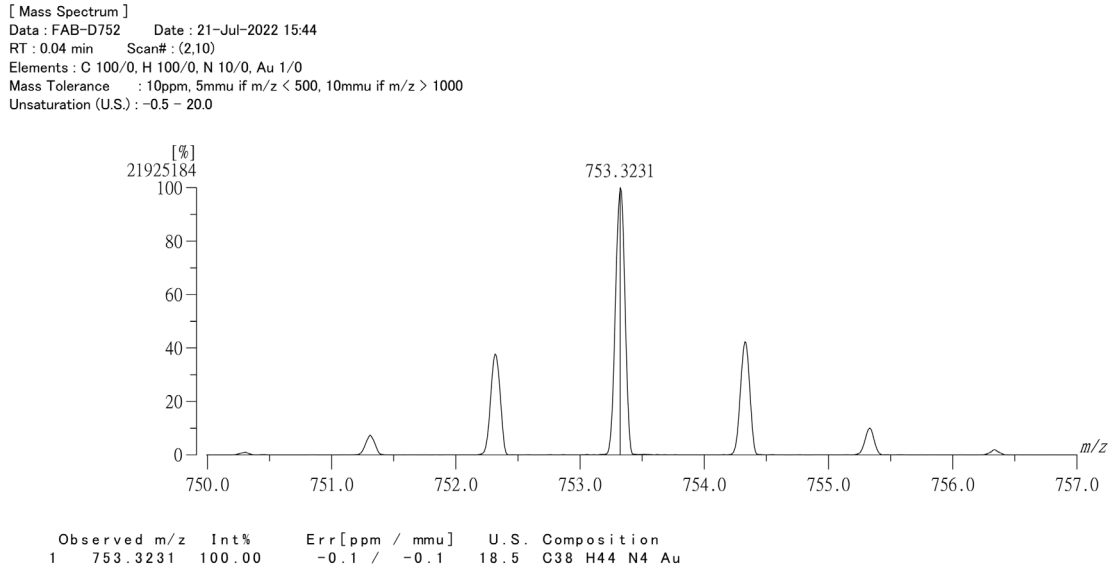

Fig. S43 | High-resolution mass spectrum (FAB, m-NBA, positive mode) of Au(^{Dipp}Im)(βCb).

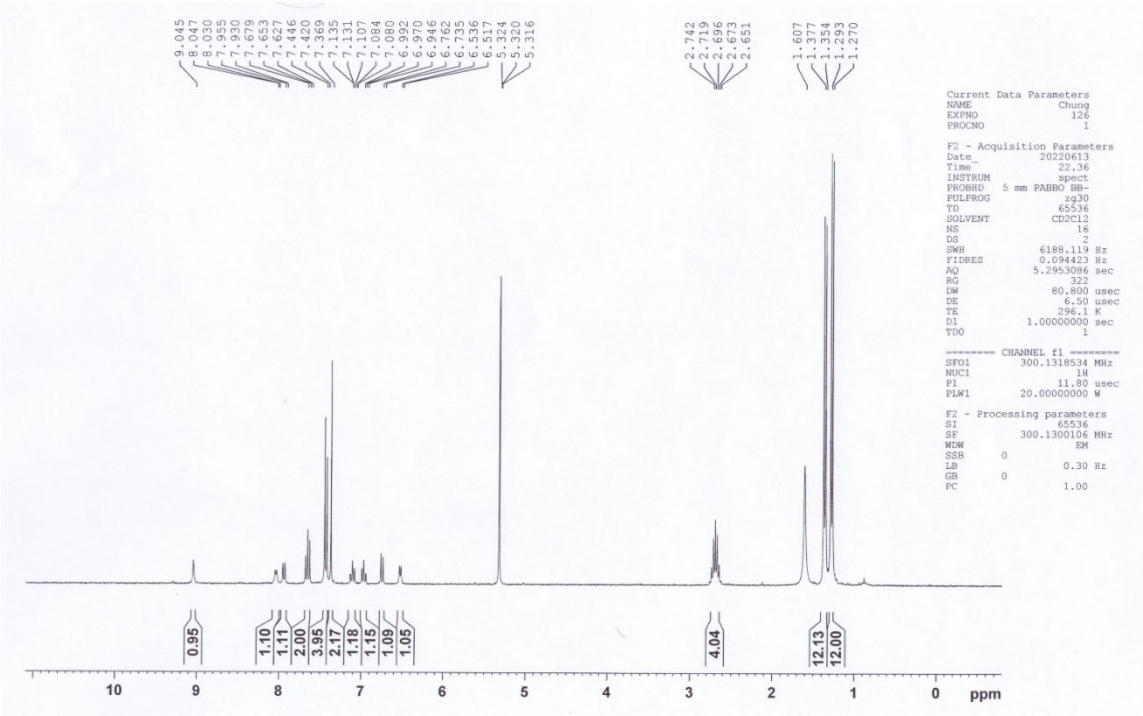

Fig. S344 | ^{1}H NMR (300 MHz, CD_2Cl_2) spectrum of Au(^{Dipp}Im)(γCb).

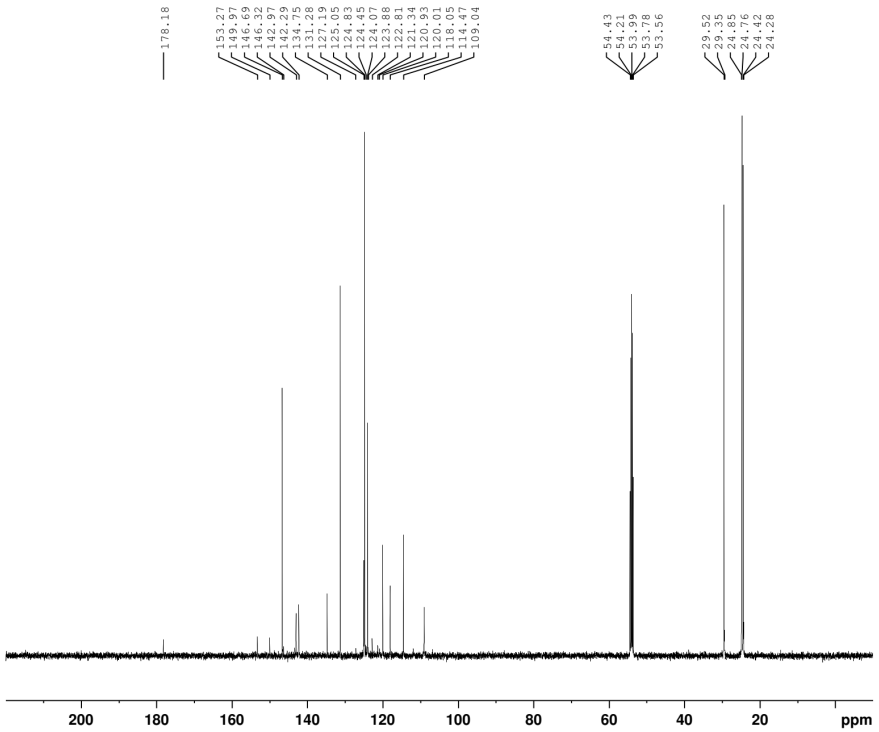

NCIRF
Seoul National University

```
Current Data Parameters
NAME      jul21-ewha-hsa
EXPNO                 6
PROCNO                1

F2 - Acquisition Parameters
Date_           20220722
Time              16.53 h
INSTRUM             spect
PROBHD   Z113652_0188 (
PULPROG             zgdc
TD                 32768
SOLVENT           CD2Cl2
NS                  1930
DS                     4
SWH            31250.000 Hz
FIDRES          1.907349 Hz
AQ              0.5242880 sec
RG                  2050
DW                16.000 usec
DE                 6.50 usec
TE                298.0 K
D1             2.00000000 sec
D11            0.03000000 sec
TD0                    1
SFO1         125.7716224 MHz
NUC1                 13C
P1                 10.00 usec
PLW1         90.00000000 W
SFO2         500.1320005 MHz
NUC2                 1H
CPDPRG[2          waltz16
PCPD2              80.00 usec
PLW2         19.00000000 W
PLW12         0.30886999 W

F2 - Processing parameters
SI                 16384
SF           125.7577175 MHz
WDW                   EM
SSB       0
LB                 1.00 Hz
GB        0
PC                 1.40
```

Fig. S45 | $^{13}C\{^{1}H\}$ NMR (126 MHz, CD_2Cl_2) spectrum of Au(^{Dipp}Im)(γCb).

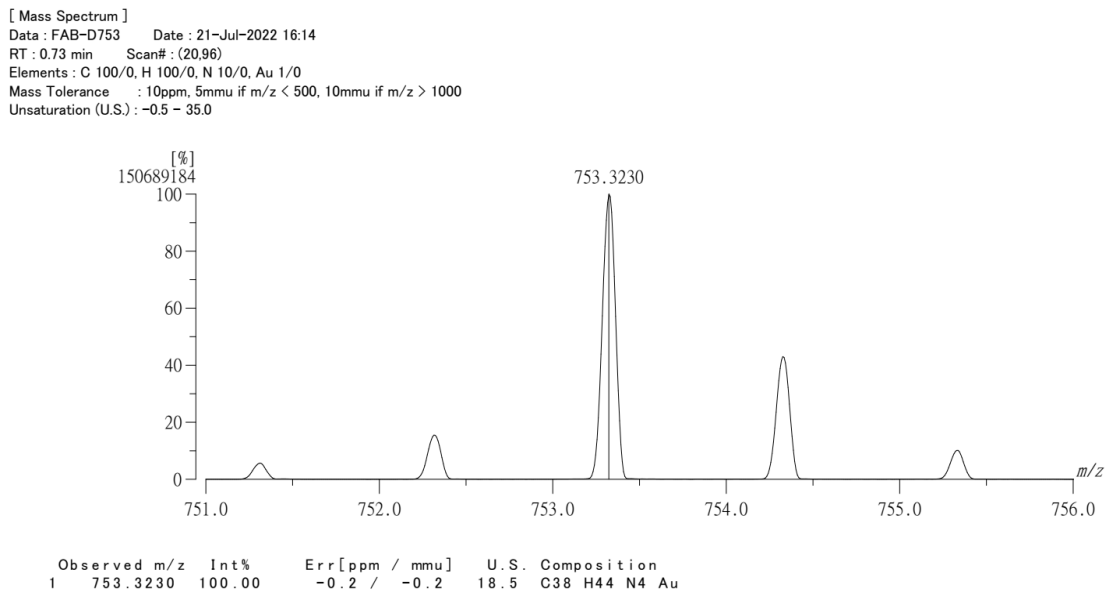

Fig. S46 | High-resolution mass spectrum (FAB, m-NBA, positive mode) of Au(^{Dipp}Im)(γCb).

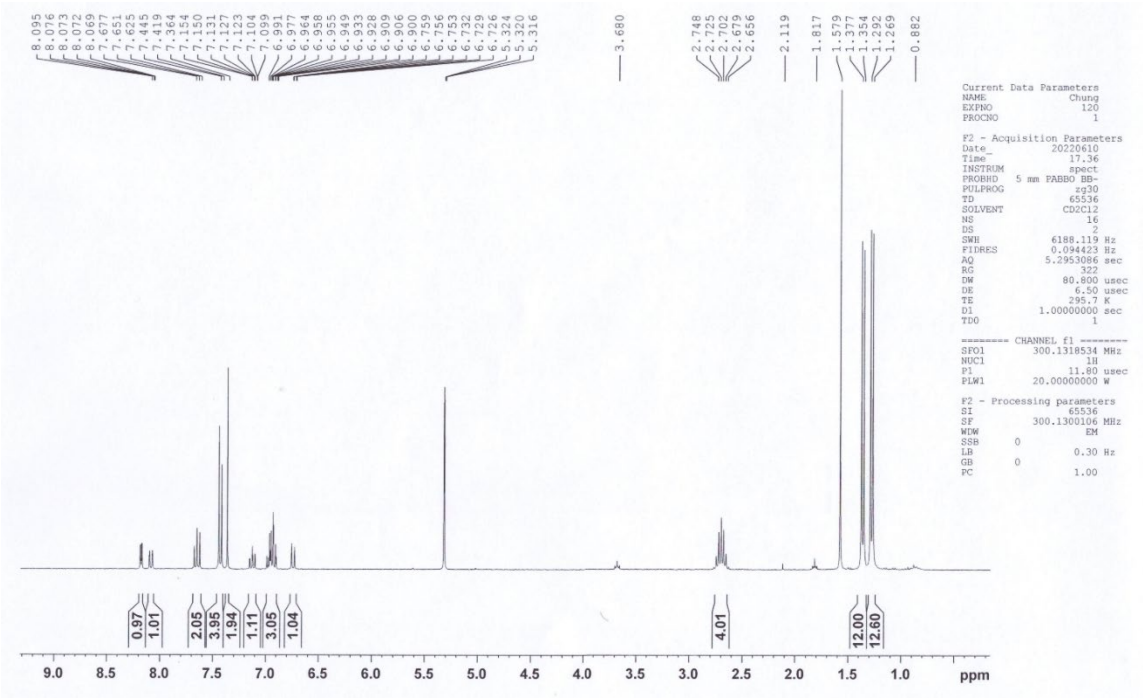

Fig. S47 | ^{1}H NMR (300 MHz, CD_2Cl_2) spectrum of Au(^{Dipp}Im)(δCb).

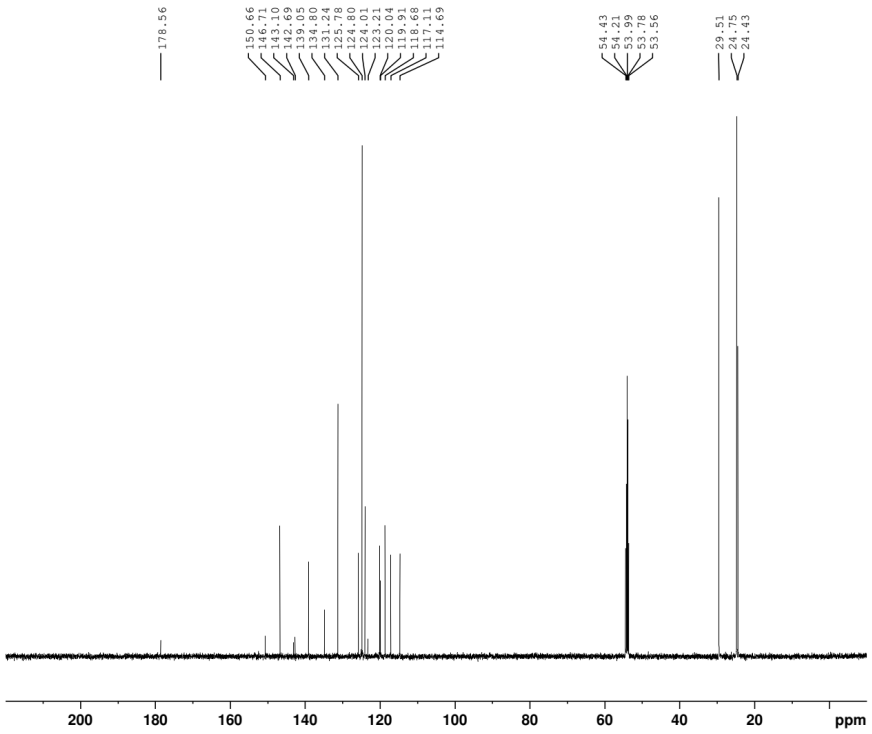

NCIRF
Seoul National University

```
Current Data Parameters
NAME      jul21-ewha-hsa
EXPNO                   7
PROCNO                  1

F2 - Acquisition Parameters
Date_           20220721
Time              22.01 h
INSTRUM             spect
PROBHD   Z113652_0188 (
PULPROG             zgdc
TD                 32768
SOLVENT           CD2Cl2
NS                   1024
DS                      4
SWH            31250.000 Hz
FIDRES          1.907349 Hz
AQ             0.5242880 sec
RG                   2050
DW                16.000 usec
DE                 6.50 usec
TE                298.0 K
D1             2.00000000 sec
D11            0.03000000 sec
TD0                     1
SFO1         125.7716224 MHz
NUC1                 13C
P1                 10.00 usec
PLW1          90.00000000 W
SFO2         500.1320005 MHz
NUC2                 1H
CPDPRG[2         waltz16
PCPD2              80.00 usec
PLW2          19.00000000 W
PLW12          0.30886999 W

F2 - Processing parameters
SI                  16384
SF           125.7577173 MHz
WDW                    EM
SSB       0
LB                 1.00 Hz
GB        0
PC                 1.40
```

Fig. S48 | $^{13}C\{^{1}H\}$ NMR (126 MHz, CD_2Cl_2) spectrum of Au(^{Dipp}Im)(δCb).

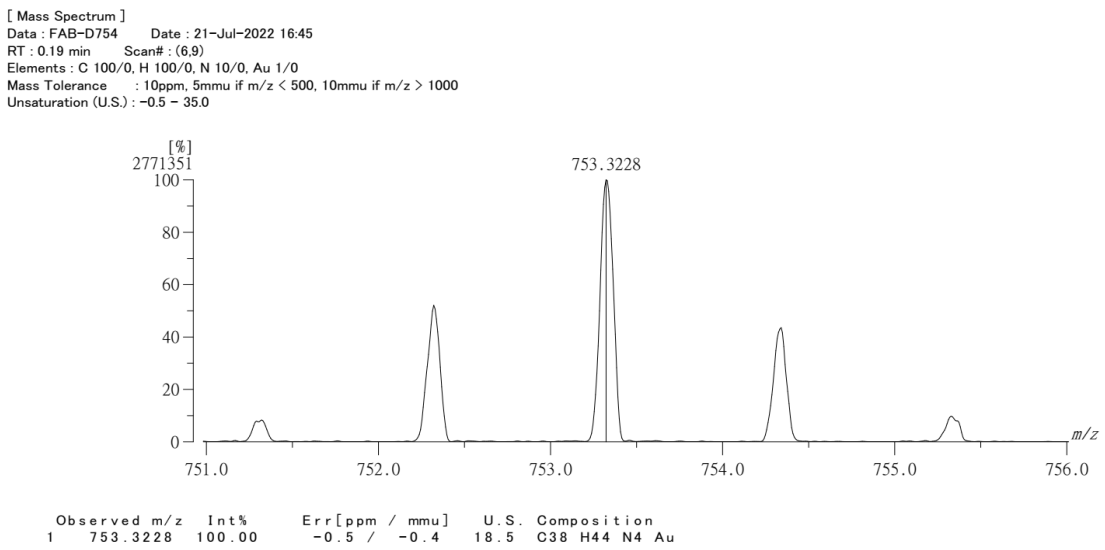

Fig. S49 | High-resolution mass spectrum (FAB, m-NBA, positive mode) of Au(^{Dipp}Im)(δCb).

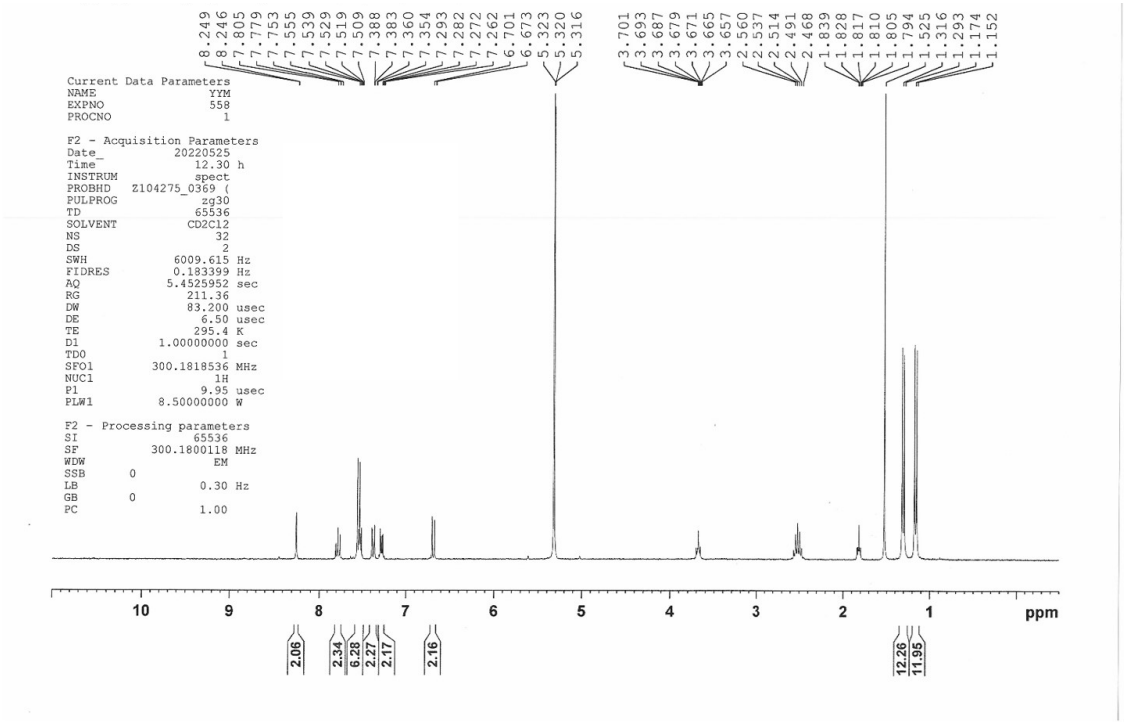

Fig. S50 | ^{1}H NMR (300 MHz, CD_2Cl_2) spectrum of Au(^{Dipp}BZI)(CNCz).

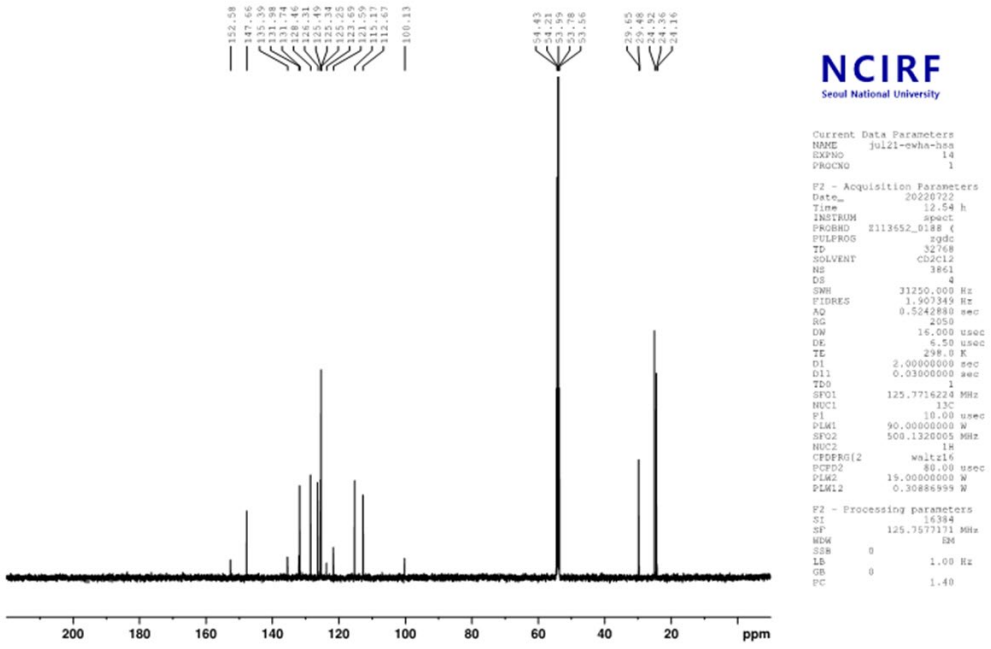

Fig. S51 | $^{13}C\{^{1}H\}$ NMR (126 MHz, CD_2Cl_2) spectrum of Au(^{Dipp}BZI)(CNCz).

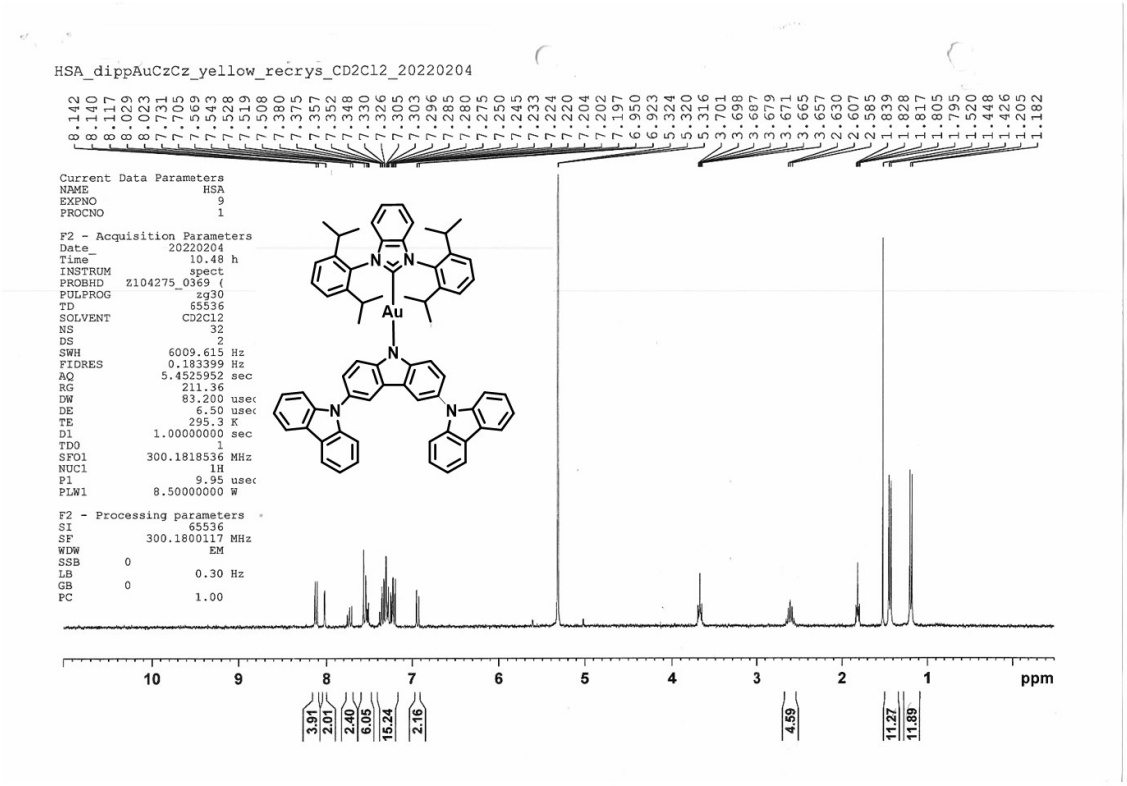

Fig. S52 | ^{1}H NMR (300 MHz, CD_2Cl_2) spectrum of Au(^{Dipp}BZI)(Cz_3).

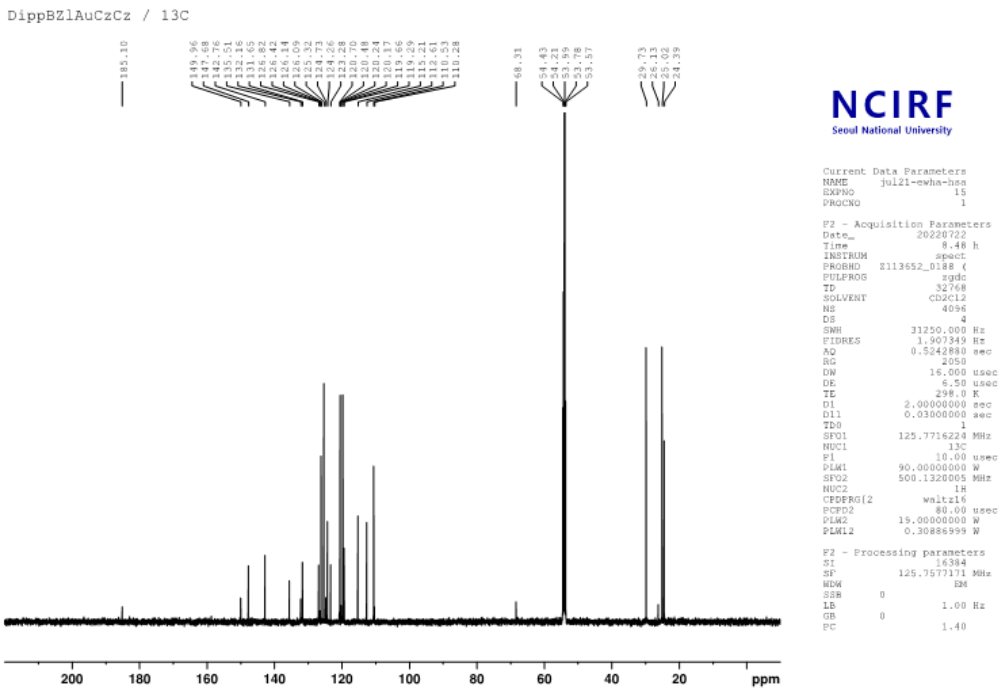

Fig. S53 | $^{13}C\{^{1}H\}$ NMR (126 MHz, CD_2Cl_2) spectrum of Au(^{Dipp}BZI)(Cz_3).

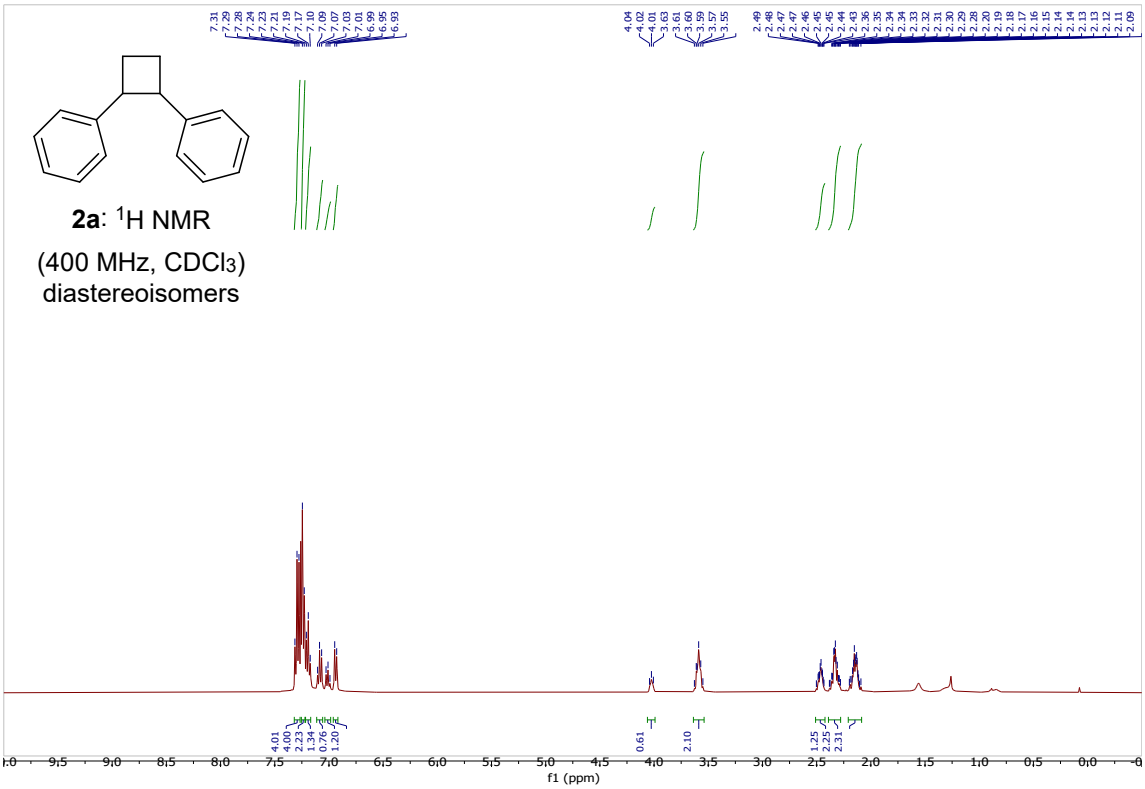

Fig. S54 | ^{1}H NMR (400 MHz, $CDCl_3$) spectrum of **2a**.

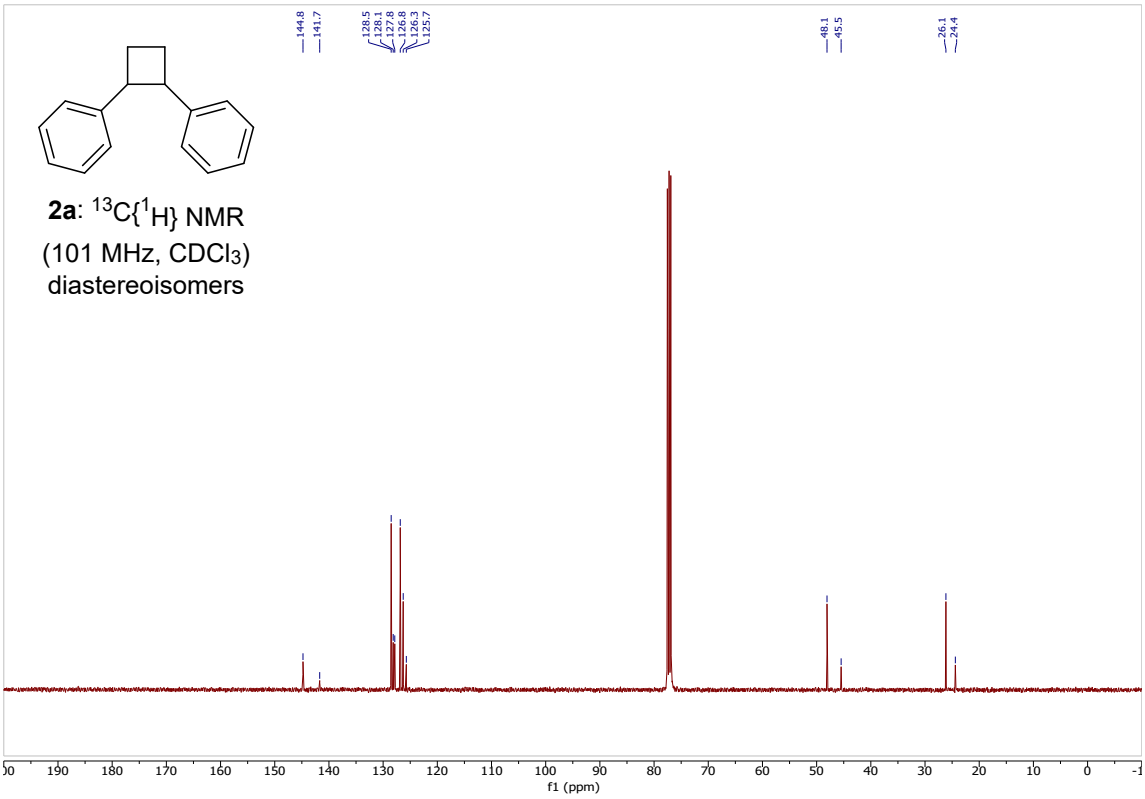

Fig. S55 | $^{13}C\{^{1}H\}$ NMR (101 MHz, $CDCl_3$) spectrum of **2a**.

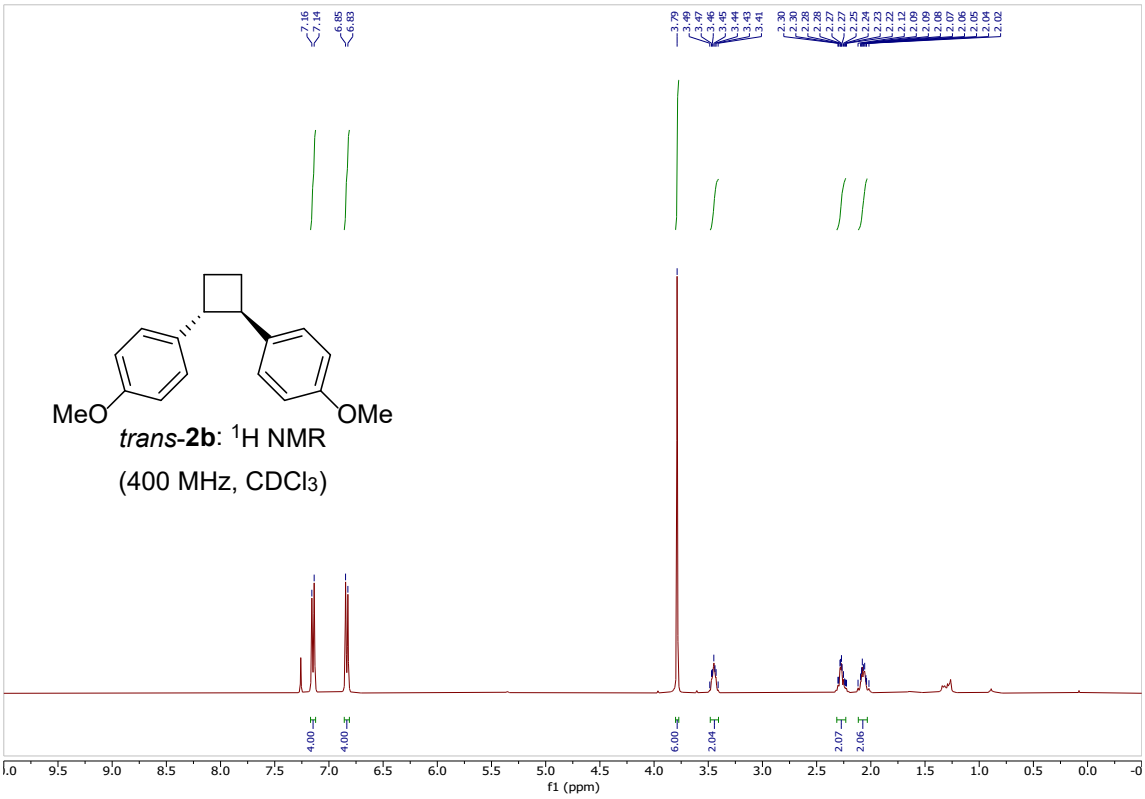

Fig. S56 | ^{1}H NMR (400 MHz, $CDCl_3$) spectrum of ***trans*-2b**.

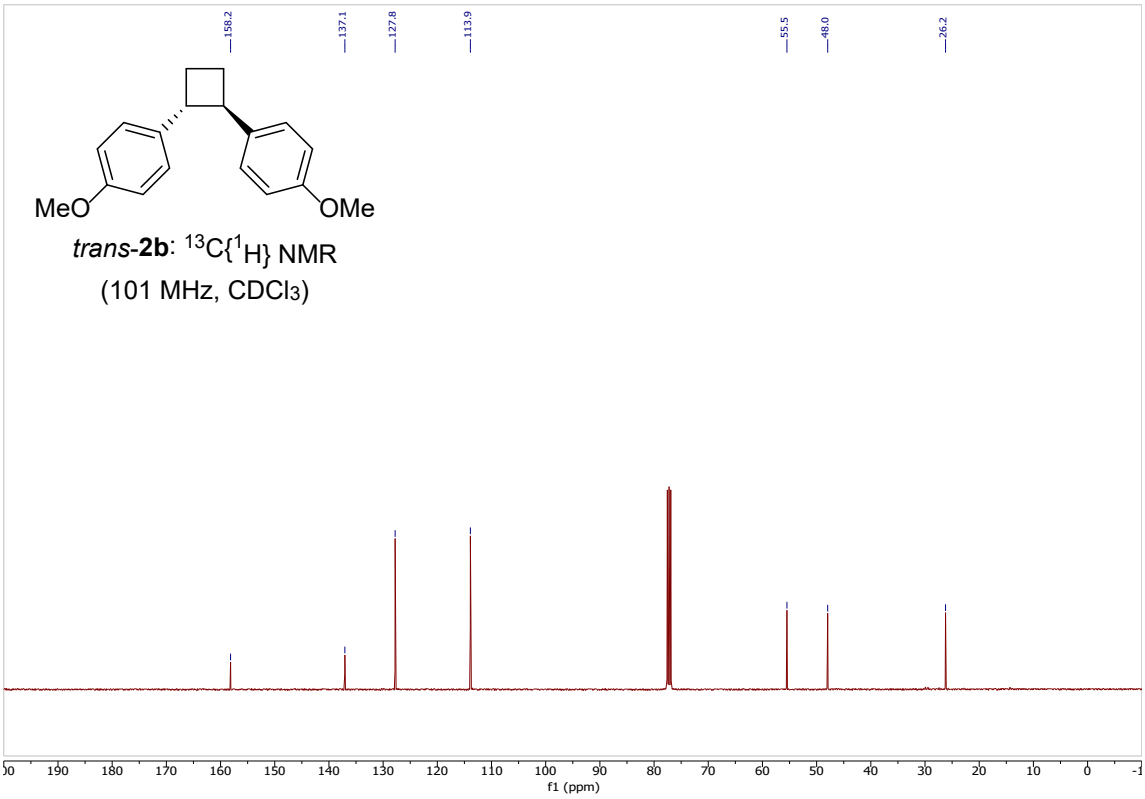

Fig. S57 | $^{13}C\{^{1}H\}$ NMR (101 MHz, $CDCl_3$) spectrum of ***trans*-2b**.

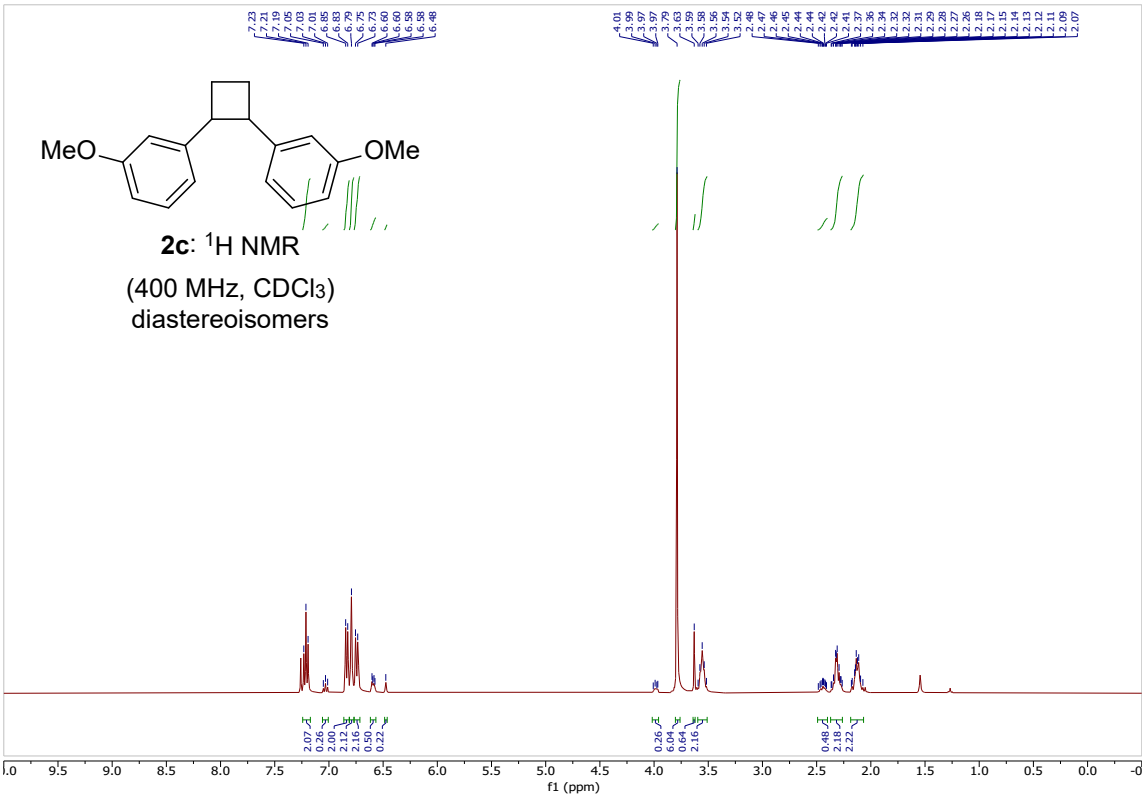

Fig. S58 | ^{1}H NMR (400 MHz, $CDCl_3$) spectrum of **2c**.

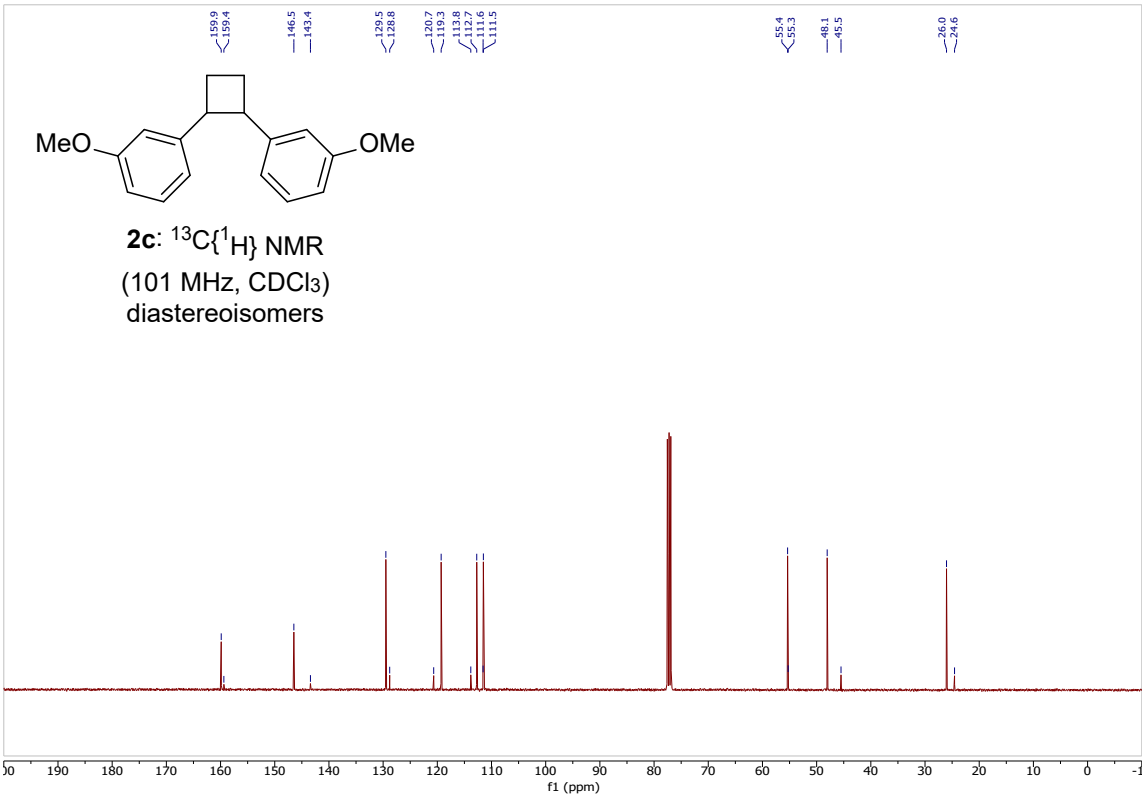

Fig. S59 | $^{13}C\{^{1}H\}$ NMR (101 MHz, $CDCl_3$) spectrum of **2c**.

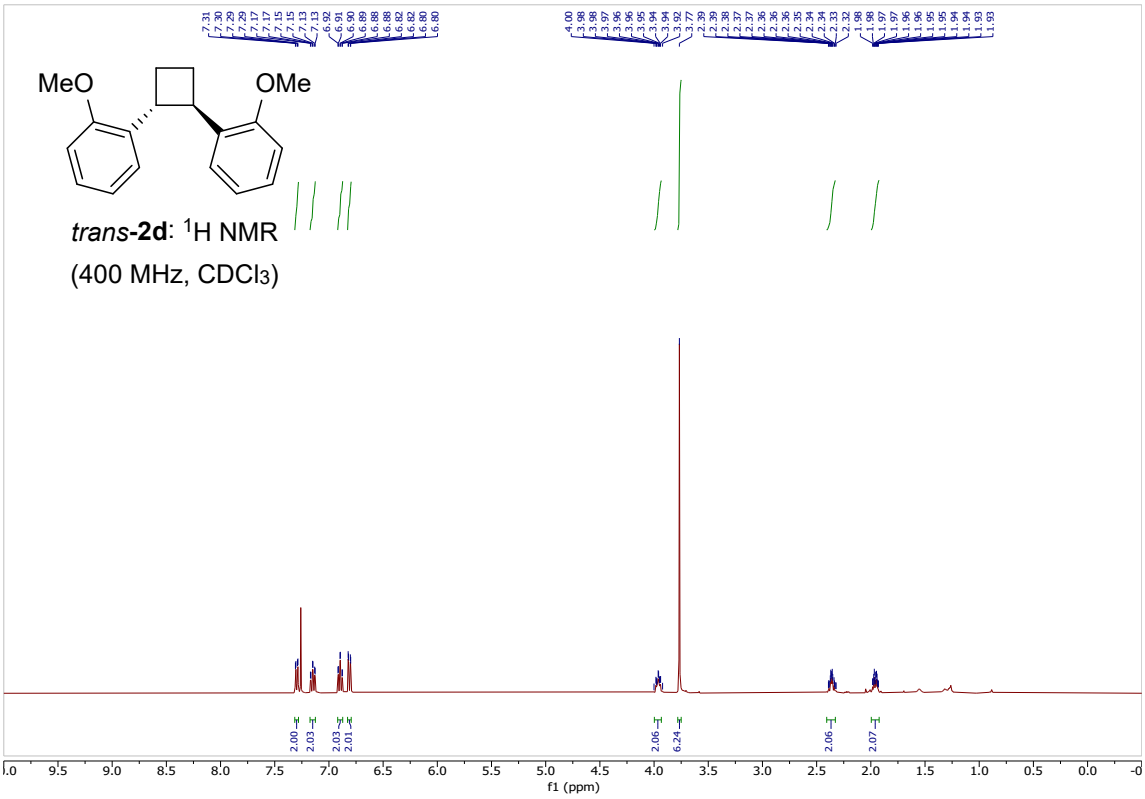

Fig. S60 | ^{1}H NMR (400 MHz, $CDCl_3$) spectrum of ***trans*-2d**.

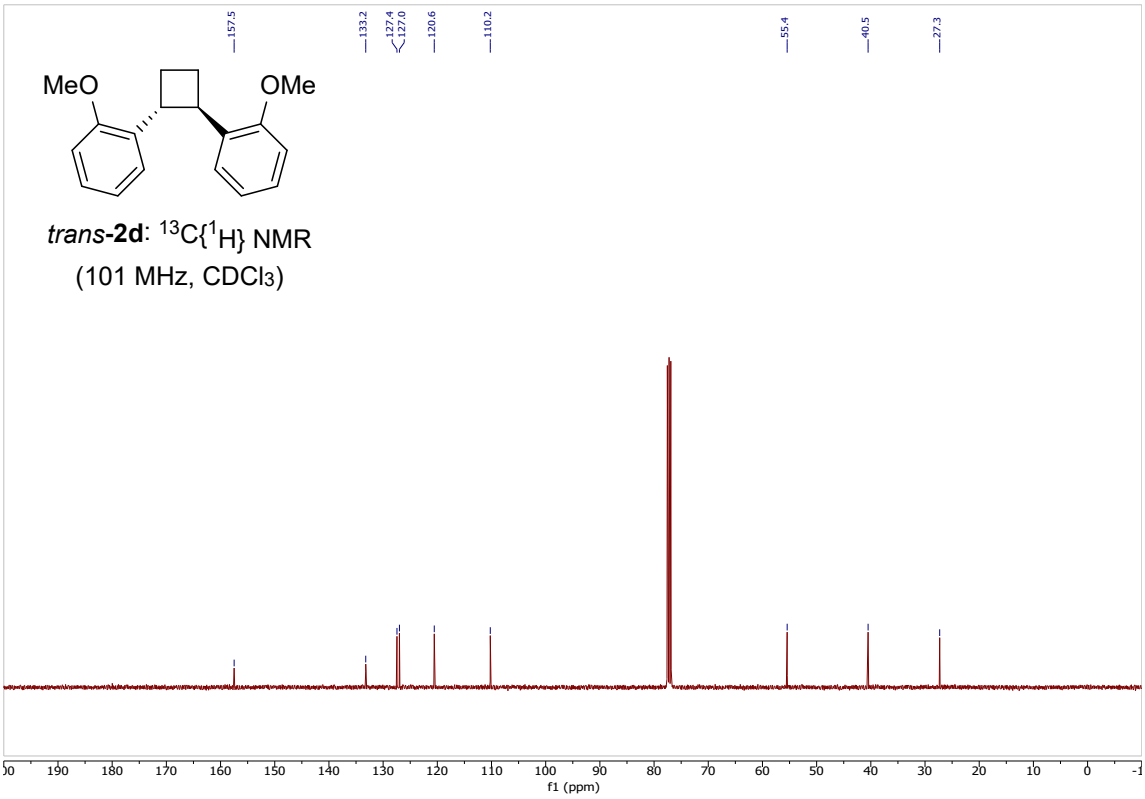

Fig. S61 | $^{13}C\{^{1}H\}$ NMR (101 MHz, $CDCl_3$) spectrum of ***trans*-2d**.

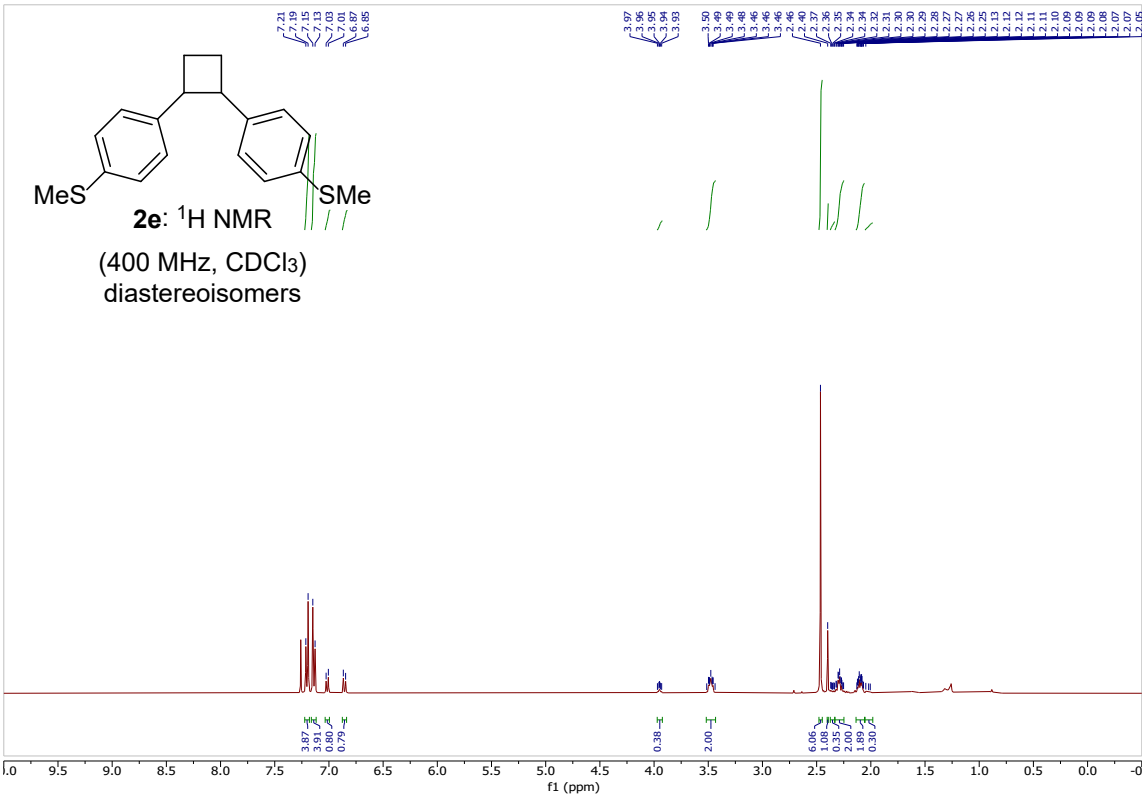

Fig. S62 | ^{1}H NMR (400 MHz, $CDCl_3$) spectrum of **2e**.

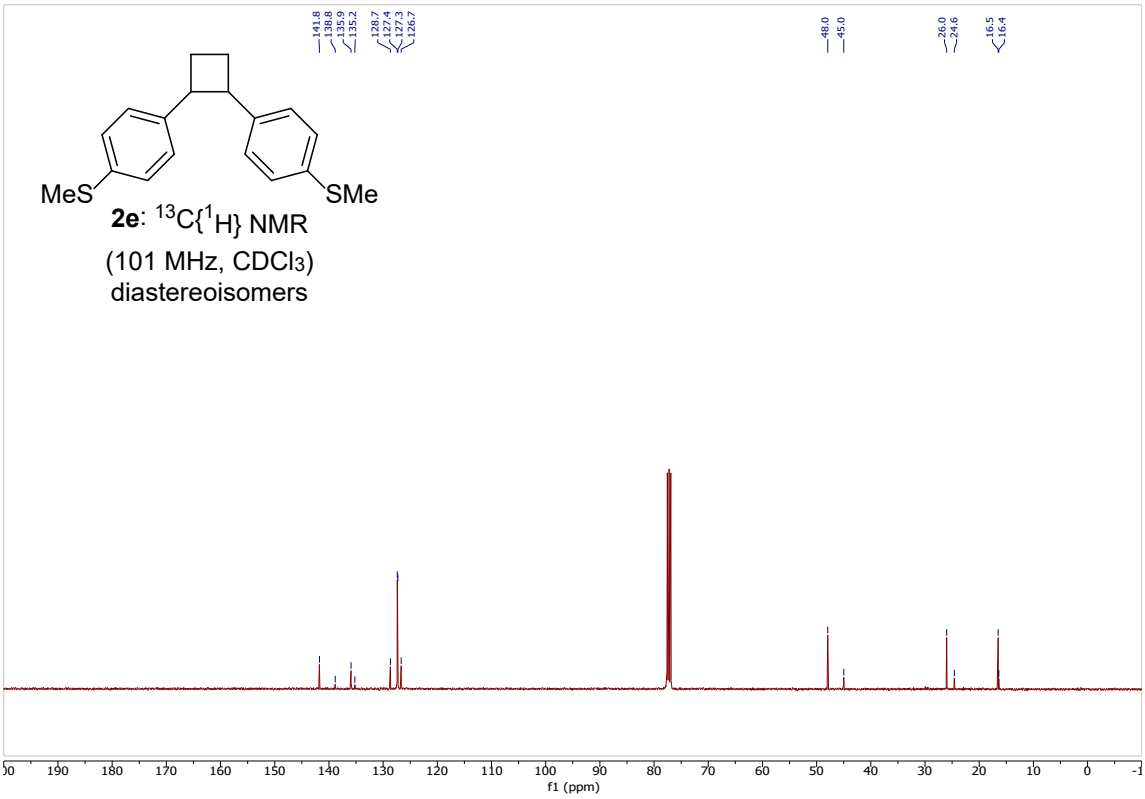

Fig. S63 | $^{13}C\{^{1}H\}$ NMR (101 MHz, $CDCl_3$) spectrum of **2e**.

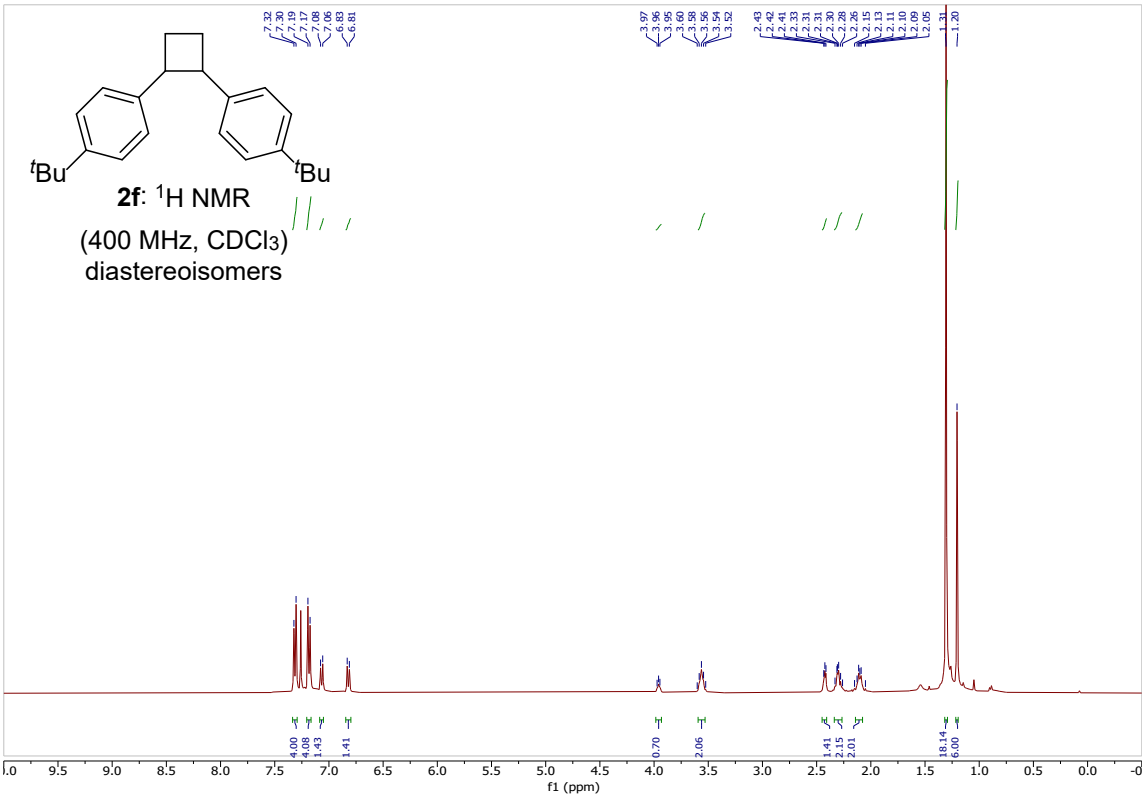

Fig. S64 | ^{1}H NMR (400 MHz, $CDCl_3$) spectrum of **2f**.

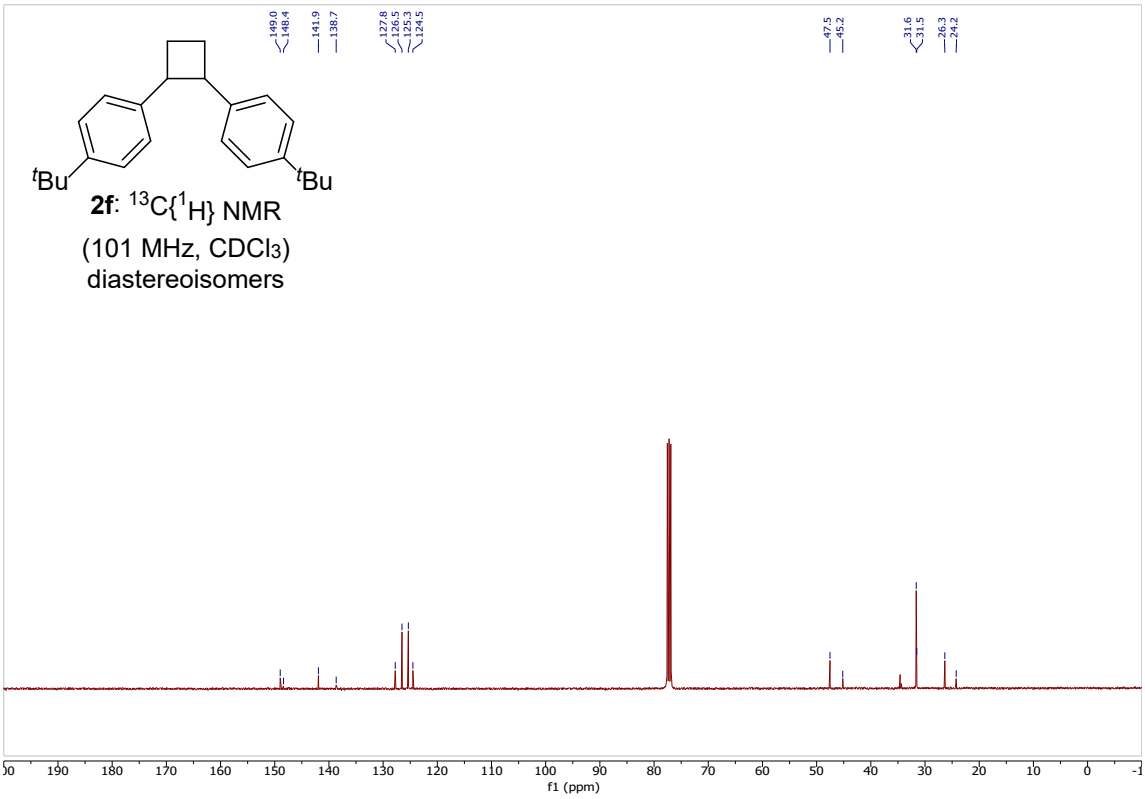

Fig. S65 | $^{13}C\{^{1}H\}$ NMR (101 MHz, $CDCl_3$) spectrum of **2f**.

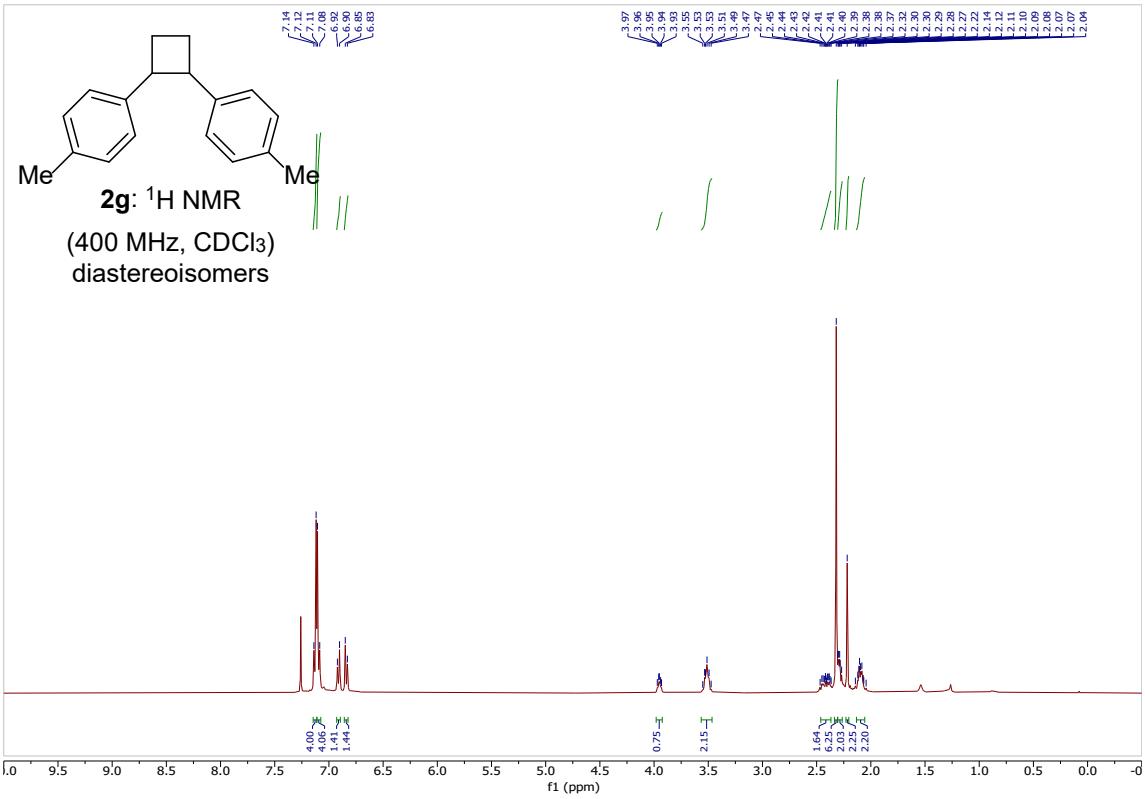

Fig. S66 | ^{1}H NMR (400 MHz, $CDCl_3$) spectrum of **2g**.

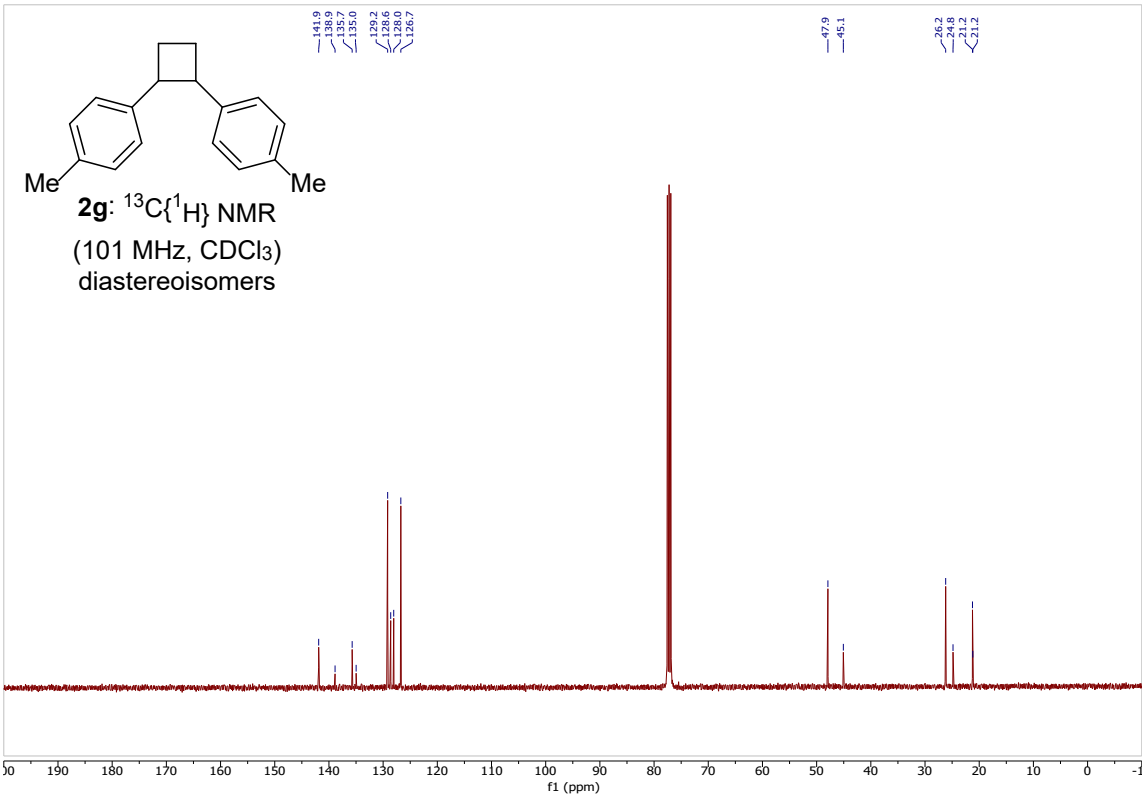

Fig. S67 | $^{13}C\{^{1}H\}$ NMR (101 MHz, $CDCl_3$) spectrum of **2g**.

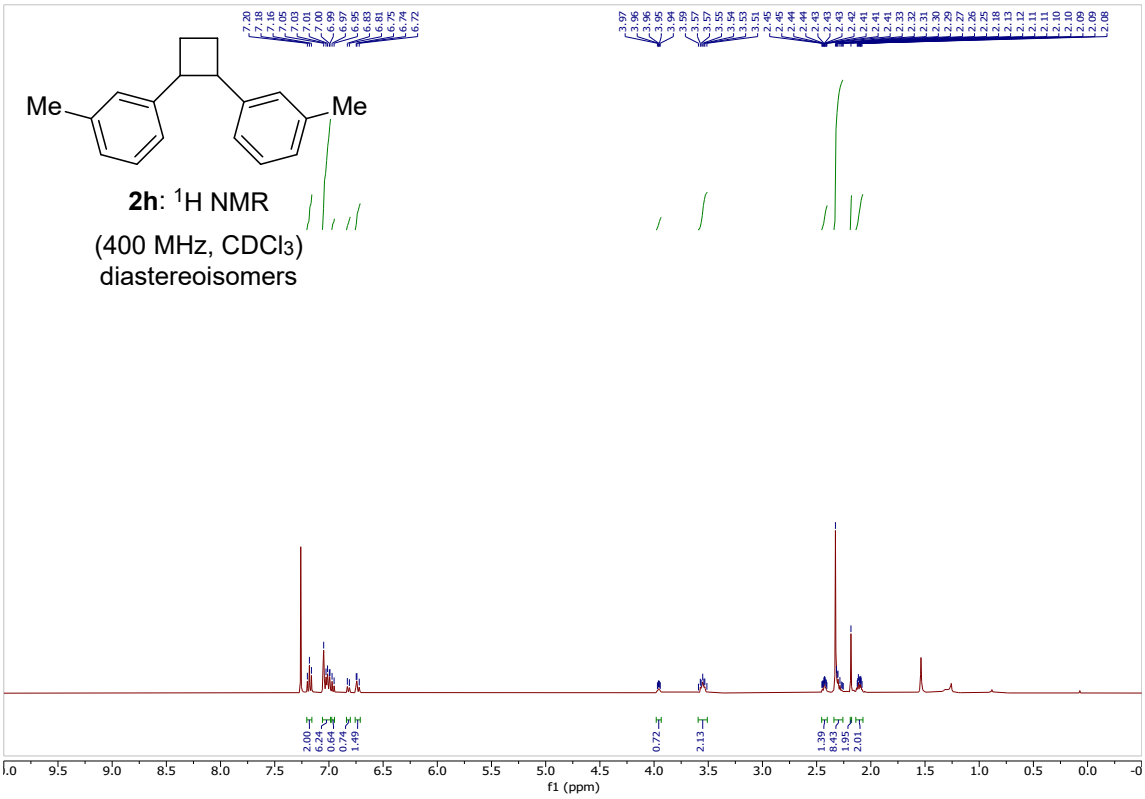

Fig. S68 | ^{1}H NMR (400 MHz, $CDCl_3$) spectrum of **2h**.

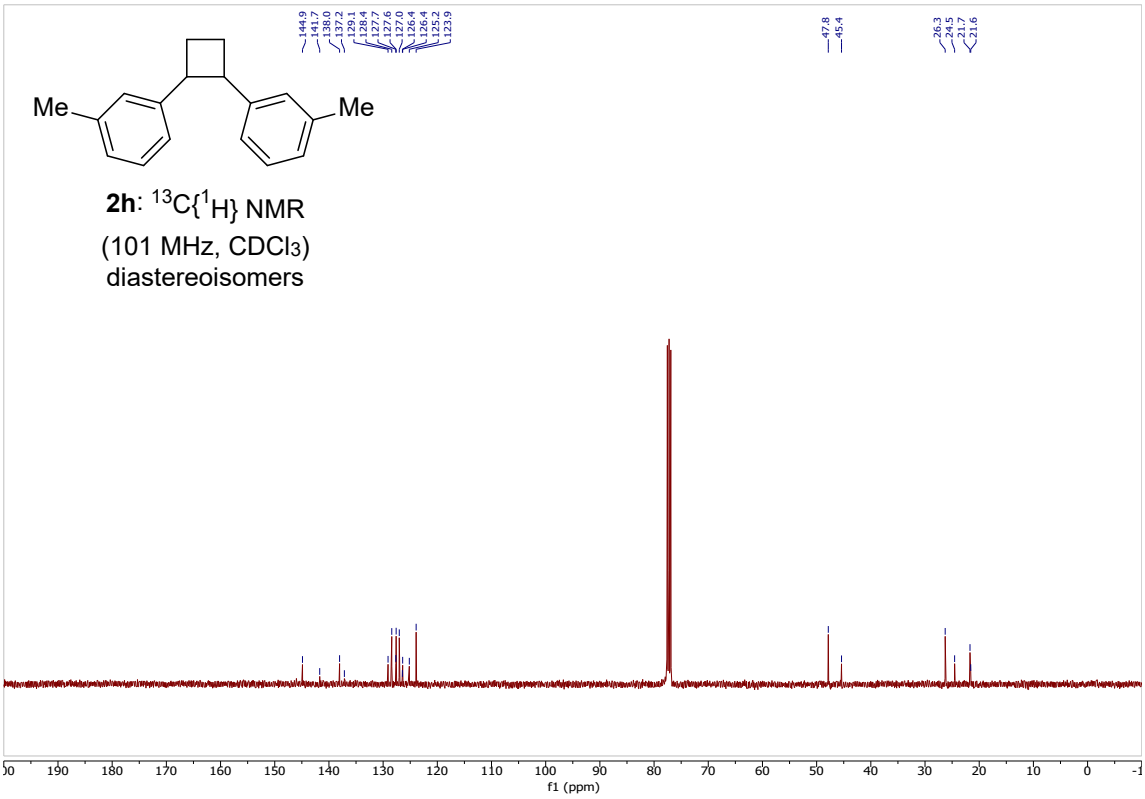

Fig. S69 | $^{13}C\{^{1}H\}$ NMR (101 MHz, $CDCl_3$) spectrum of **2h**.

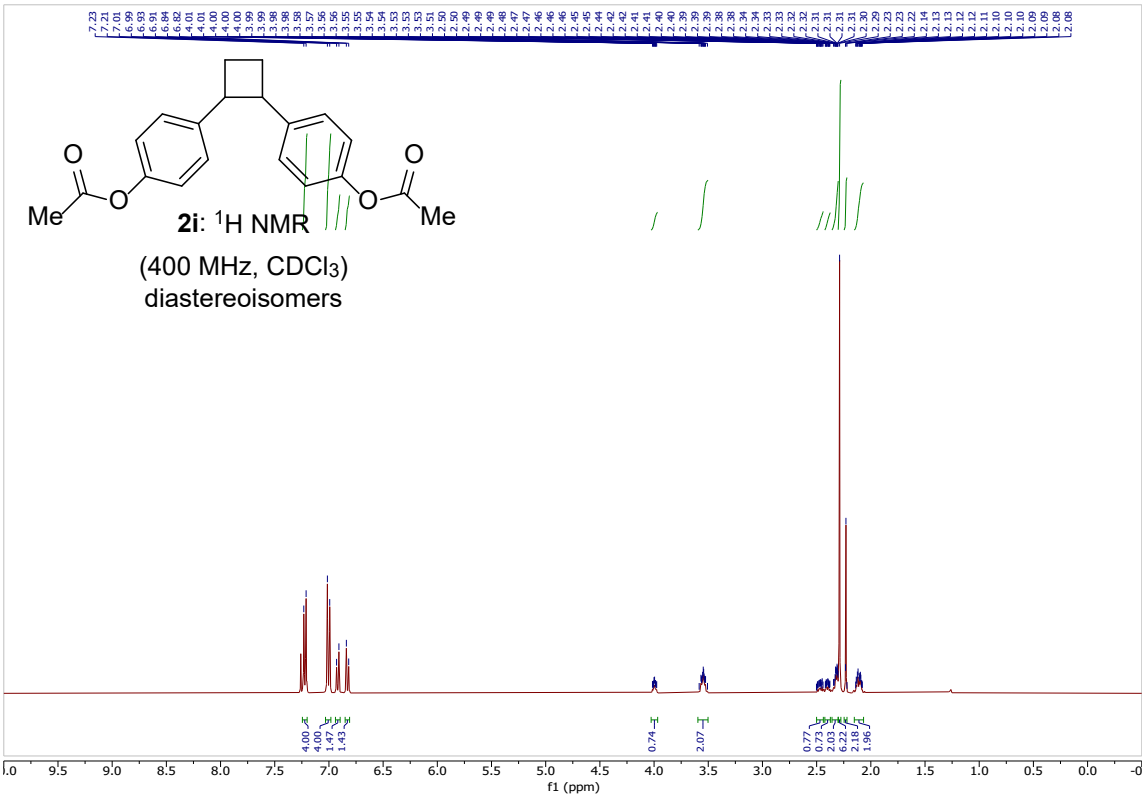

Fig. S70 | ^{1}H NMR (400 MHz, $CDCl_3$) spectrum of **2i**.

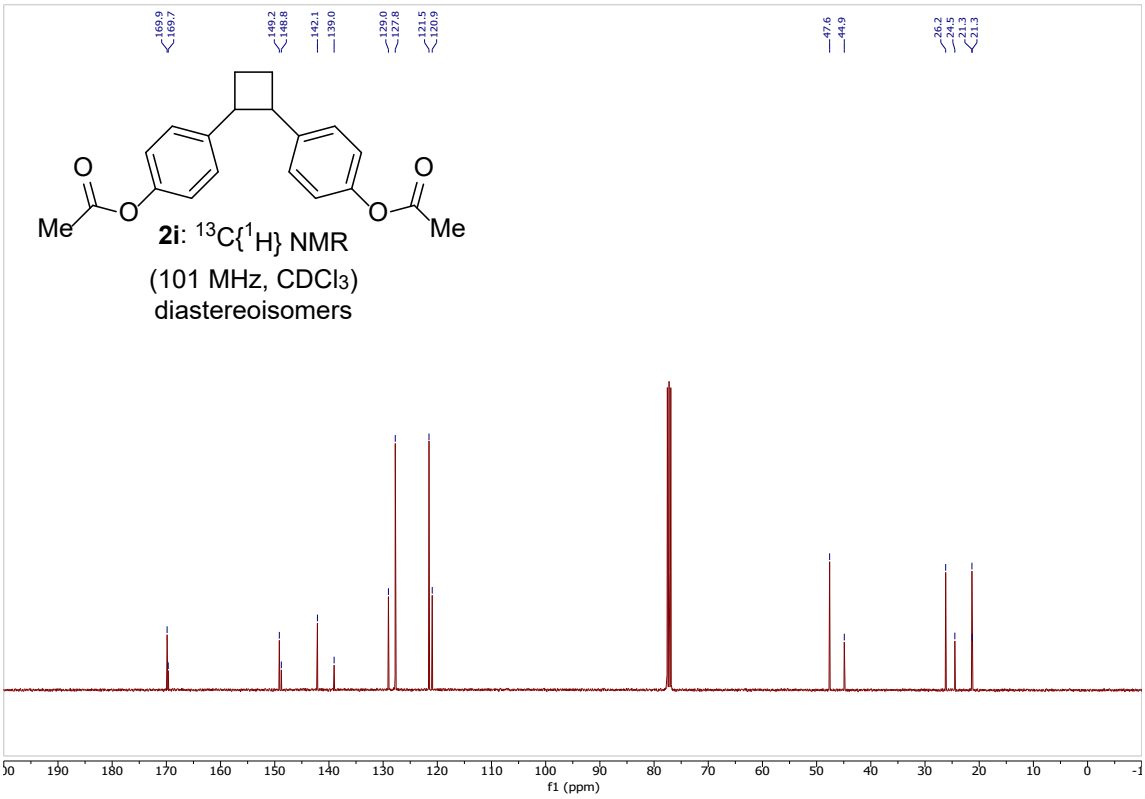

Fig. S71 | $^{13}C\{^{1}H\}$ NMR (101 MHz, $CDCl_3$) spectrum of **2i**.

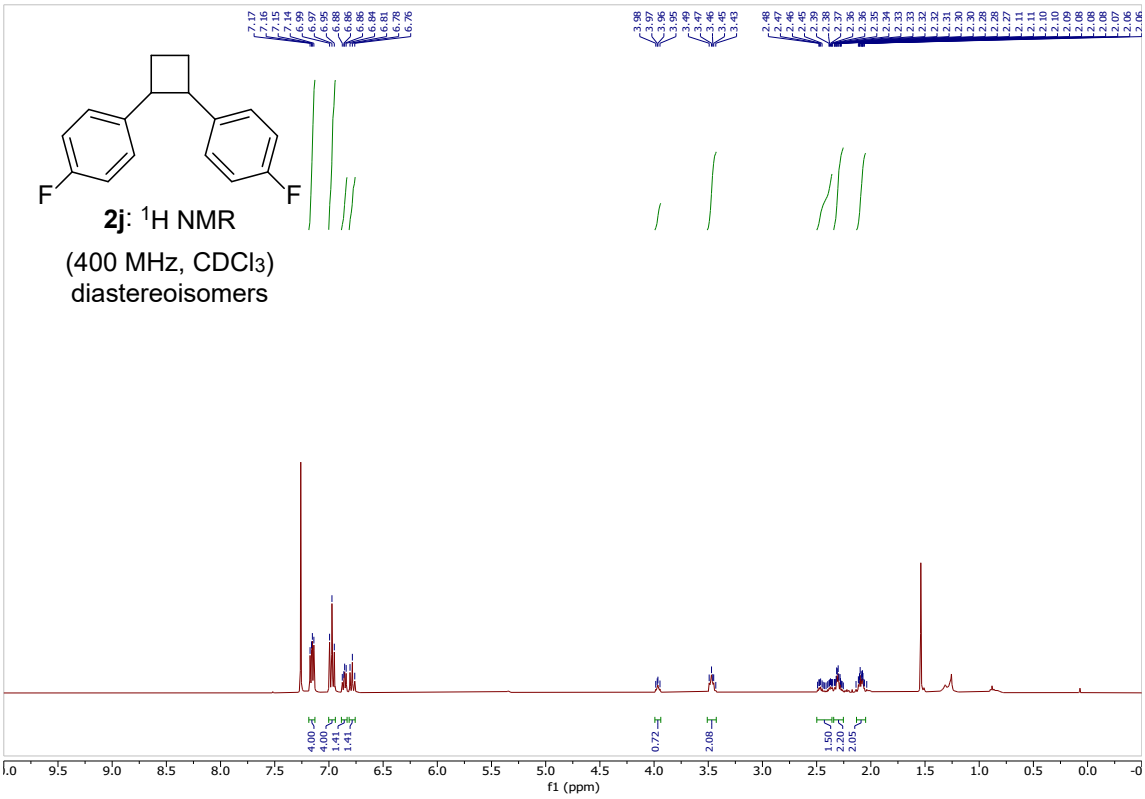

Fig. S72 | ^{1}H NMR (400 MHz, $CDCl_3$) spectrum of **2j**.

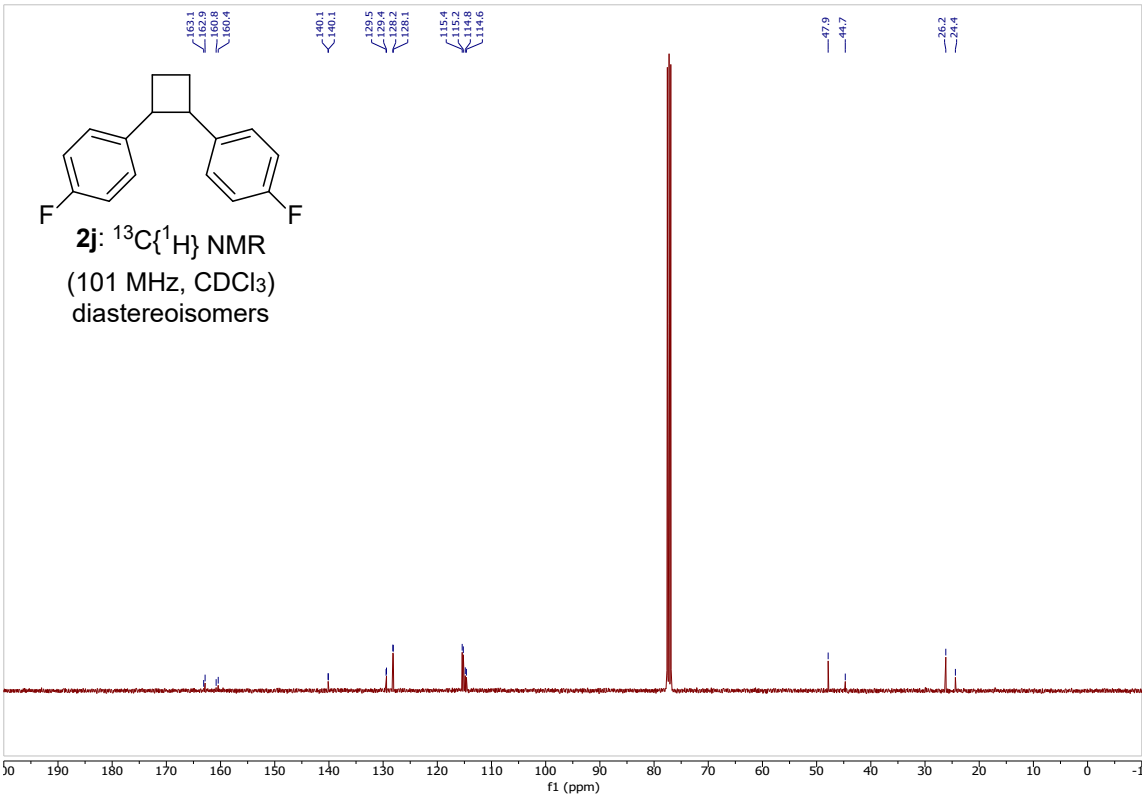

Fig. S73 | $^{13}C\{^{1}H\}$ NMR (101 MHz, $CDCl_3$) spectrum of **2j**.

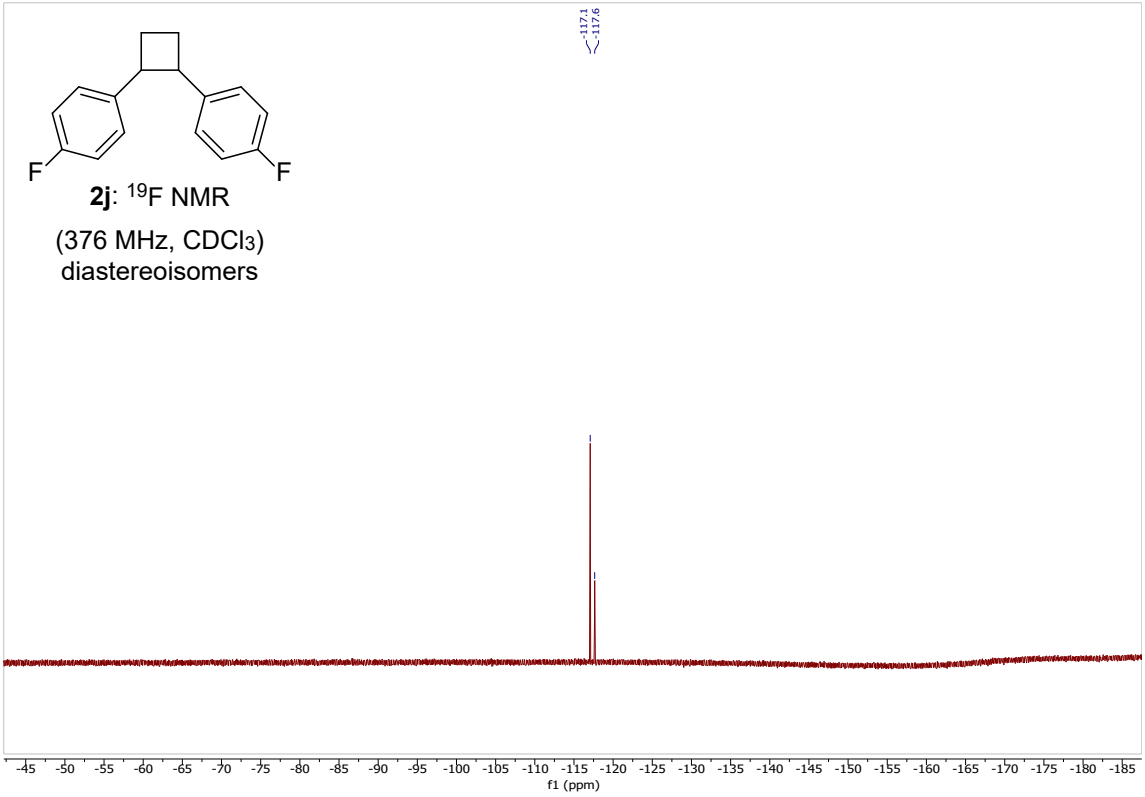

Fig. S74 | $^{19}F\{^{1}H\}$ NMR (376 MHz, $CDCl_3$) spectrum of **2j**.

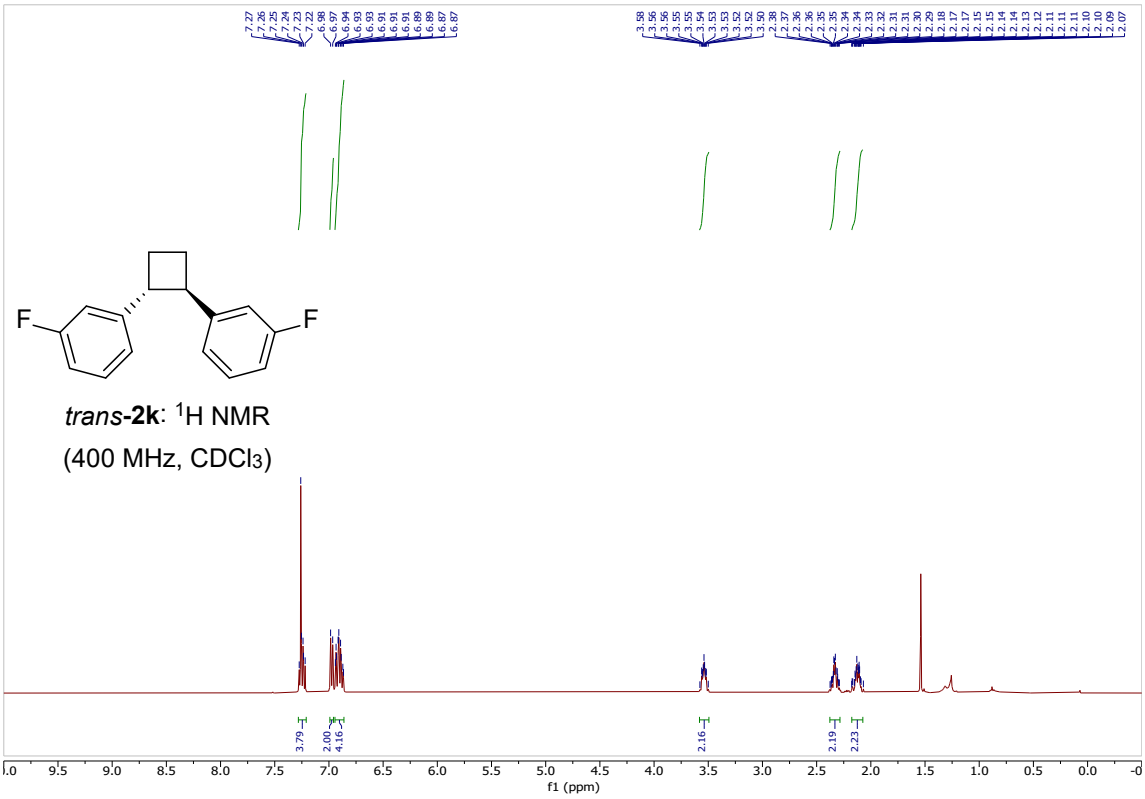

Fig. S75 | ^{1}H NMR (400 MHz, $CDCl_3$) spectrum of ***trans*-2k**.

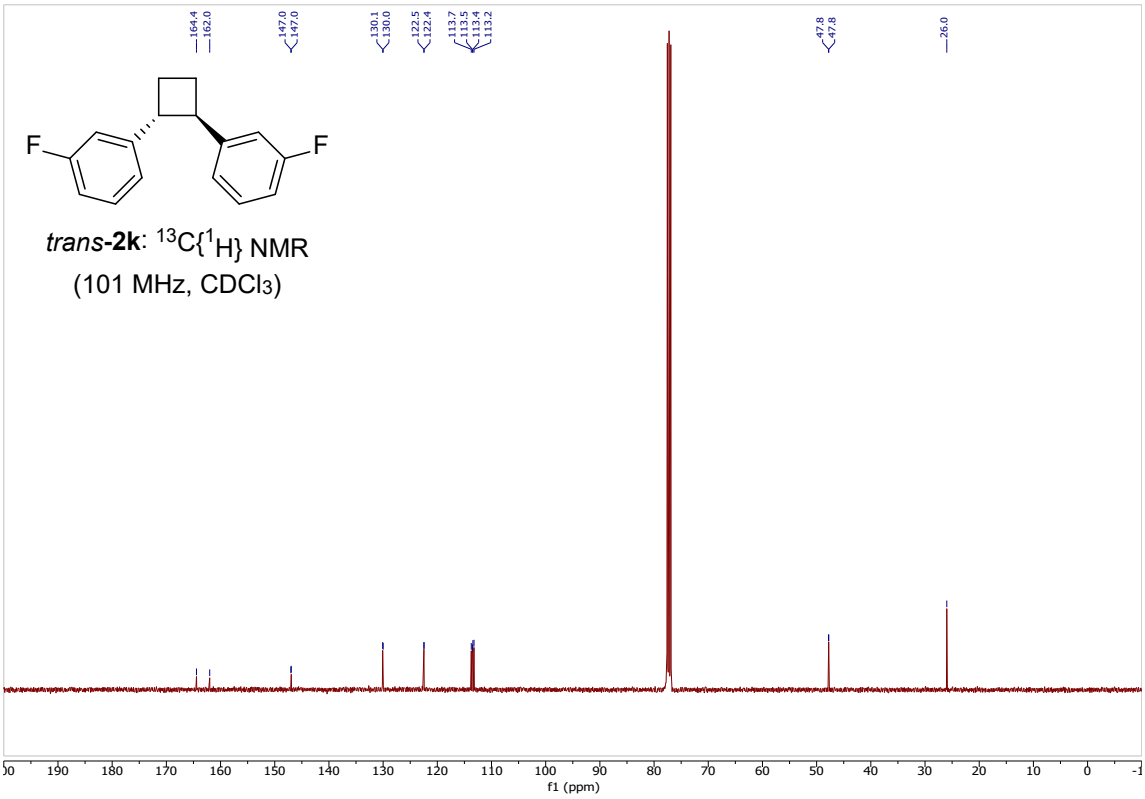

Fig. S76 | $^{13}C\{^{1}H\}$ NMR (101 MHz, $CDCl_3$) spectrum of ***trans*-2k**.

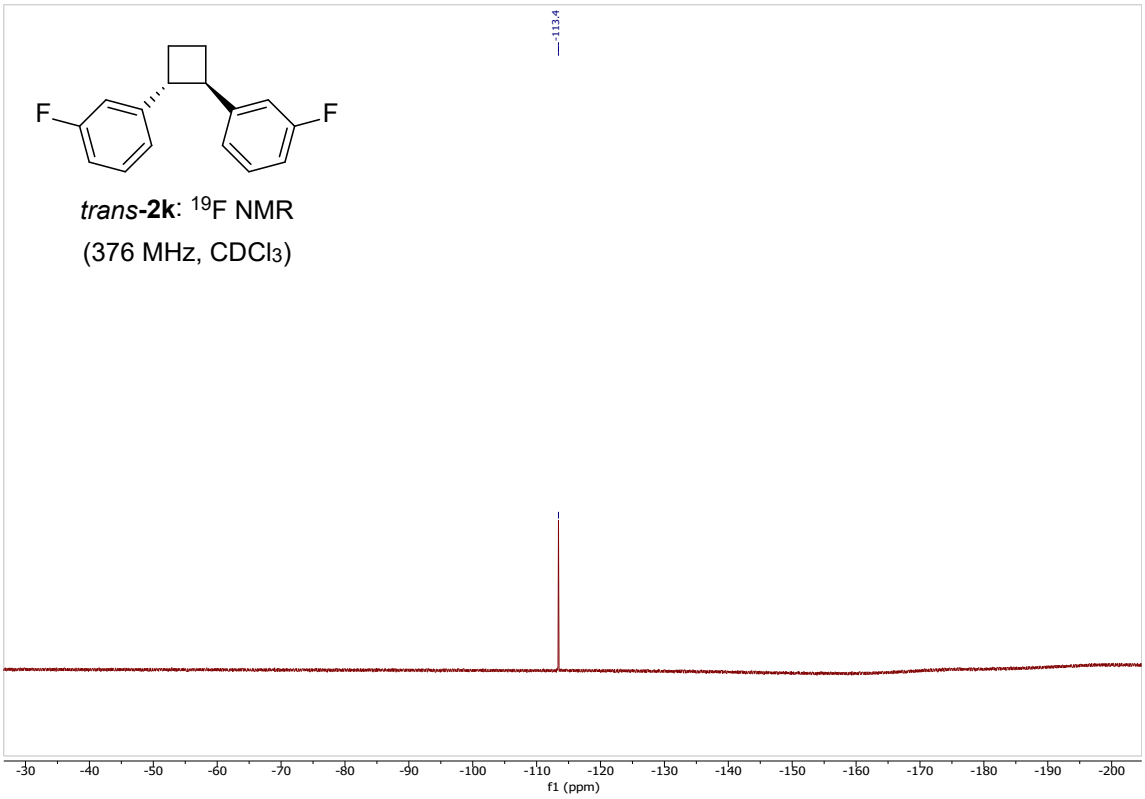

Fig. S77 | $^{19}F\{^{1}H\}$ NMR (376 MHz, $CDCl_3$) spectrum of *trans*-**2k**.

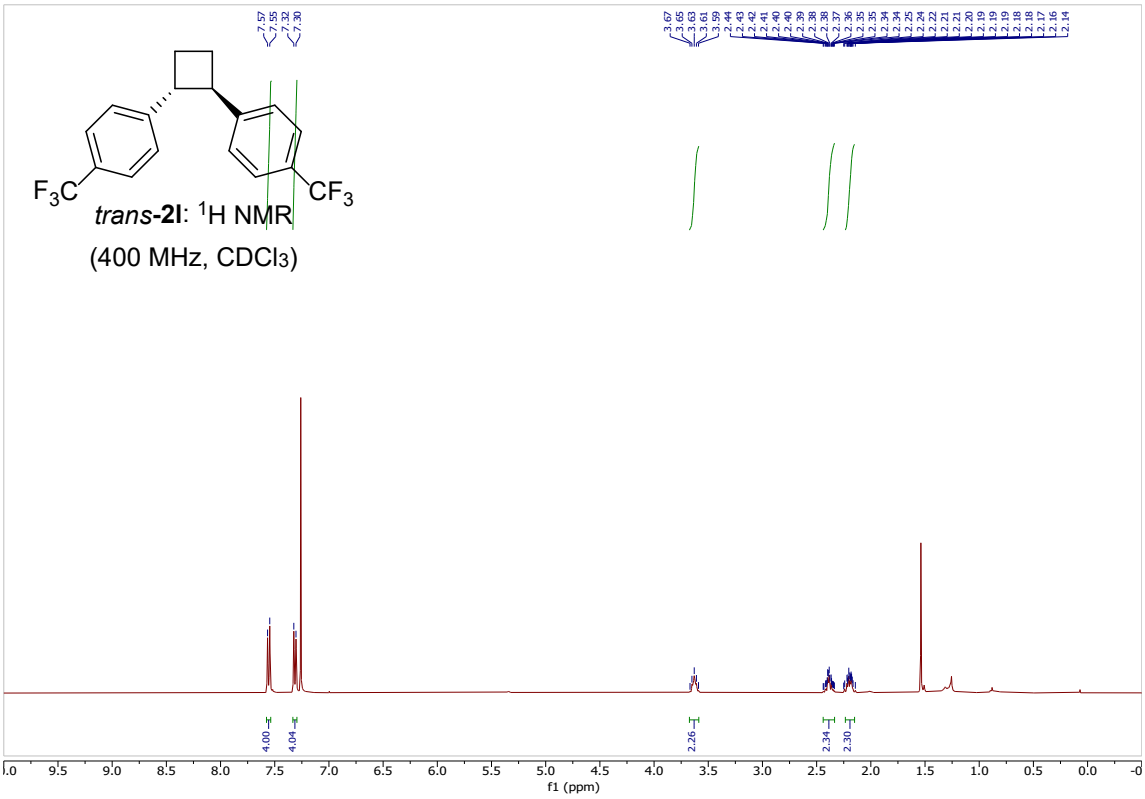

Fig. S78 | ^{1}H NMR (400 MHz, $CDCl_3$) spectrum of ***trans*-2l**.

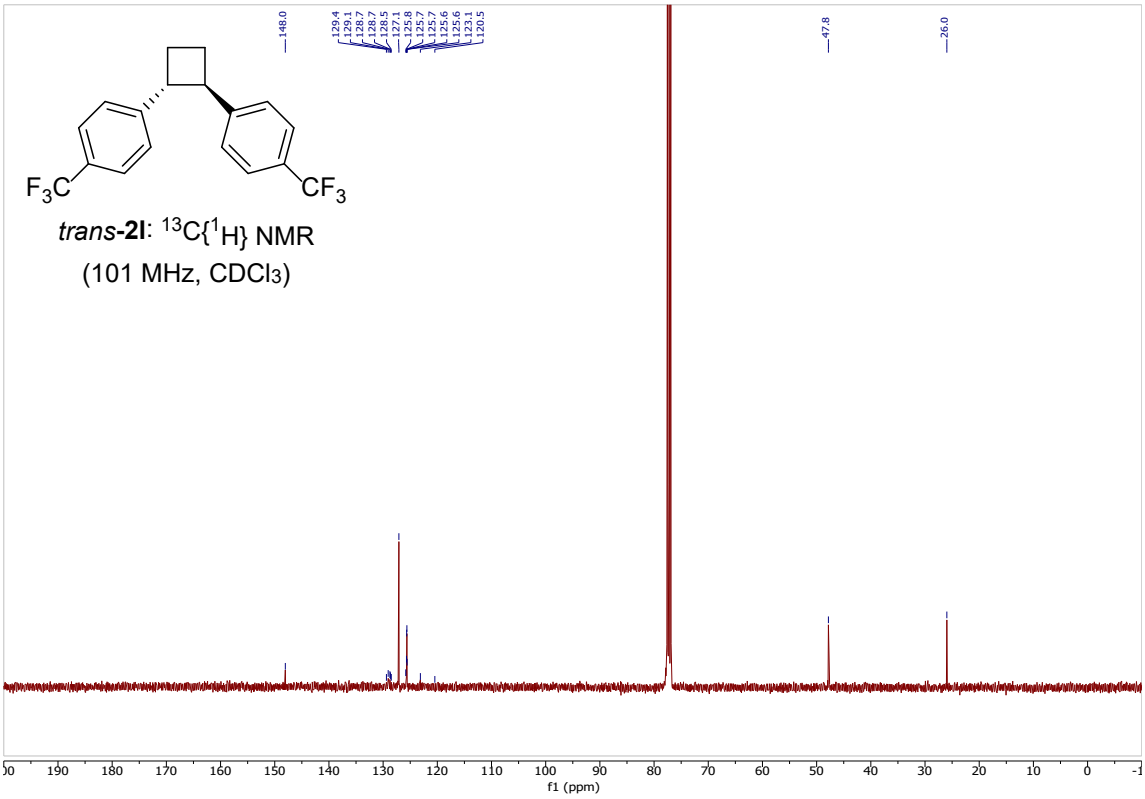

Fig. S79 | $^{13}C\{^{1}H\}$ NMR (101 MHz, $CDCl_3$) spectrum of ***trans*-2l**.

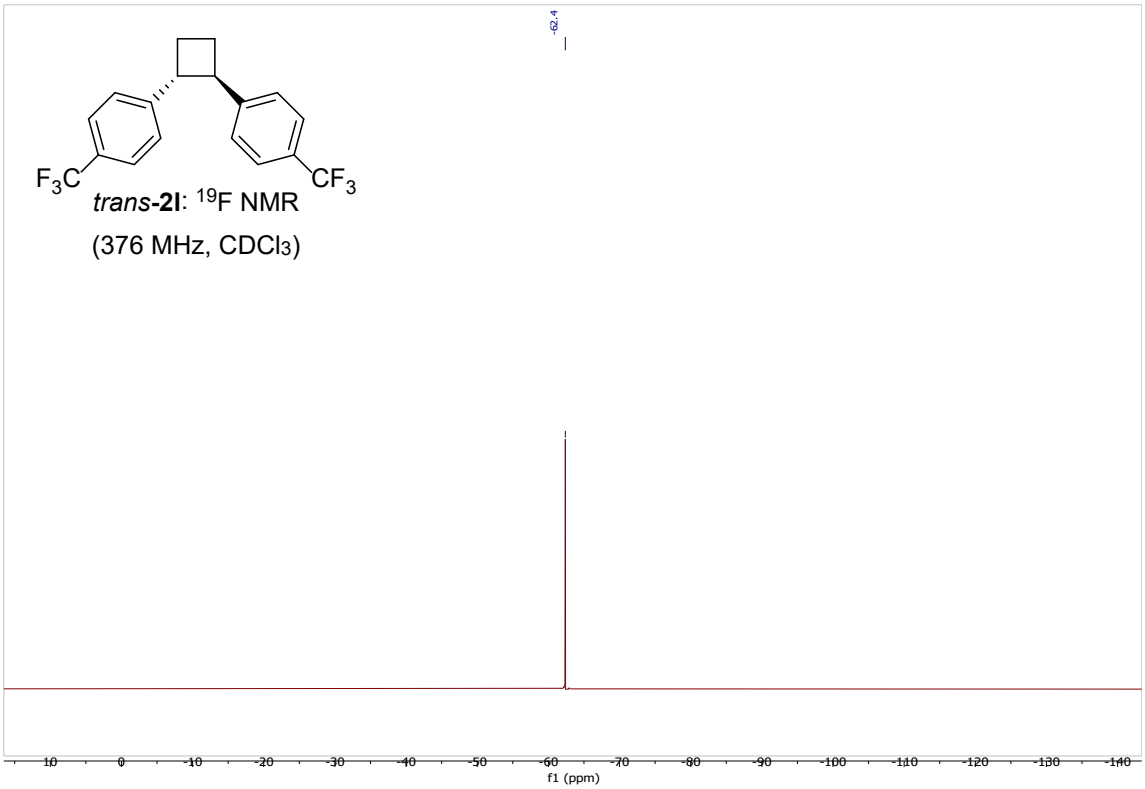

Fig. S80 | $^{119}F\{^{1}H\}$ NMR (376 MHz, $CDCl_3$) spectrum of ***trans*-2l**.

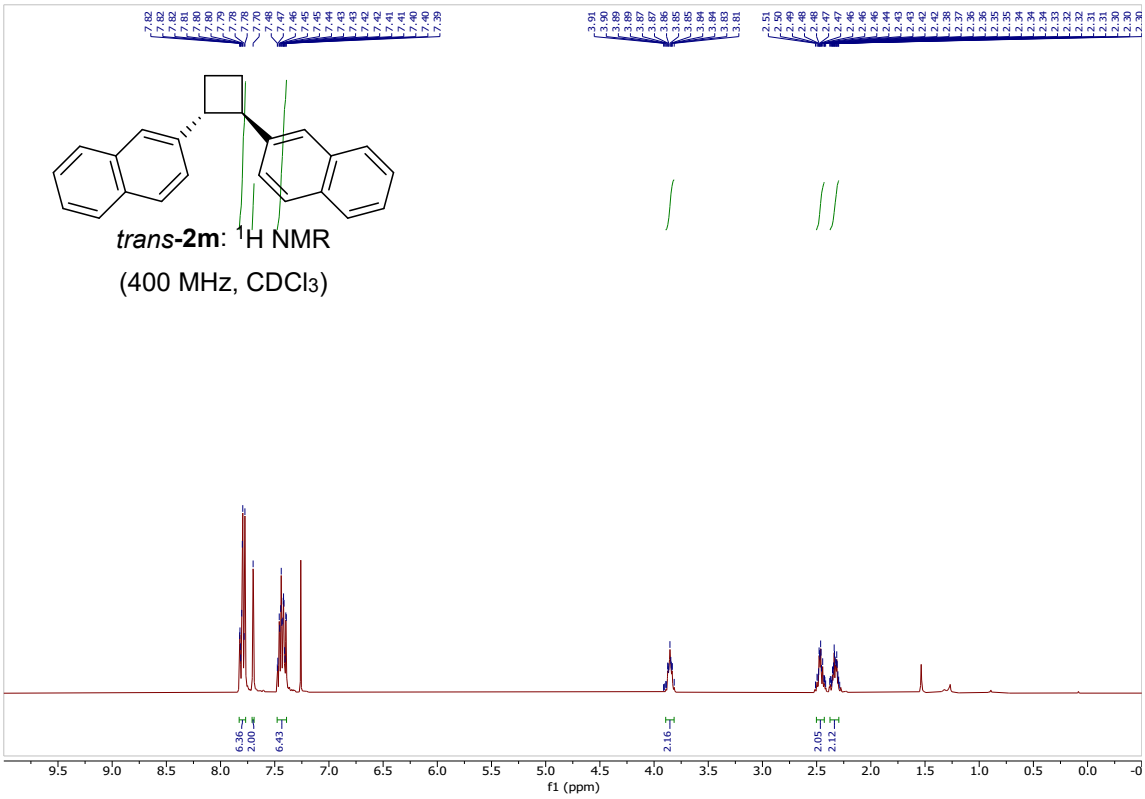

Fig. S81 | ^{1}H NMR (400 MHz, $CDCl_3$) spectrum of ***trans*-2m**.

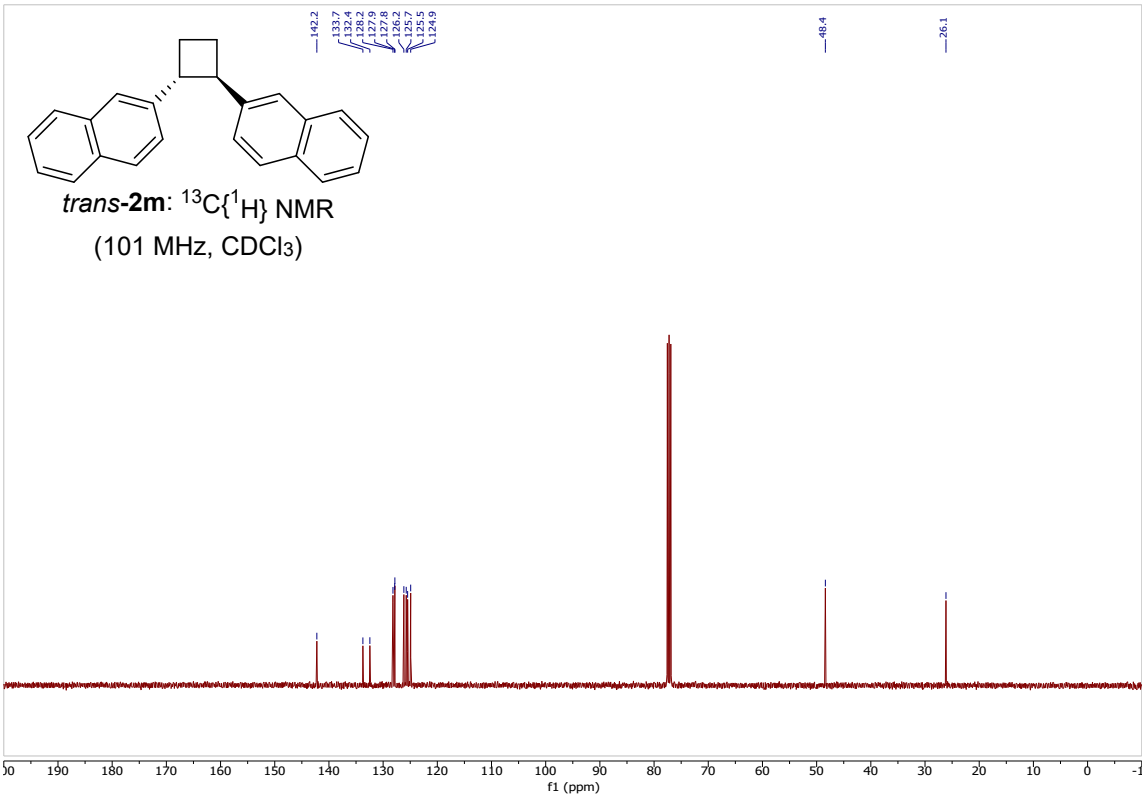

Fig. S82 | $^{13}C\{^{1}H\}$ NMR (101 MHz, $CDCl_3$) spectrum of ***trans*-2m**.

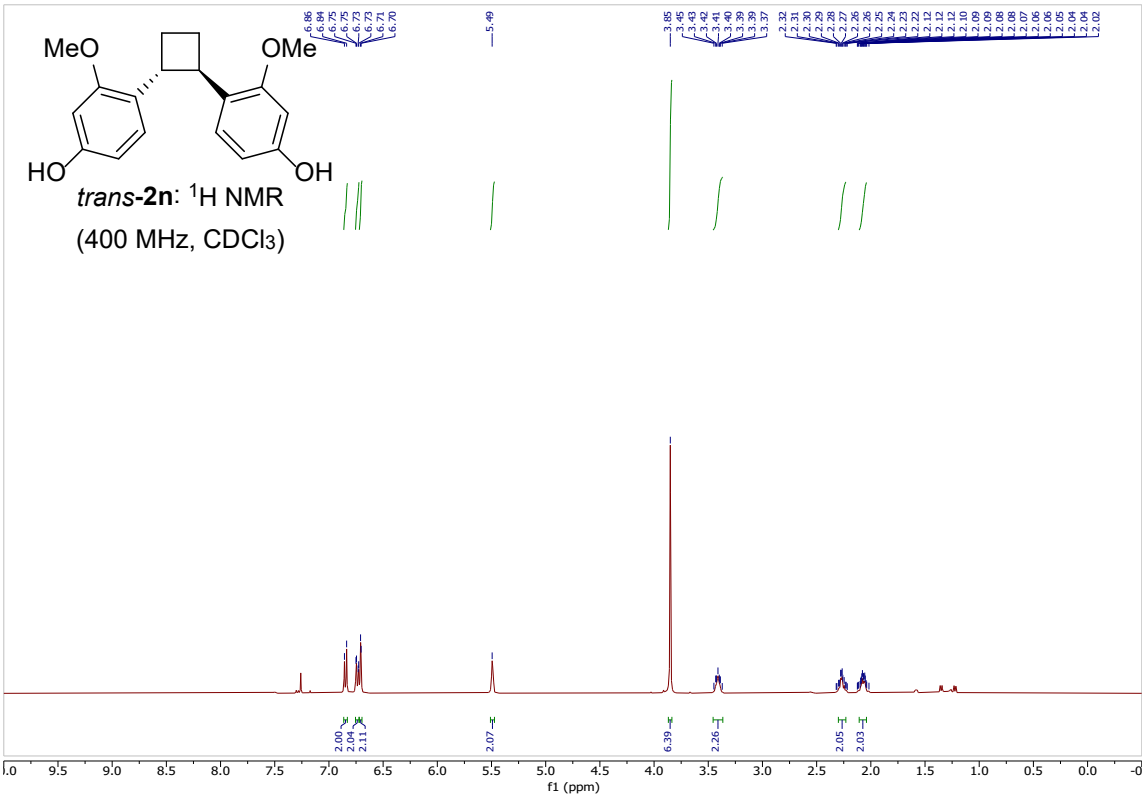

Fig. S83 | ^{1}H NMR (400 MHz, $CDCl_3$) spectrum of ***trans*-2n**.

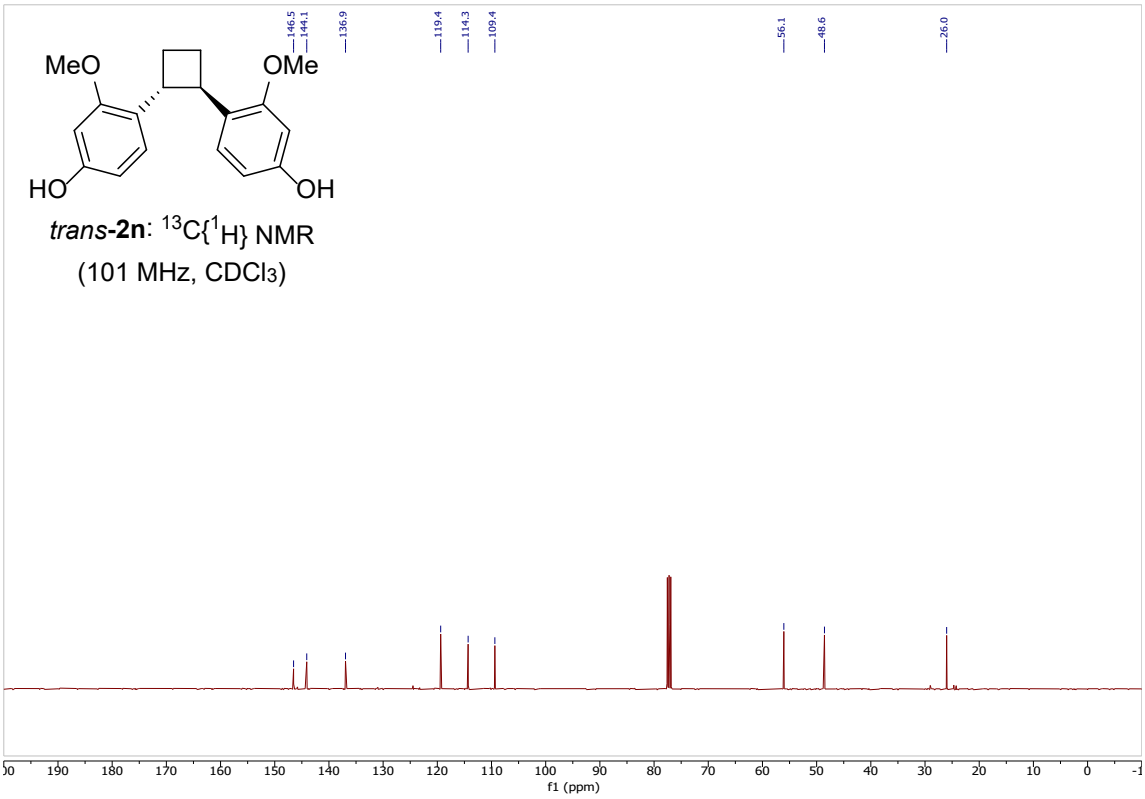

Fig. S84 | $^{13}C\{^{1}H\}$ NMR (101 MHz, $CDCl_3$) spectrum of ***trans*-2n**.

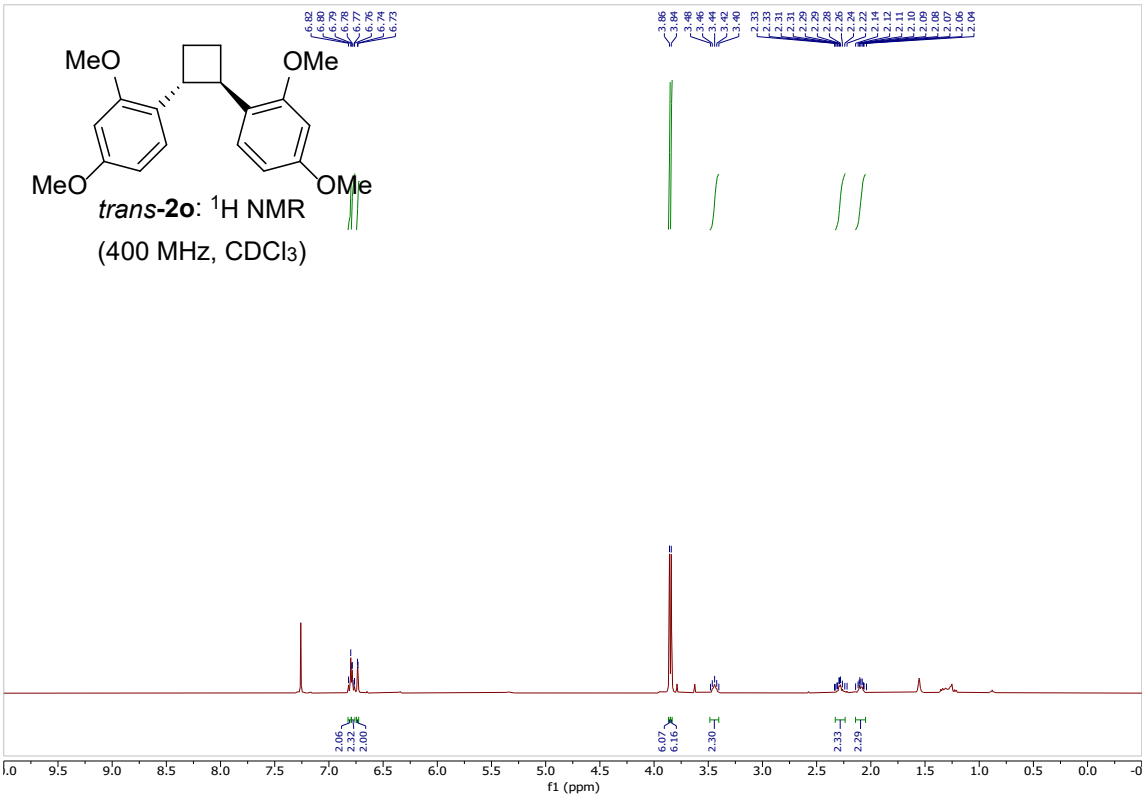

Fig. S85 | ^{1}H NMR (400 MHz, $CDCl_3$) spectrum of ***trans*-2o**.

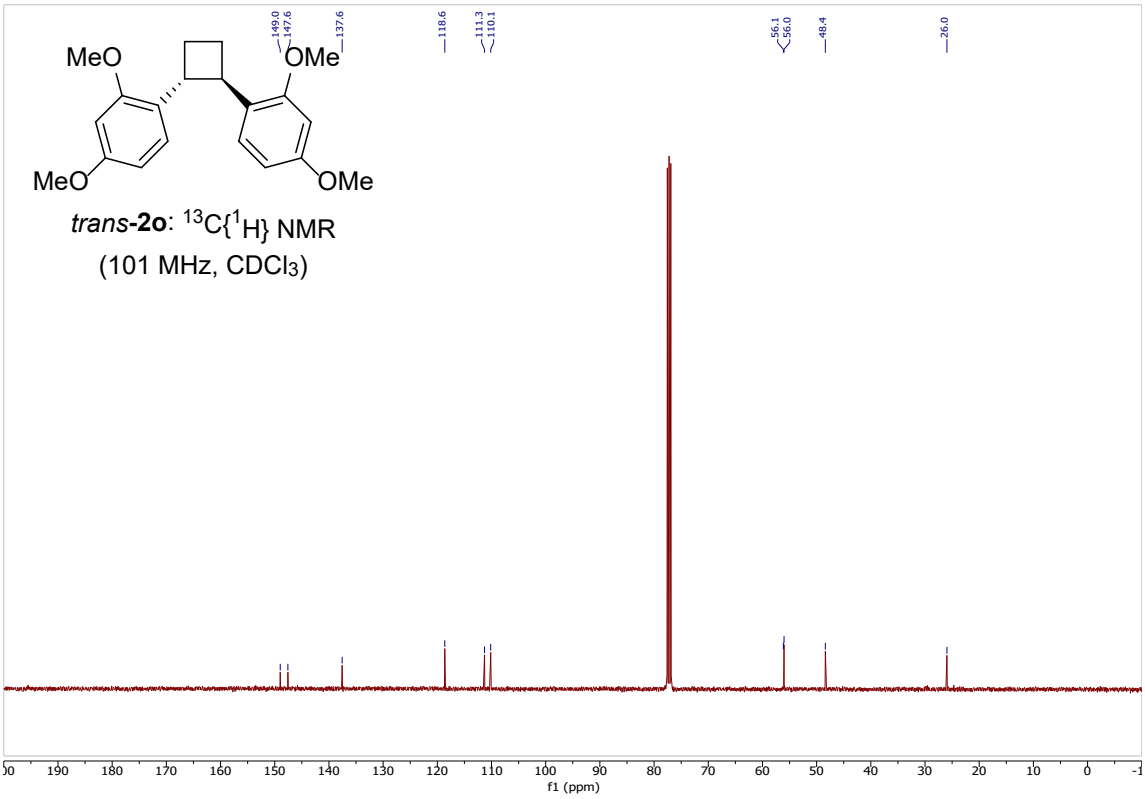

Fig. S86 | $^{13}C\{^{1}H\}$ NMR (101 MHz, $CDCl_3$) spectrum of ***trans*-2o**.

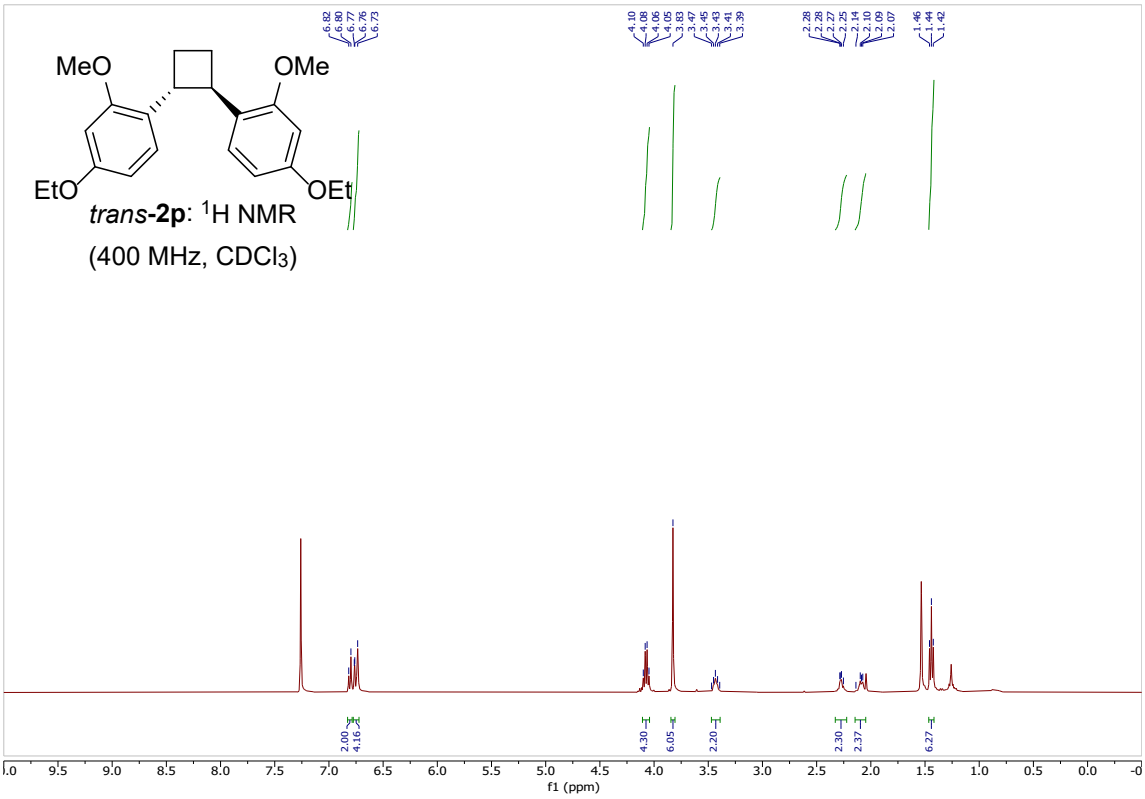

Fig. S87 | ^{1}H NMR (400 MHz, $CDCl_3$) spectrum of ***trans*-2p**.

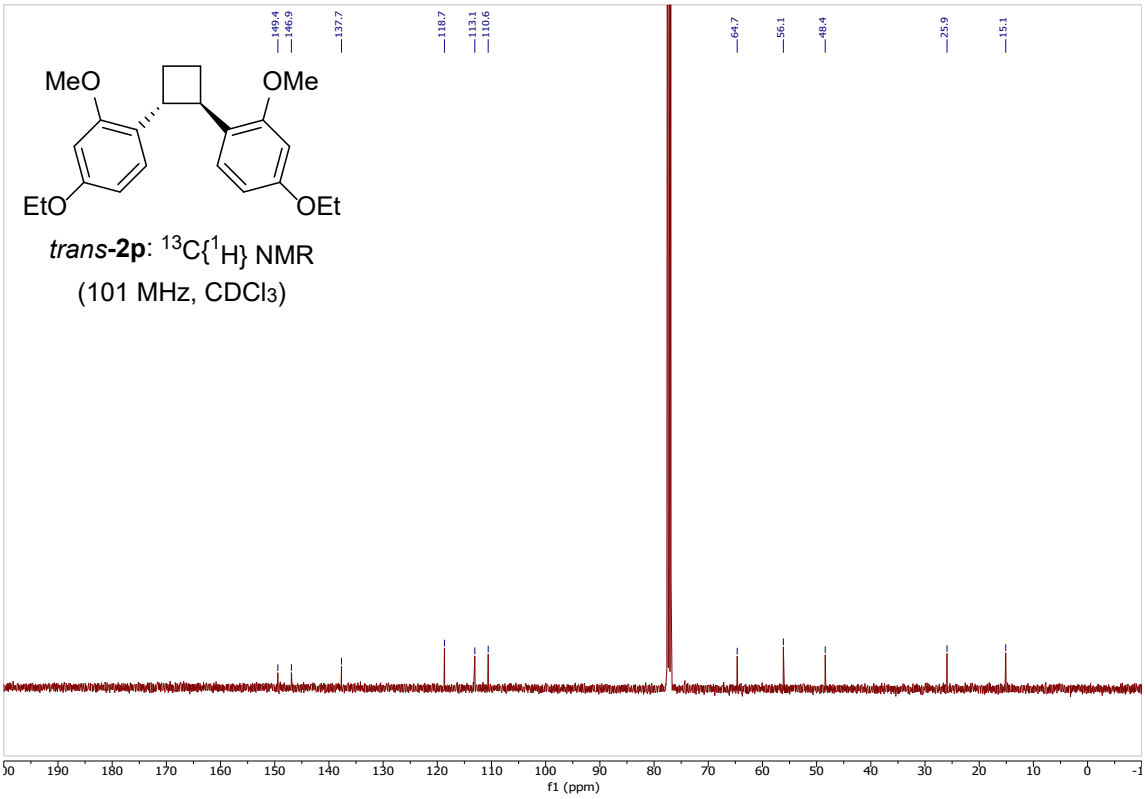

Fig. S88 | $^{13}C\{^{1}H\}$ NMR (101 MHz, $CDCl_3$) spectrum of ***trans*-2p**.

References

[1] S. Heo, Y. Jung, J. Kim, I. Kim, H. J. Bae, W.-J. Son, H. Choi, Y. You, *Adv. Optical Mater.* **2022**, 10, 2201610.

[2] N. V. Tzouras, E. A. Martynova, X. Ma, T. Scattolin, B. Hupp, H. Busen, M. Saab, Z. Zhang, L. Falivene, G. Pisanò, K. V. Hecke, L. Cavallo, C. S. J. Cazin, A. Steffen, S. P. Nolan, *Chem. Eur. J.* **2021**, 27, 11904.

[3] B. H. Jhun, J. Jang, S. Lee, E. J. Cho, Y. You, *Nat. Commun.* **2024**, 15, 6586.

[4] G. M. Sheldrick, Bruker AXS Inc., Madison, WI 2001.

[5] G. M. Sheldrick, *Acta Crystallogr., Sect. C: Found. Adv.* **2015**, 71, 3.

[6] G. Heinrich, S. Schoof, H. Gusten, *J. Photochem.* **1974**, 3, 315.

[7] Z. Lu, T. P. Yoon, *Angew. Chem., Int. Ed.* **2012**, 51, 10329.

[8] C. G. Hatchard, C. A. Parker, *Proc. R. Soc. Lond. A* **1956**, 235, 518.

[9] J. A. Kübler, B. Pfund, O. S. Wenger, *JACS Au* **2022**, 2, 2367.

[10] X. Wang, W. G. Kofron, S. Kong, C. S. Rajesh, D. A. Modarelli, E. C. Lim, *J. Phys. Chem. A* **2000**, 104, 1461.

[11] P. Müller, K. Brettel, *Photochem. Photobiol. Sci.* **2012**, 11, 632.

[12] E. S. Da Silva, P. Wong-Wah-Chung, M. Sarakha, H. D. Burrows, *J. Photochem. Photobiol. A: Chem.* **2013**, 265, 29.

[13] L. Waura-angkura, B. M. Matsagar, K. Lee, V. Pavarajarn, K. C. W. Wu, *Green Chem.* **2024**, 26, 1889.

[14] Y. J. Jang, H. An, S. Choi, J. Hong, S. H. Lee, K. H. Ahn, Y. You, E. J. Kang, *Org. Lett.* **2022**, 24, 4479.

[15] M. Golfmann, L. Glagow, A. Giakoumidakis, C. Golz, J. C. L. Walker, *Chem. Eur. J.* **2023**, 29, e202202373.

[16] Z. Liu, C. Zhou, T. Lei, X. L. Nan, B. Chen, C. H. Tung, L. Z. Wu, *CCS Chem.* **2020**, 2, 582.

[17] G. Wulff, S. Krieger, B. Kuhneweg, A. Steigel, *J. Am. Chem. Soc.* **1994**, 116, 409.

[18] M. Riener, D. A. Nicewicz, *Chem. Sci.* **2013**, 4, 2625.

[19] T. Fuchigami, M. Atobe, S. Inagi, *Fundamentals and Applications of Organic Electrochemistry: Synthesis, Materials, Devices*, Wiley-VCH, **2015**.